Hybrid nanopore field-effect transistors for controlling single-molecule transport and selective sensing of small molecules

Liang Xue

A thesis submitted in partial fulfilment of the requirement for the degree of

Doctor of Philosophy

Department of Chemistry

Imperial College London

Declaration of originality

The work presented herein was performed under the supervision of Prof. Joshua Edel and Dr Alex Ivanov Imperial College London. Except where otherwise cited or referenced, I hereby declare that the work presented in this thesis is my own. This thesis has not been submitted in whole or in part for another degree of qualification at this or any other institution of higher learning.

Liang Xue

May 2020

The copyright of this thesis rests with the author and is made available under a Creative Commons Attribution Non-Commercial No Derivatives licence. Researchers are free to copy, distribute or transmit the thesis on the condition that they attribute it, that they do not use it for commercial purposes and that they do not alter, transform or build upon it. For any reuse or redistribution, researchers must make clear to others the licence terms of this work.

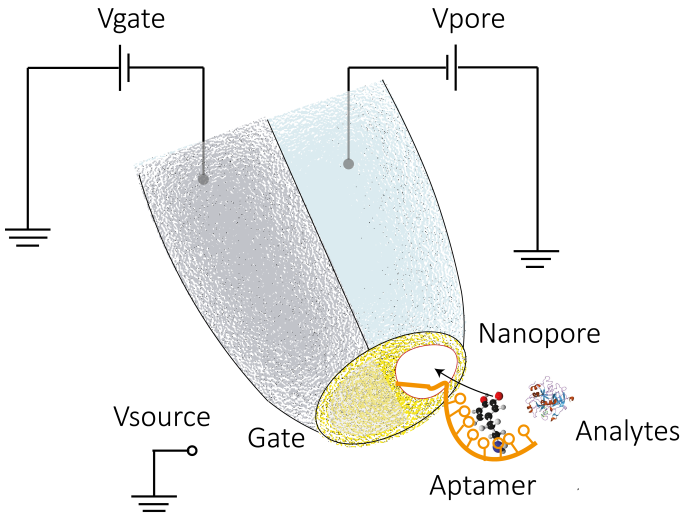
Abstract

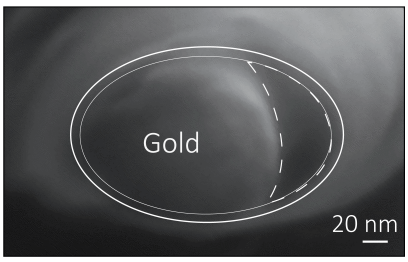
Single-molecule methods have been rapidly developing with the appealing prospect of transforming conventional analytical techniques. The selective recognition of proteins and small molecules is a major motivation in developing single-molecule detection and diagnostic techniques. However, challenges remain especially in improving detection sensitivity, selectivity and controlling molecular transport. This is compounded by the complexities in selectively detecting small molecules in biological fluids. In this thesis, we address these limitations by showing a direct fabrication method for an analytical sensor that integrates the advantages of nanopores, field-effect transistors (FET) and selective recognition of target analytes, for simultaneous single-molecule detection and manipulation of DNA, proteins and small molecules such as neurotransmitters.

In the first part of this thesis, a controlled and easy fabrication method for nanopore field-effect transistors was developed in terms of electrodeposition, facilitating the implementation of fabricated analytical sensors for the gating of molecular transport. It was demonstrated that the perfect alignment of nanopore and FET enables the gating of molecular transport across nanopore to be switched on/off in real-time. More importantly, surface functionalization of the gate electrode can be used to fine-tune transport properties enabling more active control over translocation velocity and capture rates by orders of magnitude.

Based on the established sensing platform, a novel sensing strategy was presented for selective sensing of proteins and neurotransmitters at the single-molecule level. Aptamers were attached to the surface of the gate electrode for selectively recognizing different analytes. Our results elucidated that, protein-aptamer interactions are able to generate unique fingerprints allowing for monitoring and extracting real-time binding affinity by target-induced conformational changes. The gating of binding affinity was revealed in terms of controlling protein transport. Importantly, by enhancing the affinity of aptamers, selective single-molecule detection of neurotransmitters at fM concentration was demonstrated in biological fluids such as human serum. The selective detection of neurotransmitters has yet to be achieved using solid-state nanopores. This approach was proved to be versatile for different types of neurotransmitters, including dopamine, serotonin and acetylcholine. Further development of such a strategy may enable the improvement of nanopore sensors towards different

biologically important applications such as protein fingerprinting and multiplexed sensing of different molecular targets. An outlook was made on a range of sensing modes developed on this multifunctional platform with different dynamic ranges for in-vivo monitoring of neuron activities using functionalised nanopipettes.





Acknowledgement

First of all, an enormous thank you goes to my supervisors Prof. Joshua Edel and Dr Alex Ivanov for their guidance throughout my PhD. Their enthusiasm towards science, resilience for tackling difficulties in the research and the optimism for the future have always been motivational to me. Importantly, I am grateful for them to shape me as a proper scientist to proceed further on this route.

Members of Edel/Ivanov group are always a source of joy, happiness, and positiveness. I would like to show my gratitude to postdoctoral researchers I have been interacting with, Dr Paolo Cadinu for acting as the mentor when first entering the group as a final year project student, Dr Minkyung Kang for her useful discussion during my PhD second year when experiments were challenging, Dr Longhua Tang for his motivational chats in the final year of my PhD.

The PhD journey would not have been possible without collaboration, thanks to Richard Gutierrez and Dr Andrew Heron for the projects with Oxford Nanopore Technologies, as well as Prof. Yuri Korchev for nanopore field-effect transistors.

Moreover, it is a pleasure for working alongside the colleagues in the group, Alexandra Dias-Lalaca for proof-reading on my thesis, Alfie Gatehouse for football chats, Giulia Campolo, Ye Ma, Shenglin Cai and Ben Edwards for Friday drinks in both White City and South Kensington Campuses. It is also my privilege to supervise master students in the group, including Micol Damiani, Caroline Koch, Sonalika Jain and Xun Zhou, for the pleasure and sense of achievement to help you guys develop your research skills.

Time flies since I first came to UK as a first-year undergraduate in the department, with constant contacts with my undergraduate friends during my PhD which acts as a source of motivation and encouragement, including Dong, Freeman, Wesker and Shukai.

Finally, I would like to show the greatest appreciation to my parents for their unconditional support both mentally and financially for my PhD. Also, I am so lucky to meet my girlfriend, Rachel Shi, during the graduation ceremony of my undergraduate degree at Imperial.

Table of contents

Declaration of originality 2
Abstract 3
Acknowledgement 5
Table of contents 6
List of Publications 9
List of figures 10
List of schemes 26
List of tables 27
Abbreviations 28
Chapter 1 29
Abstract 30
1.1 Biosensing and healthcare 31
1.2 Single-molecule detection 32
1.3 Single-molecule detection using nanopores 33
1.3.1 Single-molecule electrical detection using patch-clamp technologies 33
1.3.2 Nanopore sensing 34
1.3.2.1 Overview 34
1.3.2.2 Nanopore sensing – working principle 36
1.3.2.3 Biological nanopores 38
1.3.2.4 Solid-state nanopores 38
1.3.2.5 Nanopipettes 39
1.3.2.6 From protein pores to hybrid pores 39
1.3.2.7 Chemical modifications for selective sensing 40
1.3.2.8 Sensor multiplexing 42
1.3.2.9 Alternative detection strategies 43
1.3.2.10 Nanopore field-effect transistors 44
1.4 Thesis outline 46
1.5 References 48
Chapter 2 54
2.1 Introduction 55
2.2 Laser-assisted pulling of nanopipettes 55
2.3 Selective pyrolysis of butane 57
2.4 Electrochemical fabrication of nanopore-FET devices and characterisation 58

2.4.1 Feedback-controlled deposition of gold 58
2.4.2 Characterisation of nanopore-FET devices 60
2.5 Surface functionalisation of deposited gold 60
2.5.1 Functionalisation with small organic molecules 61
2.5.2 Functionalisation with oligonucleotides 61
2.5.3 Electrochemical characterisation 62
2.6 Single-molecule translocation experiments 63
2.6.1 Solutions and reagents 63
2.6.2 Electrochemical configuration 63
2.7 References 68
Chapter 3 70
Abstract 71
3.1 Introduction 72
3.1.1 General background 72
3.1.2 Electrodeposition 73
3.1.3 Cyclic voltammetry 74
3.1.4 Chronoamperometry 75
3.2 Aims and objectives 76
3.3 Results and discussion 77
3.3.1 Deposition mechanism and voltammetry characterisation 77
3.3.2 Real-time ion current feedback 79
3.3.3 Surface characterisation 84
3.4 Conclusion 86
3.5 References 87
Chapter 4 89
Abstract 90
4.1 Introduction 91
4.2 Single-molecule detection of DNA using gold-deposited nanopore-FET 92
4.3 Controlling DNA transport using gold-deposited nanopore-FET 94
4.4 Chemical modification of nanopore-FET 97
4.5 Fine-tuning single-molecule transport using amine-modified nanopore-FET 103
4.6 Conclusion and future work 106
4.7 References 107
Chapter 5 111
Abstract 112
5.1 Introduction 113

5.2 Device fabrication and chemical modification 116
5.3 Optimisation of aptamer-modified nanopore-FETs 119
5.4 Controlling protein transport by aptamer-functionalised nanopores 122
5.5 Detection of neurotransmitters 125
5.5.1 Characterisation of the binding between aptamers and neurotransmitters using electrical measurements 126
5.5.2 Selective single-molecule detection of neurotransmitters 129
5.5.3 Single-molecule binding assay for neurotransmitters 135
5.6 Conclusion and future work 138
5.7 References 140
Chapter 6 144
6.1 Project aims and outcomes 145
6.2 Future work 147
6.3 References 149

List of Publications

1) Liang Xue, Aleksandar P. Ivanov, Joshua B. Edel et al. Nanopore Ionic Field-Effect Transistors for Controlling Molecular Transport and Selective Single-Molecule Detection of Small Molecules, *in preparation (2020)*.

2) Liang Xue, Hirohito Yamazaki, Ren Ren, Meni Wanunu, Aleksandar P. Ivanov, Joshua B. Edel, Solid-state nanopore sensors, *Nature Reviews Materials* (2020), https://doi.org/10.1038/s41578-020-0229-6.

3) Liang Xue, Paolo Cadinu, Binoy Paulose Nadappuram, Minkyung Kang, Ye Ma, Yuri Korchev Aleksandar P. Ivanov, Joshua B. Edel. Gated Single-Molecule Transport in Double-Barreled Nanopores. *ACS Applied Materials & Interfaces* **10**, 38621-38629 (2018).

Conference presentation

Nanopore Ionic Field-Effect Transistors for Controlling Molecular Transport and Selective Single-Molecule Detection of Small Molecules, 2020 Nanopore electrochemistry meeting.

List of figures

Figure 1-1: Conceptual illustration of ensemble-averaged detection techniques vs single-molecule methods. Compared with conventional biosensing technologies such as enzyme-linked immunosorbent assay, which produced time-averaged properties, single-molecule methods can detect properties and interactions between each molecule by decreasing the sensing volume to a scale comparable with single biomolecules. This results in the highest levels of sensitivity and opens up the possibility of revealing the properties of single molecules that are normally masked by conventional, ensemble-averaged properties..... 32

Figure 1-2: Conceptual demonstration of the patch-clamp recording technology, a glass microelectrode is inserted into a chamber/bath filled with an electrolyte consisting of K^+, Na^+ and/or Cl^- ions. The patch (recording) electrode connected to an amplifier is inserted into the pipette, another electrode is placed in the bath acting as a ground. Typically, a voltage clamp mode is used to control the voltage across the cell membrane, and the resulting current is recorded. Alternatively, the current-clamp mode can be used where the current passing through the membrane is controlled, and the output is generated in the form of reversal potentials (E_{rev})..... 34

Figure 1-3: Comparison between (a) biological nanopores, (b) solid-state nanopores and (c) nanopipettes. Biological nanopores normally consist of a pore-forming protein supported by a lipid bilayer. The diameter of a biological nanopore is determined by the structure of the protein, mostly around 1 nm. Solid-state nanopores are fabricated by electron beam drilling on a freestanding silicon nitride membrane on a silicon substrate, generating nanopores greater than 1 nm in size. Other fabrication methods exist, such as dielectric breakdown and electrochemical etching, addressing the cost and saving time as compared to the conventional electron beam drilling processes, which are performed under ultra-high vacuum conditions. Alternatively, a subclass of solid-state nanopores, namely nanopipettes, can be fabricated by laser-assisted pulling of glass capillaries, which lasts only a few seconds and produces a pair of nanopipettes with a nanopore size greater than 15 nm. 36

Figure 1-4: Working principle of nanopore sensing. The principle behind conventional nanopore detection is called resistive pulse sensing. A constant voltage bias is applied across a pore that connects two reservoirs filled with electrolytes separated by a non-permeable membrane. (a) In most cases, the applied bias from a pair of Ag/AgCl electrodes in KCl causes a steady-state ionic current to flow through the pore as the resistance of the nanopore is greater than the electrolyte resistance. As a result, most of the potential field gradient is focused at, or close to, the pore. Ions, and any other charged molecules, are therefore translocated through the pore across the membrane, driven by this potential gradient. (b) When a charged molecule is transported through the pore, the ionic current is either enhanced (as in most cases) or blocked as part of the nanopore volume previously occupied by ions is replaced by the translocating molecule. (c) The steady-state current is recovered after the translocating molecule exits the pore. Examples of ionic current traces showing single-molecule translocation of the analyte are shown in (d). Definition of terms in the equation to estimate the current from a cylindrical nanopore: i_0 : open pore current, μ: electrophoretic mobility of ions, n: the number density of ions, d is the diameter of nanopores, l is the thickness of nanopore, V_{bias} is the applied voltage. 37

Figure 1-5: Examples of chemical modifications for both biological nanopores and solid-state nanopores. (a) Biological nanopores can be modified by attaching aptamers at the pore lumen. Note that as the size of aptamers and targeted analytes is much larger than the diameter of biological nanopores, the current fluctuations are caused by the blocking and unblocking of the nanopore entrance from the aptamer and aptamer-target complex. Therefore, interactions between aptamers and targeted analytes can be monitored by analysing the switching of different current levels, corresponding to on/off states where the nanopore is blocked and unblocked by an aptamer-target complex.[26] (b) Protein receptors can be attached to the surface of solid-state nanopores. Selective single-molecule detection of proteins is achieved by the complexation chemistry between receptors and proteins.[62] (c) To combine the robustness of solid-state nanopores with the precise structural engineering of biological nanopores, pore-forming proteins can be inserted into solid-state nanopores. A successful insertion causes a decrease of nanopore conductance and nanopore current.[60] 40

Figure 1-6: Summary of different approaches for nanopore FETs. Solid-state nanopores can be integrated with FETs by incorporating a drain-source channel above the nanopore. In most cases, synchronised electrical recording is achieved via two independent amplifiers from the

nanopore and FET channels, respectively. Representative examples are demonstrated via (a–b) a Si nanowire[93] or (d–e) graphene nanoribbon nanopores[88,89] for synchronised detection of single-molecule DNA translocation. The scale bars are 10 nm for the Si nanowire and 5 nm for the graphene nanoribbons. The single-molecule translocation can be synchronised from resistive pulse sensing in a nanopore channel, and either through capacitive coupling or gated by the charge of the translocating molecule from the FET channel (i.e. drain-source) (c, f). This process could be modelled by a nanopore overlaid with the resistance from both cis and trans chambers, as well as the resistance from the nanopore. A portion of the FET channel is coupled with the nanopore, so that the FET channel in the cis region is coupled to the voltage set at the bottom Ag/AgCl electrode, resulting in a localised potential change around the nanopore. The potential falls as 1/r away from the nanopore where r is the distance from nanopore opening.[94] The inset is a schematic of a nanopore-FET electrical circuit. In this type of devices the source-drain is either Si nanowire or graphene nanoribbons. (g) More recently, a novel class of nanopore-FET devices was constructed from dual-barrel nanopipettes, with drain-source being the empty barrel of a nanopipette and gate being gold or polypyrrole electrode. One barrel was selectively filled with carbon via pyrolytic deposition from butane, forming a carbon nanoelectrode at the tip, and an empty barrel was used as a nanopore. (h) Gold can be electrochemically deposited on the carbon nanoelectrode and functionalised with a thiolated species for use as a gate to modulate single-molecule DNA translocation from a nanopore.[32] (i) In a similar way, the gate is also fabricated by electropolymerisation of pyrrole, and artificial receptors embedded within the polymeric film for selective single-molecule sensing of targeted analytes.[35] 43

Figure 1- 7: Thesis outline in terms of the fabricating workflow of nanopore FETs based on dual-barrel nanopipettes. One barrel is selectively filled with carbon via pyrolysis of butane while another barrel remains empty, forming a carbon nanoelectrode and an open nanopore at the tip. Gold can be deposited on the surface of carbon nanoelectrode and shrinks down the nanopore by a feedback-controlled mechanism. The gold-deposited devices are functionalised by two different types of thiolated species. (d) Small organic molecules can be used to switch the surface charge of a nanopore, controlling single-molecule transport using a chemically modified nanopore-FET. (e) Thiolated oligonucleotides can be encoded onto the surface of gold to enhance the selectivity towards different targeted analytes such as proteins and small molecules. 46

Figure 2-1: Schematic demonstration of laser-assisted pulling processes. (a) Overview of a P-2000 laser puller (Sutter Instruments, USA). (b) After laser-assisted pulling, a pair of nanopipettes were fabricated. Details of the two-line laser pulling protocol: In the first line, (c) the laser beam locally heats the centre of a theta quartz capillary and then deactivates, followed by pulling on both ends to produce (d) a taper in the middle. (e) The second line generates additional heat which melts the taper, and a hard pull results in a pair of dual-barrel nanopipettes. 56

Figure 2-2: Pyrolysis of butane. (a) Schematic illustration of the experimental set-up for pyrolytic deposition of carbon. Butane was passed through one barrel via silicon tubing while the other barrel of the nanopipette was sealed. A butane torch was used to heat the tip of the pipette for pyrolytic deposition of carbon under argon flow to prevent further oxidation of the deposited carbon. A heating time of 35 s was chosen to produce an extensive filament of amorphous carbon through one barrel while leaving the other barrel open. (b) Bright-field micrographs show a change in contrast between a dual-barrel nanopipette before (left) and after (middle) carbon deposition and an SEM image (right) of a dual-barrel nanopipette before carbon deposition. (c) Photo of the set-up for pyrolytic deposition of carbon. The flowrates of argon and butane were monitored by the two flow meters labelled in the photo. The dual-barrel nanopipette was mounted on the holder first and moved inside the argon tubing to prepare for carbon deposition. (d) Schematic visualisation of the electrical contact in a dual-barrel nanopipette with one barrel filled with carbon. The deposited carbon extends up to ~60% of the length of the nanopipette barrel. However, only the section at the taper of the nanopipette is extensively filled with carbon. The pyrolytic carbon is mostly deposited on the inner walls of the barrel to form a carbon layer. A copper wire was inserted into the carbon barrel so that it is embedded into the bottom section just above the taper directly contacting the deposited carbon. 57

Figure 2-3: Schematic of the electrochemical set-up of feedback-controlled gold deposition. Two working electrodes (WEs) were placed in the carbon barrel and the open barrel, filled with the appropriate supporting electrolyte, with a quasi-reference counter electrode (QRCE) in the plating bath. A reducing potential was held at the first WE. Importantly, a potential difference of -0.1 V between the second WE and QRCE was used as feedback. 59

Figure 2-4: User interface for the nanopore app when loading the raw data from Clampfit. After loading the raw data as an ABF file from Clampfit, the output was generated as applied voltage across the nanopore and the resulting ionic current. 64
Figure 2-5: Baseline fitting using the Nanopore App. The current trace was flipped and then fitted by a Gaussian distribution function, with adjustable steps and two different polynomial factors. This was followed by defining a standard deviation relative to the fitted baseline. Determining the standard deviation was aided by fitting all points on the histogram of the current trace with a Gaussian function. In this case, three different peaks were found, which correspond to the baseline noise and folded and unfolded single-molecule DNA translocations. Therefore, the standard deviation was set to detect all translocation peaks correctly by placing it between the boundary of the baseline current and the unfolded translocation peaks. 65
Figure 2-6: Single-molecule detection of 10 kbp DNA using nanopipettes, with the patch electrode (working) in the pipette and the bath electrode (reference/ground) in the KCl bath (100 mM KCl, 10 mM Tris and 1 mM EDTA at pH 8) and 400 pM of 10 kbp DNA added in the nanopipette. (a) Under negative potential, single-molecule translocation of DNA happens from inside the nanopipette to the KCl bulk solution. The representative current traces are shown from -300 to -700 mV. (b) From the single-molecule statistics extracted and accumulated by the nanopore app, the distribution of dwell time, equivalent charge and blockade current at -400 mV is summarised in the histograms. (c) A 2D heat map demonstrates the distribution of the blockade current versus dwell time. (d) The stochastic nature of single-molecule DNA translocation was confirmed by the exponential fitting of the interevent time, obtaining a 5.94 s^{-1} capture rate. The utility of nanopipettes for single-molecule detection of 10 kbp DNA was established by the voltage dependence of (e) dwell time, (f) blockade current and (g) capture rate. As the single-molecule translocation becomes faster, there is a larger current modulation resulting in more events being captured. 66

Figure 3-1: Schematic demonstration of electrodeposition. A reducing potential is applied to the substrate. (a) The hydrated metal ions migrate from the bulk electrolyte into the electrical double layer and absorb onto the surface of the electrode with a partial detachment of the hydration layer. (b) Electron transfer from the substrate onto the absorbed metal ions occurs to reduce the metal cations with a positive valency to a zero valency. This process is repeated

to form the seed on the surface of the electrode (i.e. nucleation). (c) The deposition of metal can be accelerated based on the nucleated metal deposit, which increases the active electrode area. 73

Figure 3-2: Schematic demonstration of cyclic voltammetry. (a) The potential is swept between the anodic potential (E_a) and cathodic potential (E_c) at a constant scan rate. (b) The resulting voltammogram shows peaks in the positive and negative scan directions, corresponding to oxidation and reduction of the electroactive species, respectively. For a reversible electrochemical process, the middle point of the two redox peaks is the equilibrium potential. In both figures, black arrow indicates the initial scan direction. 74

Figure 3-3: Schematic demonstration of chronoamperometry. A constant potential of E_0 is held at the electrode until the start of the experiment at time t_0. The voltage is switched to a constant value (E_c) and held constant over time. The typical response of the chronoamperometric current is not listed in this figure as it depends on multiple parameters. 75

Figure 3-4: Comparison between (a) cyclic voltammetry and (b) chronoamperometry for electrodeposition of gold using 10-fold diluted ECF64 plating solution. (a) Cyclic voltammetry was performed with a scan rate of 0.02 V/s. The first set of CVs exhibited a small increase in electrochemical current and deposition peaks, meaning that gold is only minimally reduced from the plating solution. To investigate the precise location of the gold reduction peak on the carbon nanoelectrode, the resulting electrode was held at -0.7 V for 200 s to stimulate the nucleation of gold. The second set of CVs revealed a significant reduction peak at around -0.73 V. (b) Amperometric deposition of gold at a constant potential of -0.73 V exhibited an initial deposition current at roughly 0.01 nA for the first 100 s. This was followed by a gradual increase with the slope becoming steeper over time, indicating faster deposition. A carbon nanoelectrode was used as the working electrode, with a quasi-reference counter electrode in the plating solution..... 78

Figure 3-5: Representative examples for the feedback-controlled deposition of gold. Gold deposition was simultaneously performed using a bipotentiostatic configuration with two working electrodes inside the carbon barrel and the open barrel, respectively, where $V_{depositon}$ = -0.73 V and $V_{feedback}$ = -0.1 V. The deposition current exhibited no significant difference compared with experiments that did not incorporate the feedback (Figure 3-4). The feedback current remained roughly constant and then decreased rapidly. As the ionic current flowing

through the open barrel is a function of pore conductance, the sharp decrease in feedback current undoubtedly suggests rapid pore shrinking within this sharp transition regime..... 79
Figure 3-6: Examples demonstrating the reproducibility of the sharp decrease of feedback current. Although the time taken to reach the sharp transition varies for different pipettes, the sharp decrease of feedback current is reproducible. As a result, precise tailoring of nanopore conductance is feasible by terminating deposition processes at different currents. The data were obtained from 3 independent nanopores. 81
Figure 3-7: Controlling nanopore conductance by feedback-controlled deposition of gold. I-Vs for carbon-only nanopipettes and gold-deposited pipettes with a threshold feedback current of (a) -1.5 nA, (b) -1.0 nA and (c) -0.5 nA. (d) Detailed histograms show a large device-to-device variation (17.3 ± 6.4 nS) before gold deposition. However, the nanopore conductance was precisely tailored after feedback-controlled deposition (7.2 ± 1.4 nS for $I_{threshold}$ = -1.5 nA, 3.5 ± 1.9 nS for $I_{threshold}$ = -1.0 nA, 2.0 ± 0.4 nS for $I_{threshold}$ = -1.5 nA). The data were obtained from 90 independent nanopores. 82
Figure 3-8: Characterisation of the electrochemically active area using the redox probe for carbon-only and gold-deposited devices. The electrochemistry is based on the cathodic polarisation of either (a) the carbon nanoelectrode or (b) the gold-deposited electrode. As a result, Ru^{3+} is reduced to $Ru^{2+,}$ giving rise to diffusion-limited currents, which are indicative of an electrochemically active area. 83
Figure 3-9: Characterisation of deposited gold using dark-field microscopy. Dark-field images taken at (a) 700 s, (b) 1000 s, (c) 2000 s and (d) 3000 s during the deposition process show the gradual expansion of a gold blob. The data were obtained from 4 independent nanopores. 84
Figure 3-10: SEM and TEM characterisation of nanopore-FET devices. (a) Schematic illustrating the device configuration of gold deposited nanopipettes. (b) An SEM image of the top view shows the pore closure from the feedback-controlled deposition of gold and is confirmed by TEM images (c-d) showing the accurate deposition of gold at the tip. SEM and TEM were obtained from two independent nanopores..... 85

Figure 4-1: Validation of single-molecule functionality for the nanopore-FET devices. Representative It traces and individual translocation events recorded at the nanopore channel before (a,b) and after (c,d) feedback-controlled deposition of gold, showing a slight increase in

dwell time from (ei) 0.13 ± 0.06 ms to (eii) 0.35 ± 0.17 ms, a significant increase in peak current from (fi) 149 ± 25 pA to (fii) 510 ± 252 pA, and a reduction of capture rate from 17 ± 3 s^{-1} to 7 ± 1 s^{-1} . This was attributed to the smaller opening of the gold-coated nanopore, which induced enhanced interactions between DNA and the nanopore surface. Vpore = −700 mV, Vgate = 0 mV. 10 kbp DNA was added in the nanopipette and translocation occurred from in to out. . 93

Figure 4-2: Voltage gating of the nanopore, (a,b) I-V characterisation of the nanopore-FET before and after gold deposition, and (c,d) after gold deposition at varying V_{gate}. 95

Figure 4-3: Voltage gating of DNA translocation. (a) The variation of nanopore surface charge with gating potentials (V_{gate}) was probed by differential capacitance measurements on an ultramicron gold-deposited electrode, showing a capacitance minimum at −100 mV, which was attributed to the potential of zero charge (pzc). (b) This correlates well with the gating of 10 kbp DNA in 100 mM KCl, 10 mM Tris-HCl and 1 mM EDTA buffer at pH 8. DNA transport could be switched off or turned on depending on whether the potential applied to V_{gate} was above or below the pzc. By controlling the gate potential, translocations could be switched on and off in real time as shown in (c). Vpore = −700 mV. 10 kbp DNA was added in the nanopipette and translocation occurred from in to out..... 96

Figure 4-4: Surface functionalisation of gold-deposited nanopores with (a) 1-dodecanethiol and (b) 5-amino-2-mercaptobenzimidazole. For each case, (c,d) successful functionalisation was seen from the consecutive change of I-V with respect to the fabrication workflow of nanopore-FET devices. Electrolyte: 52 mM $(NH_4)_2SO_3$. This was further confirmed by (e) the suppression of the electrochemically active area for the gold gate functionalised by 1-dodecanethiol, the electrochemical characterisation was performed with 1 mM $Ru(NH_3)_6Cl_3$ in 100 mM KCl. (f) The inversion of I-V from negative rectification to positive rectification for gold gate functionalised by 5-amino-2-mercaptobenzimidazole in 100 mM KCl. The data were obtained from the measurements of 4 independent nanopores. 99

Figure 4-5: Fabrication process of the nanopore-FET device, starting from (a) unmodified (carbon only) pipettes, to (b) gold modified pipettes, and then (c) functionalised pipettes, with the corresponding (i) I-V characterisation after each stage of fabrication. Conductance values in 100 mM KCl were 8.13 ± 0.43 nS before deposition, 3.79 ± 0.30 nS after deposition, and 1.00 ± 0.15 nS after functionalisation. Considering the change of the nanopore surface charge after amine functionalisation, the I-V response across the nanopore revealed a significant change, from negative to positive rectification by tuning the pH from 8 to 4 in 10 mM KCl (inset, ciii).

(ii) Ion selectivity measurements across nanopores after each stage of fabrication by using current-clamp mode of a Multiclapm 700B amplifier. Potential–current (Iclamp) measurements for nanopore-FET devices (a) before deposition, (b) after deposition and (c) after functionalisation at different KCl concentration gradients. The concentration of KCl was only diluted by DI water outside of the nanopore to 75 mM, 50 mM, 25 mM, 2.5 mM, while the inside remained the same (100 mM KCl, 10 mM Tris-HCl and 1 mM EDTA buffer at pH 8). (iii) The potential at which the current is set to zero is represented as the reversal potential (E_{rev}). Before deposition, the nanopores exhibited cationic selectivity, indicated by (aiii) more negative reversal potentials as the concentration of the trans side was diluted. (biii) After deposition, the reversal potentials became less negative due to the reduction of surface charge. (ciii) The appearance of more positive reversal potentials after amine functionalisation indicated more positive nanopore surface charge. Ion-selectivity measurements showed a gradual tuning of nanopore surface charge. In all cases, the gate electrode was left floating. Potentials quoted here are relative to Ag/AgCl reference electrode in KCl bath. 101

Figure 4-6: Electrochemical characterisation of an amine-modified gate. (a) Cyclic voltammetry from −0.4 to 0.4 V showed minimal faradaic currents within the range of V_{gate}, scan rate = 0.2 V/s. (b) Differential capacitance measurements of an amine-modified electrode showed a secondary capacitance minimum at 0.15 V. Effective charge tuning at the electrode-electrolyte interface was obtained for the functionalised system, as seen from the pronounced change of capacitance at both sides of the pzc; Using an amine-functionalised nanopore-FET, (c) I-t traces recorded from the amine functionalised gate showed that the magnitude of current remained at 0 pA, indicating that was unlikely that Faradaic processes took place on the functionalised gate electrode in the potential window V_{gate} = -400 to V_{gate} = 400 mV. All characterisation was performed in 100 mM KCl, 10 mM Tris-HCl and 1 mM EDTA buffer at pH 8. 103

Figure 4-7: Voltage gating of an amine-modified nanopore-FET. Voltage gating was achieved via a stepwise increase of V_{gate} from −400 mV to 400 mV at 200 mV intervals. (a) Current–time traces showing the gating control of 10 kbp DNA translocation at an applied V_{gate} of −400 mV, −200 mV, 0 mV, 200 mV, and 400 mV. (b) The dependence on (i) dwell time, (ii) equivalent area, and (iii) event frequency is shown as a function of the gating potentials. All data were expressed as percentage change with respect to V_{gate} = 0 mV, and in all cases, V_{pore} = −500 mV. 10 kbp DNA was added in the nanopipette and translocation occurred from in to out. 104

Figure 4-8: Supplementary traces of 10 kbp DNA confirming the reproducibility of voltage gating with amine-functionalised nanopore-FETs. V_{pore} = −500 mV. V_{gate} was tuned between −400 and 400 mV. 10 kbp DNA was added in the nanopipette and translocation occurred from in to out. 105

Figure 5-1: The schematic design of aptamer-functionalised nanopore bio-transistors, feedback-controlled fabrication and single-molecule detection of targeted analytes. (a) One barrel was selectively filled with carbon while another barrel (nanopore) was left open. Gold was electrochemically deposited onto carbon. The aptamers were functionalised onto the gold via thiol self-assembly. (b) The schematic design of the nanopore bio-transistor surface chemistry. It includes the sequence information of the aptamers for proteins and neurotransmitters, and the binding mode between the targeted analyte and aptamers. For protein detection, a 15-mer thrombin binding aptamer was used, as the binding occurs between a G-quadruplex and thrombin. In contrast, for neurotransmitters, the stem-loop aptamer binds to the neurotransmitter via target-induced conformational changes, and the aptamers switch from a duplex to a G-quadruplex conformation upon analyte binding. (c) The feedback-controlled fabrication of nanopore bio-transistors. The electrochemical deposition of gold was performed using a bipotentiostatic configuration, where a reducing potential of -0.73 V was held at the carbon nanoelectrode. The deposition process was monitored by a real-time ionic current flowing through the open barrel due to the potential difference of -0.1 V between the second working electrode and a combined counter/reference electrode in the bath. The gold deposition was stopped at the specific threshold current of -1.5 nA. The gold-deposited device was functionalised by thiolated aptamers. The whole process was monitored by the consecutive change of IV (52 mM $(NH_4)_2SO_3$), as well as the change of the active electrochemical area in the presence of 1 mM $Ru(NH_3)_6Cl_3$. The representative current traces showed the single-molecule translocation of dopamine across (d) gold deposited devices, (e) scrambled sequence functionalised devices and (f) aptamer-functionalised devices. Dopamine was added in the bath. 114

Figure 5-2: The characterisation for the fabrication of nanopore bio-transistors. The process starts with a (i) carbon only device, to form a (ii) gold deposited device via the feedback-controlled deposition of gold, and an (iii) aptamer-functionalised device produced from the

surface functionalisation of deposited gold by the thiolated aptamers. To verify the successful fabrication at each step, with (a) I-V measurements demonstrating the consecutive shrinking of nanopore conductance, the inset illustrates the electrochemical measurements for the active surface area for the carbon nanoelectrode, gold deposited electrode and the aptamer-functionalised electrode. The active surface area was increased after the gold deposition and then decreased after aptamer functionalisation, as seen from the steady-state diffusing limiting current in the presence of 1 mM $Ru(NH_3)_6Cl_3$ upon cathodic polarisation from 0 mV to -400 mV. The whole process was further confirmed by (b), (c) ion-selectivity measurements. The salt concentration on the trans chamber was diluted, while the cis chamber remained unchanged. At each concentration gradient, a reversal potential (E_{rev}) was measured. After the gold deposition, Erev appeared to be more positive, which indicated the reduction of surface charge from a carbon/quartz nanopore to a gold nanopore. Aptamer-functionalized nanopore exhibited a more negative reversal potential compared to the gold deposited device due to the attachment of negatively charged oligonucleotides on the surface. In all cases, the electrolyte in the cis chamber was 100 mM KCl, 10 mM Tris and 1 mM EDTA at pH 8. The concentration of the trans chamber (KCl bath) was varied by serial dilution. Cis means in the nanopipette and trans means the KCl bath..... 117

Figure 5-3: Power spectrum density (PSD) for nanopores that are functionalised by different aptamers for (a) thrombin, (b) dopamine, (c) serotonin and (d) acetylcholine, before and after adding the targeted analytes. For all cases, the noise spectra mainly differ in the low-frequency regime (f<100 Hz). In this regime, the power spectra showed 1/f dependence. The specific binding between the aptamer and targeted analyte caused more dynamic fluctuations of thiol-modified oligonucleotides inside the pore. All PSDs were obtained by analysing 10 s current traces for each case. The current traces were low-pass filtered at 30 kHz and sampled at 250 kHz. The red dotted lines represent the linear fitting of PSD at a low-frequency regime. V_{pore} = -500 mV in all cases. The data were obtained from 8 independent nanopores. Analytes were added into the bath..... 119

Figure 5-4: The single-molecule detection of thrombin using nanopores functionalised by (a) random sequence and (b) aptamer sequence. Using nanopores functionalised by a random sequence, the translocation of thrombin produced current blockade, whereas, for the aptamer-functionalised nanopore, current enhancement was observed. (c) The specific interactions between the aptamer and thrombin caused a higher peak current and a longer

dwell time than the nanopore functionalised by a random sequence. For aptamer-functionalised nanopore, a cut down of peak current was observed for a certain threshold as a result of the binding between aptamer and thrombin. This was further revealed by the voltage dependence of the (d) dwell time, (e) peak amplitude and (f) capture rate. The 1 nM thrombin was added inside the pipette and the translocation occurred from in to out. 120

Figure 5-5: The selective single-molecule detection of thrombin using aptamer-functionalised nanopore bio-transistors. (a) The current-time traces showing the voltage dependence of single-molecule thrombin detection from (i) Vpore =-400 mV to (iv) Vpore =-700 mV. (b) A scattered diagram demonstrating the distribution of the blockade current and binding time at different voltages. (c) A unique characteristic for the translocation of thrombin through aptamer-functionalised devices is the appearance of long tails, and (d) subsequent exponential fitting of the decay gives the distribution of decay constant, which increases linearly with applied voltage. (e) The binding time (τ_{off}, dwell time) decreases exponentially with voltage, and the (f) off rate ($k_{on,}$ capture rate) increases exponentially with voltage. A semi-log plot of the binding time and off rate resulted in a linear trend with increasing V_{pore}. Thrombin was added inside the pipette at 1 nM and the translocation occurred from in to out. Error bars represent the standard deviation of 3 independent measurements..... 121

Figure 5-6: The gating of binding affinity and protein transport in an aptamer-functionalised nanopore. (a) Schematic showing that the transistor configuration carbon/gold/aptamer barrel was used as a gate to modulate single-molecule protein translocation. (b) By tuning Vgate from -400 to 400 mV, the regulation of ionic transport across the nanopore was verified by nanopore I-V collected at different gating potentials. From a single-molecule protein translocation study, (c) the dwell time (τ_{off}) was found to increase as Vgate became more positive, (d) while the blockade current increased as well. (d) This is shown as current–time traces, which demonstrates the gating of single-molecule transport of 1 nM thrombin. Vpore = -400 mV for all cases. Thrombin was added inside the pipette at 1 nM and the translocation occurred from in to out..... 123

Figure 5-7: More examples of the voltage gating of thrombin from Vgate = - 400 mV to Vgate = 400 mV. Positive Vgate increased the binding time, enhanced the signal-to-noise ratio and slowed the decay for the translocation tails. Vpore = -400 mV for all cases. The experiments were performed in 100 mM KCl, 10 mM Tris and 1 mM EDTA at pH 8. Thrombin was added inside the pipette at 1 nM and the translocation occurred from in to out. 124

Figure 5-8: I-V characterisation of (a) quartz, (b) carbon only and (c) gold devices against analyte concentration. From the experimental results of quartz and carbon/quartz nanopores, the addition of positively charged analytes, such as dopamine, caused negligible effects on the (i) I-V, (ii) conductance and (iii) rectification ratios. Therefore, the interactions between dopamine and carbon or negatively charged quartz surfaces caused almost no effect on the nanopore I-V characteristics. The nanopore conductance was obtained by a linear fitting from -50 to 50 mV. The experiments were performed in 100 mM KCl, 10 mM Tris and 1 mM EDTA at pH 8. Error bars indicate the standard deviation of 3 independent measurements. Dopamine was added in the bath. 126

Figure 5-9: I-V characterization of aptamer-functionalised devices against analyte concentration for (a) dopamine, (b) serotonin and (c) acetylcholine. For aptamer-functionalised devices, adding targeted analytes caused a change in the (i) I-V characteristics due to the specific binding. (ii) The conductance decreased with increasing concentration for both dopamine and serotonin aptamer-functionalised devices as a result of forming more G-quadruplexes. Note that the increase of I-V conductance with concentration is consistent with the current enhancement that was obtained for the single-molecule translocation of dopamine and serotonin that was achieved using functionalised nanopore. (iii) The rectification ratios (I_{-500mV}/I_{500mV}) decreased as more positively charged analytes bound with the corresponding aptamer. The sigmodal dependence of acetylcholine is caused by the use of less sensitive aptamers compared to dopamine and serotonin cases where aptamers are responsive down to fM. The targeted analytes were only added to the KCl bath. The nanopore conductance was obtained by a linear fitting from -50 to 50 mV. The experiments were performed in 100 mM KCl, 10 mM Tris and 1 mM EDTA at pH 8. Error bars indicate the standard deviation of three independent measurements. Dopamine was added in the bath. 127

Figure 5-10: The representative current traces for the translocation of dopamine across nanopores functionalised by the scrambled sequence of dopamine aptamer. No distinguishable current modulations were observed. The experiments were conducted at 100 mM KCl, 10 mM Tris and 1 mM EDTA at pH 8. Vpore= -400 mV for all concentrations. The experiments were verified by five independent nanopores functionalised with scrambled sequence of dopamine aptamer. Different concentrations of dopamine were added to the bath and any possible translocations are supposed to occur from out to in. 130

Figure 5-11: Single-molecule detection of dopamine using an aptamer-functionalised nanopore. (a) Single-molecule translocation of (b) dopamine occurred from the electrolyte bath to a nanopore functionalised by (c) dopamine aptamers under a negative V_{pore}, (d) voltage-dependent current–time traces. This illustrates the specific interactions between the stem-loop aptamers and dopamine, as suggested by the contrast between the grey (0 pM dopamine) and black (10 pM dopamine) current traces from the same device. The voltage-dependent results and detailed distribution of the (e) dwell time (dissociation time, τ_{off}), (f) blockade current and (g) on rate (capture rate, k_{on}) with increasing Vpore from -300 to -700 mV. Dopamine was added in the KCl bath, error bars indicate the standard deviation of 3 independent measurements. 131

Figure 5-12: The representative current-traces for serotonin showing the shape of the translocation peaks. In most cases, the translocation events were predominately seen as a single and rectangular peak, which suggests that each translocation event was caused by an interaction with one receptor, as multiple receptors are able to cause the inter-transfer of the targeted analyte between different ligands in the nanopore sensing region. The concentration of serotonin is 10 fM added into the KCl bath, and the translocation occurred from bath to tip, Vpore = -500 mV. 133

Figure 5-13: The hybridisation of the complementary strand to the nanopore functionalised by the serotonin aptamer. (a) The change of I-V demonstrated the formation of hybridised double-stranded DNA inside the nanopore. (b) The rectification $I-500mVI500\ mV$ changed from negative rectification to almost no rectification, and finally, a slightly positive rectification. The decrease of the rectification ratio can be attributed to the formation of ds-DNA in a nanopore, which shifts the negative charge of the attached oligonucleotides away from the surface. Interestingly, the rectification ratios became slightly less than one (i.e. positive rectification) at a 500 fM and 5 pM concentration of the complementary strand. A gold nanopore is expected to have a negative rectification due to the surface absorption of chloride anions. For the functionalised nanopore system, the linear and extended ds-DNA suppresses the chloride absorption. Therefore, it exposes more bare gold surface, which is weakly positively charged[25,48] and causes a positive rectification. (c) The real-time current traces recorded from the same device at different concentrations of the complementary strand. A current blockade was observed that is consistent with the change of I-V. Note that the blockade current is independent of the concentration. Vpore = 600 mV. The translocation of the

negatively charged complementary strand occurred from out to in. The complementary strand of serotonin aptamer was added into the KCl bath..... 133

Figure 5-14: The single-molecule sensing of neurotransmitters at fM concentration, and the capability of aptamer-functionalised nanopore bio-transistors to detect non-redox-active neurotransmitters. The single-molecule detection of serotonin at fM level was illustrated by the example of (a) serotonin, while the detection of non-redox-active neurotransmitters was demonstrated by (b) acetylcholine. For both cases, the single-molecule detection was performed via a voltage dependence of (i) dwell time (τ_{off}) and (ii) capture rate (k_{on}), with (iii) scattered diagrams to demonstrate the distribution of the blockade current and binding time at Vpore = -500 mV, and (iv) exponential distribution of interevent time (τ_{on}) demonstrating the single-molecule nature of translocation signals. Serotonin and acetylcholine were added into the KCl bath in all cases. Error bars represent the standard deivation from 3 independent measurements. 135

Figure 5-15: Further details of the calculation of K_D from single-molecule translocation data. The voltage dependence of the dwell time (τ_{off}) and capture rate (k_{on}) was extrapolated to discover the values at which no voltage wasapplied to calculate the K_d and compare it with the literature values. 136

Figure 5-16: The correlation between the concentration dependence of nanopore conductance and the single-molecule translocation of serotonin. Increasing the concentration of serotonin caused the transition from the current enhancement to the current blockade. Within the range where the nanopore conductance increased with concentration, the current enhancement was obtained, whereas the current blockade appeared after the plateau was reached. Vpore = -400 mV and the concentration of serotonin was varied in the KCl bath in all cases. Serotonin was added into the KCl bath. 137

Figure 5-17: The selective electrochemical response for the gate electrodes of aptamer-functionalised nanopore bio-transistors. The electrochemical response from (a) carbon nanoelectrode, (b) gold deposited gate, (c) gold gate functionalised by the scrambled sequence of dopamine aptamer and (d) gold gate functionalised by dopamine aptamer. The aptamer functionalised gate generated the most significant electrochemical response. Dopamine was added into the KCl bath. 140

Figure 6-1: Summary of key conclusions and future work based on hybrid nanopore bio-transistors developed in this thesis. Overall, conclusions can be drawn from two different components of the device. (a) For aptamer-functionalised nanopores, the single-molecule detection of neurotransmitters was achieved via the target-induced conformational changes of aptamers functionalised onto the surface of gold. (b) By using aptamers with sufficiently high affinity with the targets, fM sensitivity can be attained. More importantly, the binding kinetics and thermodynamics can be extracted from resistive pulse-sensing methods and correlated with bulk measurements, confirming the robustness of the approach. (c) The strategy proposed in this thesis has implications on the detection of short fragments of nucleic acids via the base-pairing interactions between the target and the complementary strand, suggesting a novel way of detecting important potential biomarkers such as miRNAs. (d) To truly take advantage of this platform, the electrochemistry of the aptamer-functionalised gate was incorporated with a significantly broader dynamic range, up to hundreds of micron molar, from the oxidation of redox-active neurotransmitters. To summarise, a range of detection methods were integrated into this sensing platform, with different dynamic ranges from fM to μM. Promising applications regarding in-vivo detection of neuron activities can be expected. 147

List of schemes

Scheme 2-1: Surface functionalisation of deposited gold. Thiolated small molecules can be attached to the gold surface. Methanol was used as the solvent as it solubilises most organic molecules and simultaneously encourages the wetting of the nanopore surface. Modification with thiolated oligos was performed in DI water because it fully wets the nanopore and solubilises thiol-modified oligos. 60

Scheme 2-2: Deprotection of disulfide bonds using TCEP. Thiol-modified oligos protected with a C6 S-S modifier were treated with 100-fold molar excess of TCEP to form reactive-thiol oligos that can be attached to the surface of gold through thiol-gold self-assembly. The surface of the gold was modified by the oligonucleotide with a C6 spacer linked in between. 62

Scheme 2-3: Electrochemical reactions on the surface of Ag/AgCl electrodes. 63

Scheme 3-1: Electrochemical deposition of gold using ECF64 plating solution containing gold sulphite. The deposition mechanism proceeds via absorption of the gold (I) complex followed by electron transfer to reduce the absorbed gold (I). 77

Scheme 5-1: The electrochemical oxidation of dopamine oxidising phenol groups into ketones and releasing protons. 139

List of tables

Table 2-1: Detailed settings for the protocol for pulling dual-barrel nanopipettes. The first line results in a taper in the middle of the capillary, and the second line produces a pair of nanopipettes. 57

Table 5-1: List of DNA oligonucleotide sequences that are used in this work. All sequences were written in the form from 5' end to 3' end. For thiol-modified DNA oligonucleotides, the oligos were synthesised with an S-trityl-6-mercaptohexyl derivative protecting group. 100 times the excess amount of TCEP (tris (2-carboxyethyl) phosphine) was used to cleave the disulphide bond and form the reactive thiol-modified oligos. The thiol group was separated from the oligo with a C6 spacer arm. 116

Table 5-2: The summary of the experimental and literature evidence of the structural switching of aptamers and its relation to I-V and translocation studies. The aptamers switched from a duplex conformation to either a parallel or anti-parallel G-quadruplex, which becomes more compressed upon binding with dopamine or serotonin. This created a knock-on effect on the concentration dependence of nanopore conductance, which increased with more targets being bound, and therefore, more G-quadruplex formations. The rectification decreased due to more binding between the positively charged analytes and the aptamer. This was further reflected in the results of the single-molecule translocation experiments where current enhancement was observed. 136

Abbreviations

bp	Base pair
CV	Cyclic voltammetry
DNA	Deoxyribonucleic acid
ds	Double-stranded
EDTA	Ethylenediaminetetraacetic acid
Erev	Reversal potential
FET	Field-effect transistor
FraC	Fragaceatoxin C
I.D.	Inner diameter
I-t	Current-time
I-V	Current-voltage
LSV	Linear sweep voltammetry
MspA	Mycobacterium smegmatis porin A
O.D.	Outer diameter
PCR	Polymerase chain reaction
pzc	Potential of zero charge
QRCE	Quasi reference-counter electrode
RE	Reference electrode
SAM	Self-assembled monolayer
SECM	Scanning electrochemical microscopy
SELEX	Systematic evolution of ligands by exponential enrichment
SEM	Scanning electron microscopy
SICM	Scanning ion-conductance microscopy
TCEP	Tris(2-carboxyethyl)phosphine
TEM	Transmission electron microscopy
Tris	Tris(hydroxymethyl)aminomethane
WE	Working electrode

Chapter 1

Introduction

Contents

Abstract 30
1.1 Biosensing and healthcare 31
1.2 Single-molecule detection 32
1.3 Single-molecule detection using nanopores 33
1.3.1 Single-molecule electrical detection using patch-clamp technologies 33
1.3.2 Nanopore sensing 34
1.3.2.1 Overview 34
1.3.2.2 Nanopore sensing – working principle 36
1.3.2.3 Biological nanopores 38
1.3.2.4 Solid-state nanopores 38
1.3.2.5 Nanopipettes 39
1.3.2.6 From protein pores to hybrid pores 39
1.3.2.7 Chemical modifications for selective sensing 40
1.3.2.8 Sensor multiplexing 42
1.3.2.9 Alternative detection strategies 43
1.3.2.10 Nanopore field-effect transistors 44
1.4 Thesis outline 46
1.5 References 48

Abstract

This chapter outlines the importance of biosensing and healthcare, and more importantly, how the development of biosensors is fuelled by single-molecule detection, which has the ultimate in sensitivity. Among the different single-molecule methods developed to date, nanopore-based sensing represents one of the more promising methods, mainly due to its label-free operation. Pore-forming proteins, silicon and quartz can be used to assemble nanopores with unique chemical and physical properties. A special focus is made on nanopipettes as compared with biological nanopores and solid-state nanopores as a result of easy and low-cost fabrication via laser pulling. In addition to the materials aspect, the grand challenges of biosensing using nanopores are also presented. In this thesis, perhaps two of the most important of these, controlling molecular transport and enhancing selectivity, are addressed by proposing a novel strategy to incorporate nanopipette nanopores with chemical modification and field-effect transistors.

1.1 Biosensing and healthcare

Detecting and analysing the key building blocks of life, such as nucleic acids, proteins and neurotransmitters, has been a core driving force for the innovation of biosensors. Essentially, sensing biomolecules has crucial implications for healthcare, specifically, the early diagnosis of diseases, sequencing information on the human genome, uncovering molecular activities in neuron networks, and improving our understanding of the mechanisms of different biological systems.

To date, an innovative range of biosensing techniques has been developed to fulfil the aims outlined above. Along with advancements in biological chemistry, surface modification, molecular recognition, molecular spectroscopy, signal recording and processing, and even data science and deep learning, biosensing techniques are rapidly advancing – conventional methods include polymerase chain reaction and enzyme-linked immunosorbent assay. Indeed, these have formed the basis of most biosensing techniques and although their robustness and usability have been proved by the number of applications and amount of investment, the requirement for more time-efficient, cost-effective, sensitive and selective biosensing techniques has driven the continuous evolvement of novel methods and applications in this field.[1–3]

Outside of pure scientific research, the development of materials processing and assembly techniques, such as lithography, has also boosted the miniaturisation of sensor components and 'lab-on-a-chip' applications.[4,5] Moreover, the use of miniaturised components and chips greatly facilitates the commercialisation of biosensing techniques, with some established examples from PacBio,[6] Oxford Nanopores[7] and Illumina.[8]

1.2 Single-molecule detection

As stated in Section 1.1, the miniaturisation of sensor components is on the right course for aiding the biosensing evolution. The ultimate one can achieve is to reduce the dimensions of a sensor to the scale of the biological components, to attain the detection of single molecules. This idea was first mentioned by Richard Feynman in his landmark talk in 1959, with the claim that '*there is plenty of room at the bottom*'.[9] Since then, there has been a significant drive to optimise further or develop conventional sensing techniques such as fluorescent spectroscopy, [10,11] surface-enhanced Raman spectroscopy[12] and atomic force spectroscopy[13,14] to a single-molecule level. In 2014, Eric Bertzig, Stefan W. Hell and William E. Moerner were awarded the Nobel Prize in Chemistry based on their work to develop super-resolved fluorescent spectroscopy for sensing single molecules, originating from one of the first breakthroughs of the optical detection of a single molecule inside a solid crystal.[15]

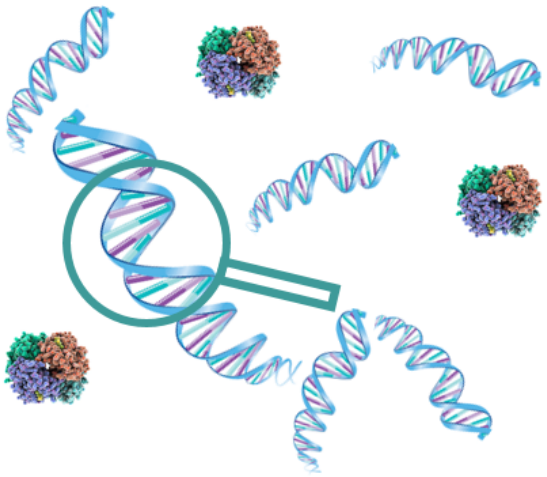


Figure 1-1: Conceptual illustration of ensemble-averaged detection techniques vs single-molecule methods. Compared with conventional biosensing technologies such as enzyme-linked immunosorbent assay, which produced time-averaged properties, single-molecule methods can detect properties and interactions between each molecule by decreasing the sensing volume to a scale comparable with single biomolecules. This results in the highest levels of sensitivity and opens up the possibility of revealing the properties of single molecules that are normally masked by conventional, ensemble-averaged properties.

While the majority of conventional experimental techniques yield time-averaged population-based information, single-molecule measurements allow us to investigate, with resolved

structural and spatial dynamics, how individual members of a molecular population behave and interact. The challenges associated with probing a single molecule, or the equivalent of 1.66 yoctomole, necessitate sensitive methods that amplify measurement signal, either a photon flux emitted from a single dye, or, in the case of traditional nanopore sensors, a residual ion flux passing through a molecule as it transiently occludes the pore void volume.[1,2] Typically, a small concentration is needed to capture the analytes of interest, and a low detection volume is required to isolate a single analyte from the background. In most cases, a low-abundance analyte is extracted from the background and measured in the detection volume. This is especially salient for improving our understanding of the interactions between individual biomolecules and has implications for providing answers to complicated questions regarding biological systems.[4,16]

1.3 Single-molecule detection using nanopores

1.3.1 Single-molecule electrical detection using patch-clamp technologies

Single-molecule electrical methods are predominant in the study of biological molecules and processes in solution because of their label-free feature.[1,2,17,18] The idea can be traced back to the 1950s, when the concept of the Coulter Counter was introduced based on counting charged particles in a solution, passing through a small aperture one by one under an applied potential.[19] Later on, in the 1970s, this sensing principle was introduced to biological systems with patch-clamp techniques, where an extremely fine glass pipette was used to make contact with the outer membrane of a cell, forming a single ion channel.[20] Erwin Neher and Bert Sakmann were awarded the Nobel Prize in Physiology or Medicine for the innovation of this technology in 1991.[21]

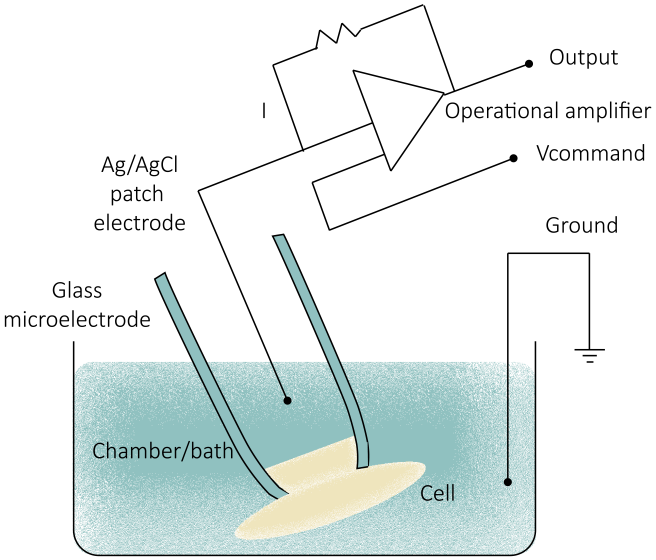


Figure 1-2: Conceptual demonstration of the patch-clamp recording technology, a glass microelectrode is inserted into a chamber/bath filled with an electrolyte consisting of K^+, Na^+ and/or Cl^- ions. The patch (recording) electrode connected to an amplifier is inserted into the pipette, another electrode is placed in the bath acting as a ground. Typically, a voltage clamp mode is used to control the voltage across the cell membrane, and the resulting current is recorded. Alternatively, the current-clamp mode can be used where the current passing through the membrane is controlled, and the output is generated in the form of reversal potentials (E_{rev}).

1.3.2 Nanopore sensing

1.3.2.1 Overview

Nanopore sensing using patch-clamp recordings has largely been motivated by the sequencing of nucleic acids since David Deamer sketched the concept in which bases of a DNA strand passing through a nanopore by an applied voltage produced base-specific readouts.[22] It took just under two decades for the first sequential reads of DNA strands using nanopores to be published,[23] after which, commercialisation of the nanopore sequencing concept by Oxford Nanopore Technologies sparked a wide range of applications and interest beyond the nanopore community.[5,7] Today, it is rapidly advancing, not only in the context of sequencing but also in the exploration of other applications, such as biological screening, diagnostics and the grand challenge of protein sequencing.[24,25]

At the core of every single molecule method is the necessity to confine individual analytes in space and time during the measurement. In traditional optical methods, a 'virtual' volume often defines a region within which molecules can be detected. This is unlike nanopores, where a molecule is confined in a physical volume. One requirement is that the diameter of the nanopore is on a scale similar to that of the molecule, to facilitate detection. At the same time, the nanopore depth or thickness should, ideally, be as thin as possible to maximise the detected signal. Of course, many challenges have been overcome to achieve the present potential of the technology, including improvements in the tuning of material properties, dimensions, selectivity and detection modality. Recent advances of nanopore sensing will be discussed by introducing different types of nanopores, with a special focus on the use of a range of different materials including proteins,[26,27] silicon,[28,29] quartz,[30,31] metals,[32,33] polymeric films,[34,35] nanowires[36] and 2D materials such as graphene.[37]

Overall, the nanopore field has grand tasks ahead. From a materials perspective, it seeks to invent novel nanopore architectures and materials, achieve multiplexed detection, high-throughput analysis, enhanced sensitivity and selective/specific detection. Apart from DNA and RNA sequencing, the prospects for clinical adoption of nanopore technologies are high, but most likely, delivery on this promise hinges on more colourful signals than ionic currents alone. This is, in part, due to the need for detecting small molecular differences in complex biofluids such as serum, cerebrospinal fluid and urine. Such measurements often require the use of a 'spectroscopic' fingerprinting approach rather than the more typical one-dimensional signals often obtained.

In this thesis, how these materials are enabling novel sensing functionalities were discussed, and also highlight recent solutions to one of the greatest drawbacks associated with nanopore sensing: the lack of selectivity. I discuss recent strategies, where the much-needed analyte selectivity can be achieved via chemical modification of the nanopore material. This happens through growing areas of research within the community that aim to capitalise on the advantages of nanopore sensing coupled with other detection modalities such as field-effect transistors (FETs). Finally, I discuss how this approach was used in this thesis to address the challenges of nanopore sensing mentioned above.

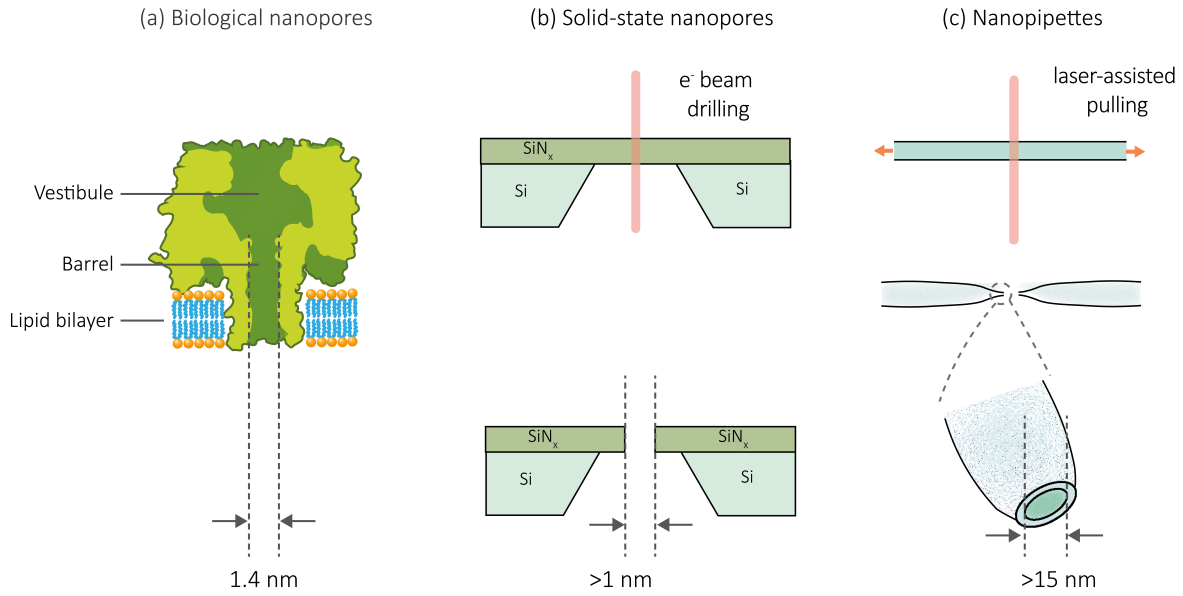


Figure 1-3: Comparison between (a) biological nanopores, (b) solid-state nanopores and (c) nanopipettes. Biological nanopores normally consist of a pore-forming protein supported by a lipid bilayer. The diameter of a biological nanopore is determined by the structure of the protein, mostly around 1 nm. Solid-state nanopores are fabricated by electron beam drilling on a freestanding silicon nitride membrane on a silicon substrate, generating nanopores greater than 1 nm in size. Other fabrication methods exist, such as dielectric breakdown and electrochemical etching, addressing the cost and saving time as compared to the conventional electron beam drilling processes, which are performed under ultra-high vacuum conditions. Alternatively, a subclass of solid-state nanopores, namely nanopipettes, can be fabricated by laser-assisted pulling of glass capillaries, which lasts only a few seconds and produces a pair of nanopipettes with a nanopore size greater than 15 nm.

1.3.2.2 Nanopore sensing – working principle

The principle behind conventional nanopore detection is called resistive pulse sensing. Two reservoirs filled with an electrolyte (usually a buffered salt solution such as potassium chloride (KCl), sodium chloride or lithium chloride) are separated by a thin, non-permeable membrane and linked only via a single nanopore. Electrodes such as silver/silver chloride (Ag/AgCl) are immersed in each compartment, and a voltage bias across the nanopore is applied over time (i.e. clamping the voltage), causing a steady-state ionic current flux through the pore. During an analyte's passage through the pore (sometimes called translocation), the ionic current

usually decreases due to hindered access of the ions to the pore volume.[38,39] In some cases, such as double-stranded DNA transport in low salt concentrations, recruitment of mobile counterions by the DNA backbone to the pore vicinity enhances the ionic current. Other factors, such as salt concentration and pH, can influence the interplay between the electrophoretic and electro-osmotic flow. By analysing the different characteristics of the current pulse, such as amplitude (ΔI), duration (Δt) and noise, one can obtain important information on the analyte, including size, charge, affinity with the nanopore surface and, in some cases, even shape, dipole moments and sequence. Additionally, the frequency of these modulations informs on the analyte's concentration.

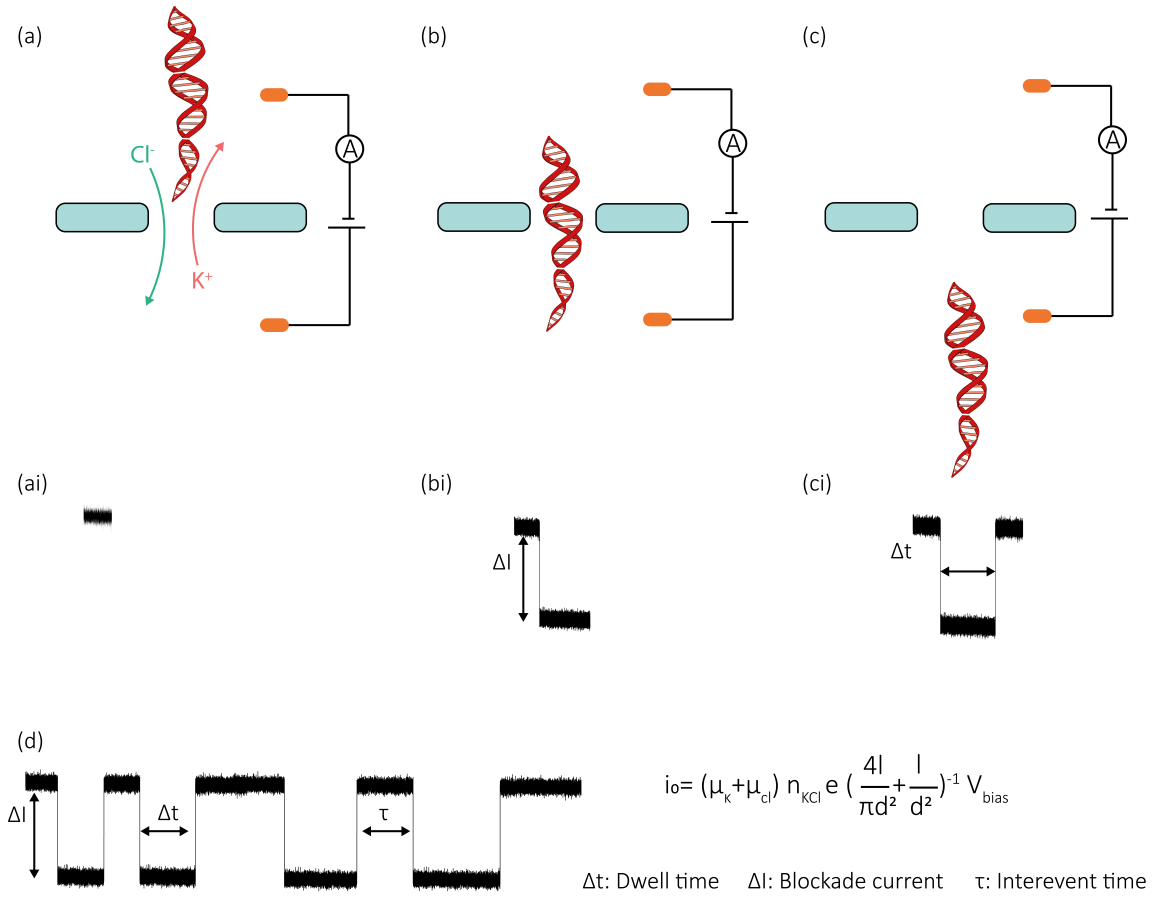


Figure 1-4: Working principle of nanopore sensing. The principle behind conventional nanopore detection is called resistive pulse sensing. A constant voltage bias is applied across a pore that connects two reservoirs filled with electrolytes separated by a non-permeable membrane. (a) In most cases, the applied bias from a pair of Ag/AgCl electrodes in KCl causes a steady-state ionic current to flow through

the pore as the resistance of the nanopore is greater than the electrolyte resistance. As a result, most of the potential field gradient is focused at, or close to, the pore. Ions, and any other charged molecules, are therefore translocated through the pore across the membrane, driven by this potential gradient. (b) When a charged molecule is transported through the pore, the ionic current is either enhanced (as in most cases) or blocked as part of the nanopore volume previously occupied by ions is replaced by the translocating molecule. (c) The steady-state current is recovered after the translocating molecule exits the pore. Examples of ionic current traces showing single-molecule translocation of the analyte are shown in (d). Definition of terms in the equation to estimate the current from a cylindrical nanopore: i_0 : open pore current, μ: electrophoretic mobility of ions, n: the number density of ions, d is the diameter of nanopores, l is the thickness of nanopore, V_{bias} is the applied voltage.

1.3.2.3 Biological nanopores

Starting from biological nanopores, the unique structural feature of pore-forming proteins (e.g. α-haemolysin, MspA, CsgG and FraC) offers excellent channel length and nanopore size at nanoscale in a reproducible manner by inserting them into supporting lipid bilayers. Therefore, biological nanopores have found a plethora of applications, such as the high throughput sequencing of nucleic acids, and have even been commercialised by Oxford Nanopore Technologies. The fixed nanopore size in a sub 5 nm regime opens up different possibilities for resolving small molecular differences such as different lengths and sequences of homopolymers,[40,41] single DNA methylation,[42] protein sequencing[25] and conformational analysis.[43] While the robustness of proteins and lipid bilayers represents a general challenge for biological nanopores, part of this limitation has been solved by inserting proteins into polymeric membranes for improving their stability.[44]

1.3.2.4 Solid-state nanopores

Along with the advancement of processing techniques for solid-state materials over the last two decades, solid-state nanopores, which have the advantages of robustness and stability, are being developed. Comparable to biological nanopores where the amino acid composition of pore-forming proteins can be changed to vary the surface charge, solid-state nanopores also offer the flexibility of pore size, tuneable surface charge and functionality via chemical or physical modification.[32,45,46] Moreover, the solid-state approach makes it possible to integrate with other external forces and fields to pre-concentrate analytes at the mouth of nanopores,

heightening sensitivity towards sub-pM regimes.[47] To combine the robustness of solid-state materials with the precise structural engineering of pore-forming proteins, a protein pore can also be inserted into a solid-state nanopore for the discrimination of different types of biomolecules.[48]

1.3.2.5 Nanopipettes

In recent years, the emergence of a subclass of solid-state nanopores, namely nanopipettes, has initiated a range of studies, particularly in the area of what might be achieved beyond a single nanopore. Their fabrication can be performed via laser-assisted pulling of quartz/borosilicate capillaries, which are significantly cheaper and more time-efficient than the e-beam lithography fabrication of conventional solid-state nanopores. Moreover, the conical geometry of nanopipettes makes it possible for them to be inserted into cells for different biopsy applications.[49,50] The single-barrel nanopipettes have demonstrated their excellent potential for single-molecule detection, with some examples using molecular carriers to sense proteins in complex biological media.[31,51] Importantly, the incorporation of multi-barrel capillaries opens up the possibility of joining multiple pores together, even with only tens of nanometres' separation. Inspired by the pioneering work on scanning ion conductance microscopy and scanning electrochemical microscopy,[52,53] a range of novel applications relating to the optimisation and controlling of single-molecule translocation have been developed based on double and multiple nanopipette architectures, such as single-molecule 'tug of war',[54,55] tuning translocation speeds and capture rates.[32,35]

1.3.2.6 From protein pores to hybrid pores

While protein nanopores have been constantly innovated for numerous sequencing and sensing applications, their precise structural engineering at the atomic level is still being envisaged for novel molecular assembly of nanopore architectures such as Rosette nanotubes[56]. Similarly, other biological components such as DNA can also be used to assemble a range of nanopore architectures, with examples including using unique DNA nanoscalffolds to assemble nanopores with rationally engineered shapes and properties[57–59].

Not only from the structural perspective, the robustness of those unique pore architectures afforded from biomolecular assembly could be enhanced by insertion into solid-state or

polymeric membranes, originating from hybrid pore formation by directed insertion of α-haemolysin into solid-state nanopores. [60]More recently, this insertion approach was extended beyond typical pore-forming proteins to thermostable viral portal proteins[48] and DNA origamis[61], with single-molecule sensing capability established down to ssDNA and peptides.

1.3.2.7 Chemical modifications for selective sensing

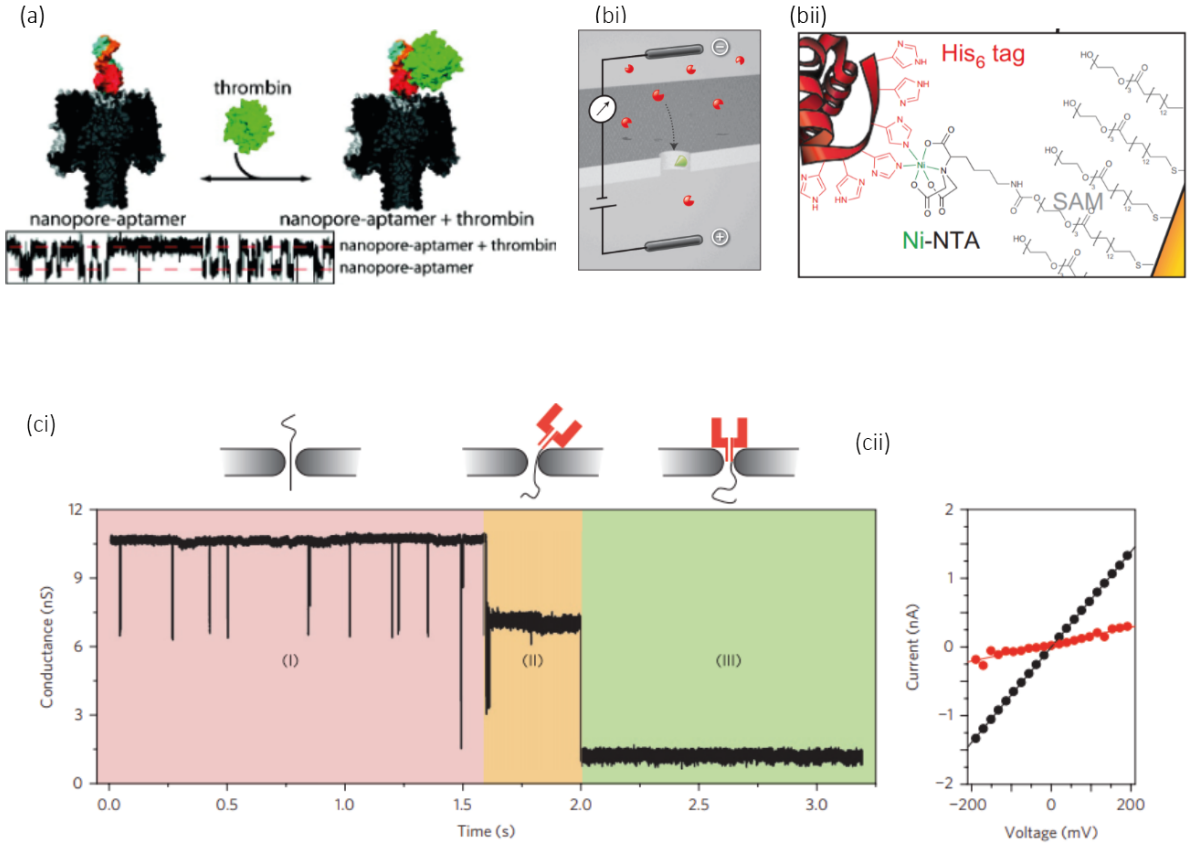


Figure 1-5: Examples of chemical modifications for both biological nanopores and solid-state nanopores. (a) Biological nanopores can be modified by attaching aptamers at the pore lumen. Note that as the size of aptamers and targeted analytes is much larger than the diameter of biological nanopores, the current fluctuations are caused by the blocking and unblocking of the nanopore entrance from the aptamer and aptamer-target complex. Therefore, interactions between aptamers and targeted analytes can be monitored by analysing the switching of different current levels, corresponding to on/off states where the nanopore is blocked and unblocked by an aptamer-target complex.[26] (b) Protein receptors can be attached to the surface of solid-state nanopores. Selective single-molecule detection of proteins is achieved by the complexation chemistry between receptors and proteins.[62] (c) To combine the robustness of solid-state nanopores with the precise structural engineering of biological

nanopores, pore-forming proteins can be inserted into solid-state nanopores. A successful insertion causes a decrease of nanopore conductance and nanopore current.[60]

Nanopore sensing is an exceptionally versatile tool for the detection of biological analytes at the single-molecule level; however, this is generally not considered a selective detection strategy. Any molecule that can be electrokinetically driven through the nanopore can disrupt the flow of ions and produce a signal. The similarity in signal is particularly problematic in the discrimination of proteins, and it is essential to solve, in nanopore platforms, for the fingerprinting of individual biomarkers and for screening complex biological fluids such as serum, urine or cerebrospinal fluid. For example, human serum contains thousands of proteins in a broad range of concentrations, and the ability to detect a single protein type within this mixture, especially at low concentrations, is critical for diagnostic and screening applications. Extensive efforts have been made to address this fundamental limitation by incorporating a selective component to the detection modality. To date, nanopore selectivity has been achieved via two routes: 1) functionalising the nanopore with a receptor tailored for a specific analyte; and 2) introducing probes into the solution that can `fish out` the molecules of interest.

Some of the earlier attempts to achieve selectivity relied on chemical means to modify the nanopore surface, whether biological[63–65] or solid-state.[66] One common strategy was the use of DNA aptamers.[26] Aptamers are nucleic acids that bind to target molecules with high specificity and affinity. Unlike antibodies, aptamers can be efficiently designed and selected to work in a range of buffer and pH conditions.[67,68] One of the first instances was the attachment of a thrombin-binding aptamer to an α-hemolysin pore. Thrombin, a biological enzyme with a crucial role in physiological and pathological coagulation, has been extensively used for the development of aptamer-based therapeutics and diagnostics, in large part due to the system being exceptionally well studied.[69] The DNA aptamer was covalently attached through a disulphide bond to a single cysteine residue near the opening of the pore. In this case, on binding to the thrombin, the nanopore opening could be switched on or off by the DNA formed cation-stabilised G-quadruplex (secondary structures of nucleic acids that are formed by G-rich sequences), altering the ionic current. Although biological pores are not always as easy to modify as their solid-state analogues, they have the advantage that it is relatively easy to precisely control the site modification of the pore along with the number of receptors that can

be incorporated.[26,70] Alternatively, in solid-state nanopores, functionality can be incorporated via the design of biomimetic platforms such as those incorporating single protein receptors via a thiol-terminated self-assembled monolayer. Wei et al.[62] demonstrated metallised silicon nitride nanopores chemically modified with nitrilotriacetic acid receptors that allowed for the reversible binding and unbinding of the proteins to the receptors observed in real-time. Although the functionalised site of the nanopore (the receptor) was arbitrarily located on the nanopore surface, it was possible to quantitatively determine the intrinsic binding strength (dissociation rate) of a molecular interaction from voltage-dependent measurements.

1.3.2.8 Sensor multiplexing

Although great strides have been made to improve selectivity and sensitivity in nanopore measurements, the time a molecule spends inside the detection volume ultimately governs how accurately a target/probe complex can be detected. A strategy first implemented by Gershow and Golovchenko was to read a translocating molecule repeatedly through a single pore by rapidly reversing the bias.[71] Using this strategy, it was possible to read the same molecule up to 12 times over 250 ms. Although this was not used for the detection of a particular biological target, it opened the door to developing double nanopore platforms for performing electrophoretic time-of-flight measurements by determining the time it takes for a molecule to transit through two nanopores spaced 1.5 µm apart.[72] More recently, there have been extensive efforts to reduce spacing down to gap sizes of 10 nm in order to improve the capture and recapture efficiency.[54,73,74] It was shown that with such small gaps, a molecule could be recaptured, and even stalled, with near 100% efficiency. This paved the way for using such devices to perform targeted sensing with heightened sensitivity. Furthermore, the slowing down facilitates recording the translocations at lower bandwidth and hence improving the signal to noise. Building on this strategy, Liu et al.[74] showed that it is possible to not only sense the same molecule but also use molecular carriers to detect monovalent streptavidin bound to the DNA. This strategy could be used to detect more biologically relevant molecules and, potentially, even be used with fluids such as serum. Perhaps the most well-established multiplexing strategy can be traced to nanopore sequencers from Oxford Nanopore Technologies, where there are hundreds of active nanopores in a commercially available flow cell.

1.3.2.9 Alternative detection strategies

While electrical sensing provides excellent temporal resolution and wealthy details about analytes at the single-molecule level, alternative detection strategies are being developed to enrich the single-molecule information that can be obtained from conventional electrical sensing and multiplexing nanopore detection. Charge-based and capacitance-based Field-Effect Transistor (FET) detection can be integrated with nanopore sensing using FET-coupled nanopores. Furthermore, photon-based detection has been increasingly used to eliminate false positives when sensing proteins using molecular carriers,[51] giving more positional information for both targeted analytes and nanopores,[75,76] detecting vibrational information[77] and, in some cases, the sequence information.[78]

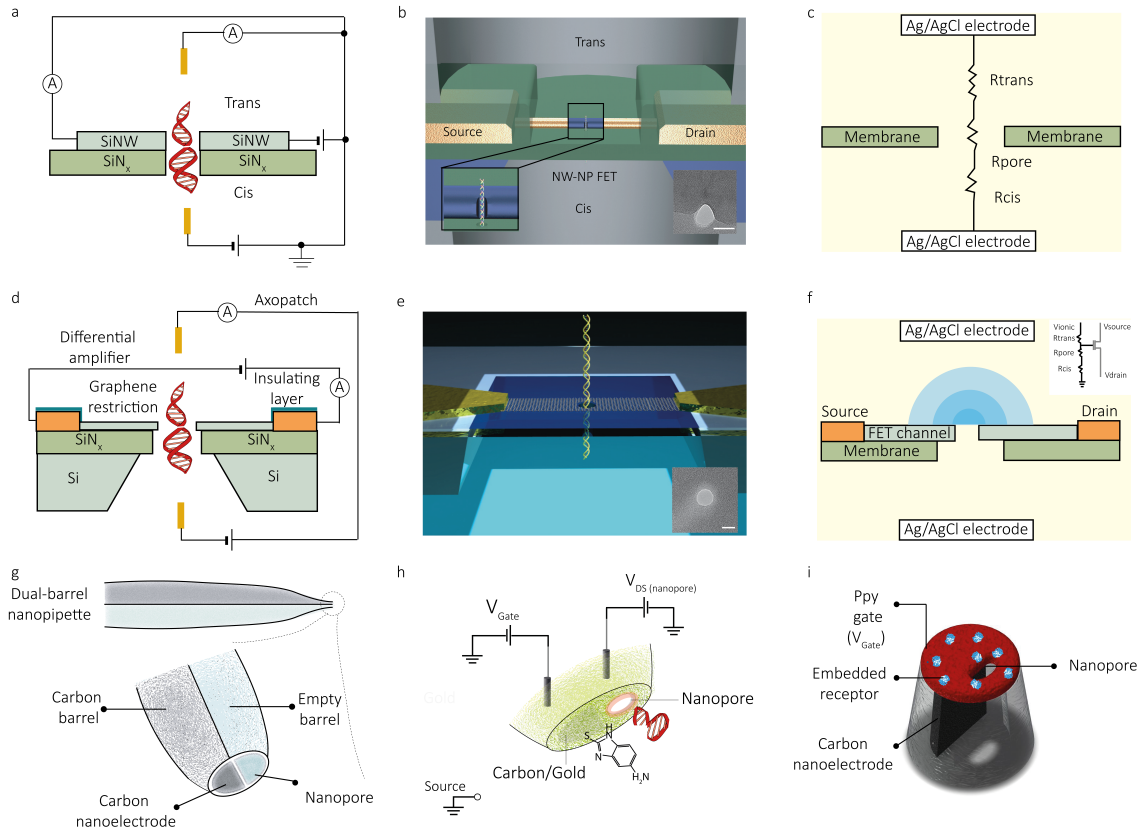


Figure 1-6: Summary of different approaches for nanopore FETs. Solid-state nanopores can be integrated with FETs by incorporating a drain-source channel above the nanopore. In most cases, synchronised electrical recording is achieved via two independent amplifiers from the nanopore and FET channels, respectively. Representative examples are demonstrated via (a–b) a Si nanowire[93] or (d–e) graphene nanoribbon nanopores[88,89] for synchronised detection of single-molecule DNA translocation. The scale bars are 10 nm for the Si nanowire and 5 nm for the graphene nanoribbons.

The single-molecule translocation can be synchronised from resistive pulse sensing in a nanopore channel, and either through capacitive coupling or gated by the charge of the translocating molecule from the FET channel (i.e. drain-source) (c, f). This process could be modelled by a nanopore overlaid with the resistance from both cis and trans chambers, as well as the resistance from the nanopore. A portion of the FET channel is coupled with the nanopore, so that the FET channel in the cis region is coupled to the voltage set at the bottom Ag/AgCl electrode, resulting in a localised potential change around the nanopore. The potential falls as 1/r away from the nanopore where r is the distance from nanopore opening.[94] The inset is a schematic of a nanopore-FET electrical circuit. In this type of devices the source-drain is either Si nanowire or graphene nanoribbons. (g) More recently, a novel class of nanopore-FET devices was constructed from dual-barrel nanopipettes, with drain-source being the empty barrel of a nanopipette and gate being gold or polypyrrole electrode. One barrel was selectively filled with carbon via pyrolytic deposition from butane, forming a carbon nanoelectrode at the tip, and an empty barrel was used as a nanopore. (h) Gold can be electrochemically deposited on the carbon nanoelectrode and functionalised with a thiolated species for use as a gate to modulate single-molecule DNA translocation from a nanopore.[32] (i) In a similar way, the gate is also fabricated by electropolymerisation of pyrrole, and artificial receptors embedded within the polymeric film for selective single-molecule sensing of targeted analytes.[35]

1.3.2.10 Nanopore field-effect transistors

Similar to nanopores, FET sensors are highly versatile for the label-free detection of biological species in solution, or complex biological media. Examples include Si nanowire,[79,80] graphene[81] and carbon nanotubes.[82] The detection principle is based on monitoring the change of the source-drain conductance or transient changes in the gate conductance after affinity-based binding between the analytes and the transistor surface. Although promising, like most sensors, analyte detection is diffusion-limited. Furthermore, the active sensing volume is limited by the Debye screening length. Different approaches have been developed to address these issues, including working in a dilute electrolyte, which effectively increases the Debye screening length, and functionalising transistor channels with small receptors, such as aptamers[83] and antibodies,[84] facilitating the detection of proteins[81] and viruses.[85]

Integrating nanopores with FETs by confining charged analytes in a nanoscale pore offers advantages including enabling active transport to the FET. Nanopore integration can be

achieved via the incorporation of nanowires, graphene nanoribbons and gold electrodes aligned to the pore lumen. Operationally, detection between both the FET and the nanopore channels can be synchronised, as has been shown for the detection of DNA and nanoparticles. The synchronisation mechanism is based on either capacitive coupling[86,87] or electrostatic gating[36,88–90] as a result of a change in local potential at the gate electrode during DNA translocation, or gating by the charge of the translocating molecule (Figure 1-6 a–e).

The concept of ionic FETs combined with nanopores was first demonstrated by Nam et al.,[91] in which electrode-embedded nanopore structures were fabricated by e-beam lithography and atomic layer deposition. Ionic transport in sub 10 nm nanopores can be effectively manipulated by using electrodes embedded in the membrane. Building on earlier work, controlling analyte transport across nanopores was also realised for the single-molecule translocation of DNA. More recently, double-barrelled nanopores have been used to control single-molecule transport via the integration of a gate electrode. Xue et al.[32] showed that it is possible to combine the unique advantages of nanopores and FETs and that these hybrid sensors have perfectly aligned nanopore and FET components, making it possible to detect molecular events with near 100% synchronisation. Surface functionalisation of the gate electrode was shown to be capable of fine-tuning transport properties, enabling more active control over the translocation velocity and capture rates (Figure 3d-f). Such an approach can be used in combination with aptamer- and antibody-modified surfaces, to selectively target different proteins and even small molecules such as neurotransmitters, which are exceptionally challenging to detect using conventional nanopore platforms.[92] Although currently, there is still some room for improvement, the ultimate aim is to make full use of the potential and harness the unique advantages of both techniques to extract molecular fingerprints, and possibly, perform sequencing for a range of analytes.

1.4 Thesis outline

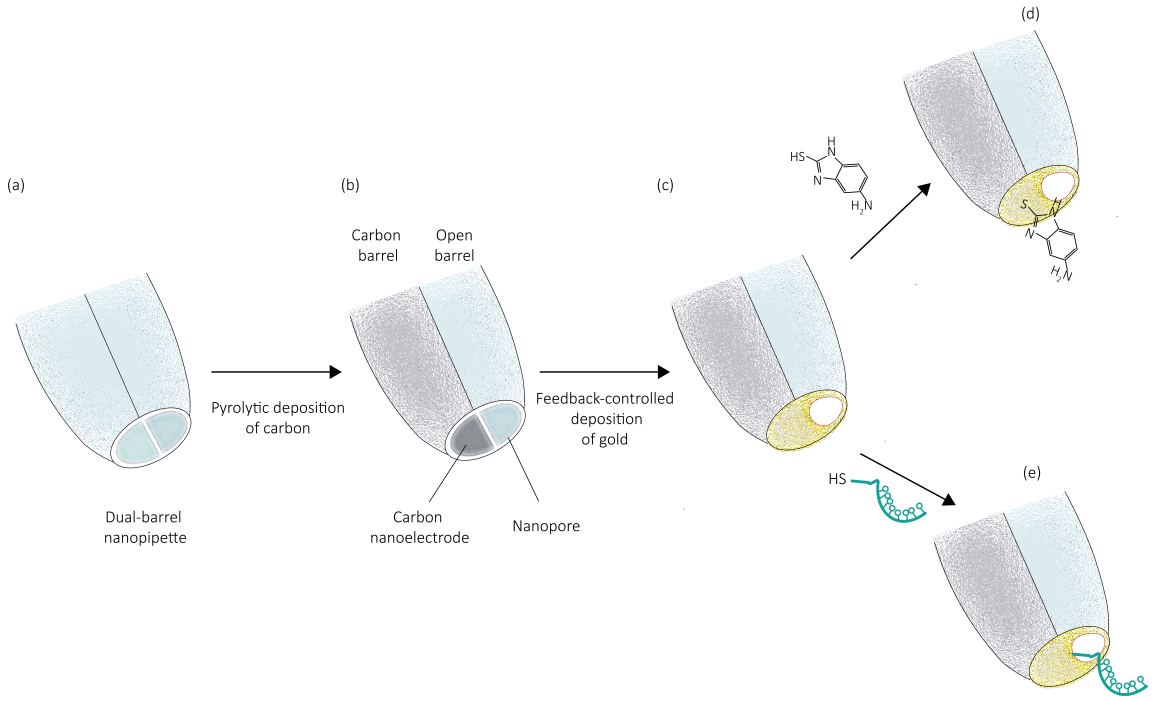


Figure 1- 7: Thesis outline in terms of the fabricating workflow of nanopore FETs based on dual-barrel nanopipettes. One barrel is selectively filled with carbon via pyrolysis of butane while another barrel remains empty, forming a carbon nanoelectrode and an open nanopore at the tip. Gold can be deposited on the surface of carbon nanoelectrode and shrinks down the nanopore by a feedback-controlled mechanism. The gold-deposited devices are functionalised by two different types of thiolated species. (d) Small organic molecules can be used to switch the surface charge of a nanopore, controlling single-molecule transport using a chemically modified nanopore-FET. (e) Thiolated oligonucleotides can be encoded onto the surface of gold to enhance the selectivity towards different targeted analytes such as proteins and small molecules.

To address two of the most important challenges outlined above, controlling single-molecule transport and enhancing selectivity, we present a new fabrication strategy for efficiently designing and aligning a sub-30 nm nanopore to a gate electrode to control molecular transport at a single-molecule level. Rapid fabrication was achieved by controlled electrodeposition of gold onto a nanoscale carbon electrode formed inside one of the barrels of a double-barrel nanopore/nanopipette. Ion current feedback was used to fabricate the gold gate electrode localised at the nanopore opening while monitoring and tuning the pore conductance in real time. I show that single-molecule events can be detected in both nanopore

and gate channels with enhanced sensitivity and up to almost 100% synchronisation. Furthermore, voltage gating, as well as surface functionalisation (Figure 1-6 c, d), can be used to tune the nanopore surface charge, and, in turn, to switch on or off, or to accurately control the rate of single-molecule transport. The results demonstrate that these hybrid nanopore–FET devices can be readily used to control molecular transport by tuning nanopore charges both electrically and chemically.

Primarily, nucleic acid aptamers have been used as artificial receptors to increase the sensitivity and selectivity of both nanopores and FETs. Selected from the systematic evolution of ligands by exponential enrichment (SELEX) processes, high specificity and affinity afforded from unique molecular conformations allows the selective recognition of a target with enhanced sensitivity. In this thesis, I propose a strategy to combine the advantages of nanopore sensors, aptamer molecular recognition chemistry and FETs (Figure 1-6 e). For example, nanopores can be functionalised with aptamers to target specific analytes, and this can be further combined with voltage gating to control the physical interactions between analytes and receptors. We have previously demonstrated routes towards the fabrication of hybrid nanopore-FET systems for simultaneous single-molecule detection and manipulation. In the present work, we build on these concepts for the selective sensing of small neurotransmitter molecules, including dopamine, serotonin, and acetylcholine. Compared with existing approaches for selective detection at low concentrations, our strategy has the advantages of no need for sample pre-treatment and freedom from any external applied fields or forces to pre-concentrate analytes at the entrance of nanopores, thus enabling easy operation; in particular, stem-loop aptamers attached to the surface of the nanopore, enabling ligand-induced conformational rearrangements in close proximity to the nanopore surfaces. The single-molecule detection of neurotransmitters can be achieved at fM level, which is 6–9 magnitudes lower than the conventional electrochemical or optical methods.

1.5 References

(1) Varongchayakul, N.; Song, J.; Meller, A.; Grinstaff, M. W. Single-Molecule Protein Sensing in a Nanopore: A Tutorial. *Chem. Soc. Rev.* **2018**, *47* (23), 8512–8524.

(2) Miles, B. N.; Ivanov, A. P.; Wilson, K. a; Doğan, F.; Japrung, D.; Edel, J. B. Single Molecule Sensing with Solid-State Nanopores: Novel Materials, Methods, and Applications. *Chem. Soc. Rev.* **2013**, *42* (1), 15–28.

(3) Turner, A. P. F. Biosensors: Sense and Sensibility. *Chem. Soc. Rev.* **2013**, *42* (8), 3184–3196.

(4) Zhang, A.; Lieber, C. M. Nano-Bioelectronics. *Chem. Rev.* **2016**, *116*, 215–257.

(5) Rusk, N. MinION Takes Center Stage. *Nat. Methods* **2015**, *12* (1), 12–13.

(6) Buck, D.; Weirather, J. L.; de Cesare, M.; Wang, Y.; Piazza, P.; Sebastiano, V.; Wang, X. J.; Au, K. F. Comprehensive Comparison of Pacific Biosciences and Oxford Nanopore Technologies and Their Applications to Transcriptome Analysis. *F1000Research* **2017**.

(7) Ashton, P. M.; Nair, S.; Dallman, T.; Rubino, S.; Rabsch, W.; Mwaigwisya, S.; Wain, J.; O'Grady, J. MinION Nanopore Sequencing Identifies the Position and Structure of a Bacterial Antibiotic Resistance Island. *Nat. Biotechnol.* **2015**, *33* (3), 296–300.

(8) Quail, M. A.; Kozarewa, I.; Smith, F.; Scally, A.; Stephens, P. J.; Durbin, R.; Swerdlow, H.; Turner, D. J. A Large Genome Center's Improvements to the Illumina Sequencing System. *Nat. Methods* **2008**.

(9) Feynman, R. P. There's Plenty of Room at the Bottom. In *Engineering and Science magazine*; 1960; Vol. XXIII.

(10) Eid, J.; Fehr, A.; Gray, J.; Luong, K.; Lyle, J.; Otto, G.; Peluso, P.; Rank, D.; Baybayan, P.; Bettman, B.; Bibillo, A.; Bjornson, K.; Chaudhuri, B.; Christians, F.; Cicero, R.; Clark, S.; Dalal, R.; DeWinter, A.; Dixon, J.; Foquet, M.; Gaertner, A.; Hardenbol, P.; Heiner, C.; Hester, K.; Holden, D.; Kearns, G.; Kong, X.; Kuse, R.; Lacroix, Y.; Lin, S.; Lundquist, P.; Ma, C.; Marks, P.; Maxham, M.; Murphy, D.; Park, I.; Pham, T.; Phillips, M.; Roy, J.; Sebra, R.; Shen, G.; Sorenson, J.; Tomaney, A.; Travers, K.; Trulson, M.; Vieceli, J.; Wegener, J.; Wu, D.; Yang, A.; Zaccarin, D.; Zhao, P.; Zhong, F.; Korlach, J.; Turner, S. Real-Time DNA Sequencing from Single Polymerase Molecules. *Science* **2009**, *323* (5910), 133–138.

(11) Juette, M. F.; Terry, D. S.; Wasserman, M. R.; Zhou, Z.; Altman, R. B.; Zheng, Q.; Blanchard, S. C. The Bright Future of Single-Molecule Fluorescence Imaging. *Curr. Opin. Chem. Biol.* **2014**, *20* (1), 103–111.

(12) Le Ru, E. C.; Etchegoin, P. G. Single-Molecule Surface-Enhanced Raman Spectrosscopy. *Annu. Rev. Phys. Chem.* **2009**, *63*, 65–87.

(13) Kodera, N.; Yamamoto, D.; Ishikawa, R.; Ando, T. Video Imaging of Walking Myosin V by High-Speed Atomic Force Microscopy. *Nature* **2010**, *468* (7320), 72–76.

(14) Katan, A. J.; Dekker, C. High-Speed AFM Reveals the Dynamics of Single Biomolecules at the Nanometer Scale. *Cell* **2011**, *147* (5), 979–982.

(15) Burgess, N. The 2014 Nobel Prize in Physiology or Medicine: A Spatial Model for Cognitive Neuroscience. *Neuron*. 2014.

(16) Sang, J. C.; Meisl, G.; Thackray, A. M.; Hong, L.; Ponjavic, A.; Knowles, T. P. J.; Bujdoso, R.;

Klenerman, D. Direct Observation of Murine Prion Protein Replication in Vitro. *J. Am. Chem. Soc.* **2018**.

(17) Di Ventra, M.; Taniguchi, M. Decoding DNA, RNA and Peptides with Quantum Tunnelling. *Nat. Nanotechnol.* **2016**, *11* (2), 117–126.

(18) Ivanov, A.; Actis, P.; Jönsson, P. On-Demand Delivery of Single DNA Molecules Using Nanopipets. *ACS Nano* **2015**, *9* (4), 3587–3595.

(19) Coulter, W. H. US Patent Specification BT - Means for Counting for Counting Particles Suspended in a Fluid. US Patent 2656508 A, 1953.

(20) Neher, E.; Sakmann, B. Single-Channel Currents Recorded from Membrane of Denervated Frog Muscle Fibres. *Nature* **1976**.

(21) Nobel Prize 1991 in Chemistry. *Appl. Magn. Reson.* **1992**.

(22) Deamer, D.; Akeson, M.; Branton, D. Three Decades of Nanopore Sequencing. *Nat. Biotechnol.* **2016**, *34* (5), 518–524.

(23) Cherf, G. M.; Lieberman, K. R.; Rashid, H.; Lam, C. E.; Karplus, K.; Akeson, M. Automated Forward and Reverse Ratcheting of DNA in a Nanopore at 5-Angstrom Precision. *Nat. Biotechnol.* **2012**, *30* (4), 344–348.

(24) Restrepo-Pérez, L.; Joo, C.; Dekker, C. Paving the Way to Single-Molecule Protein Sequencing. *Nat. Nanotechnol.* **2018**, *13* (9), 786–796.

(25) Ouldali, H.; Sarthak, K.; Ensslen, T.; Piguet, F.; Manivet, P.; Pelta, J.; Behrends, J. C.; Aksimentiev, A.; Oukhaled, A. Electrical Recognition of the Twenty Proteinogenic Amino Acids Using an Aerolysin Nanopore. *Nature Biotechnology*. 2019.

(26) Rotem, D.; Jayasinghe, L.; Salichou, M.; Bayley, H. Protein Detection by Nanopores Equipped with Aptamers. *J. Am. Chem. Soc.* **2012**, *134* (5), 2781–2787.

(27) Qing, Y. J.; Ionescu, S. A.; Pulcu, G. S.; Bayley, H. Directional Control of a Processive Molecular Hopper. *Science* **2018**, *361* (6405), 908–911.

(28) Plesa, C.; Ruitenberg, J. W.; Witteveen, M. J.; Dekker, C. Detection of Individual Proteins Bound along DNA Using Solid-State Nanopores. *Nano Lett.* **2015**, *15* (5), 3153–3158.

(29) Chien, C.-C.; Shekar, S.; Niedzwiecki, D. J.; Shepard, K. L.; Drndić, M. Single-Stranded DNA Translocation Recordings through Solid-State Nanopores on Glass Chips at 10 MHz Measurement Bandwidth. *ACS Nano* **2019**, *13* (9), 10545–10554.

(30) Lin, X.; Ivanov, A.; Edel, J. Selective Single Molecule Nanopore Sensing of Proteins Using DNA Aptamer-Functionalised Gold Nanoparticles. *Chem. Sci.* **2017**, *8*, 3905–3912.

(31) Sze, J. Y. Y.; Ivanov, A. P.; Cass, A. E. G.; Edel, J. B. Single Molecule Multiplexed Nanopore Protein Screening in Human Serum Using Aptamer Modified DNA Carriers. *Nat. Commun.* **2017**, *8* (1), 1552.

(32) Xue, L.; Cadinu, P.; Paulose Nadappuram, B.; Kang, M.; Ma, Y.; Korchev, Y. E.; Ivanov, A. P.; Edel, J. B. Gated Single-Molecule Transport in Double-Barreled Nanopores. *ACS Appl. Mater. Interfaces* **2018**, *10* (44), 38621–38629.

(33) Ivanov, A. P.; Instuli, E.; McGilvery, C. M.; Baldwin, G.; McComb, D. W.; Albrecht, T.; Edel, J. B. DNA Tunneling Detector Embedded in a Nanopore. *Nano Lett.* **2011**, *11*, 279–285.

(34) Al Sulaiman, D.; Cadinu, P.; Ivanov, A. P.; Edel, J. B.; Ladame, S. Chemically Modified Hydrogel-

Filled Nanopores: A Tunable Platform for Single-Molecule Sensing. *Nano Lett.* **2018**, *18* (9), 6084–6093.

(35) Ren, R.; Zhang, Y.; Nadappuram, B. P.; Akpinar, B.; Klenerman, D.; Ivanov, A. P.; Edel, J. B.; Korchev, Y. Nanopore Extended Field-Effect Transistor for Selective Single-Molecule Biosensing. *Nat. Commun.* **2017**, *8* (1), 586.

(36) Xie, P.; Xiong, Q.; Fang, Y.; Qing, Q.; Lieber, C. M. Local Electrical Potential Detection of DNA by Nanowire–Nanopore Sensors. *Nat. Nanotechnol.* **2011**, *7* (2), 119–125.

(37) Rollings, R. C.; Kuan, A. T.; Golovchenko, J. A. Ion Selectivity of Graphene Nanopores. *Nat. Commun.* **2016**, *7*, 11408.

(38) Kesselheim, S.; Muller, W.; Holm, C. Origin of Current Blockades in Nanopore Translocation Experiments. *Phys. Rev. Lett.* **2014**, *112* (1), 18101.

(39) Wilson, J.; Sarthak, K.; Si, W.; Gao, L. Y.; Aksimentiev, A. Rapid and Accurate Determination of Nanopore Ionic Current Using a Steric Exclusion Model. *ACS Sensors* **2019**, *4* (3), 634–644.

(40) Cao, C.; Li, M.-Y.; Cirauqui, N.; Wang, Y.-Q.; Dal Peraro, M.; Tian, H.; Long, Y.-T. Mapping the Sensing Spots of Aerolysin for Single Oligonucleotides Analysis. *Nat. Commun.* **2018**, *9* (1), 2823.

(41) Stoddart, D.; Heron, A. J.; Mikhailova, E.; Maglia, G.; Bayley, H. Single-Nucleotide Discrimination in Immobilized DNA Oligonucleotides with a Biological Nanopore. *Proc. Natl. Acad. Sci. U. S. A.* **2009**.

(42) Ying, Y. L.; Long, Y. T. Nanopore-Based Single-Biomolecule Interfaces: From Information to Knowledge. *J. Am. Chem. Soc.* **2019**.

(43) Galenkamp, N. S.; Soskine, M.; Hermans, J.; Wloka, C.; Maglia, G. Direct Electrical Quantification of Glucose and Asparagine from Bodily Fluids Using Nanopores. *Nat Commun* **2018**, *9* (1), 4085.

(44) Harnack, O.; Wessels, J.; Yasuda, A.; Clarke, J.; REID, T. Method of Fabricating a Membrane Having a Tapered Pore. US8137569B2, 2008.

(45) Yusko, E. C.; Johnson, J. M.; Majd, S.; Prangkio, P.; Rollings, R. C.; Li, J.; Yang, J.; Mayer, M. Controlling Protein Translocation through Nanopores with Bio-Inspired Fluid Walls. *Nat. Nanotechnol.* **2011**, *6* (4), 253–260.

(46) Kowalczyk, S. W.; Kapinos, L.; Blosser, T. R.; Magalhães, T.; van Nies, P.; Lim, R. Y. H.; Dekker, C. Single-Molecule Transport across an Individual Biomimetic Nuclear Pore Complex. *Nat. Nanotechnol.* **2011**, *6* (7), 433–438.

(47) Freedman, K. J.; Otto, L. M.; Ivanov, A. P.; Barik, A.; Oh, S.-H.; Edel, J. B. Nanopore Sensing at Ultra-Low Concentrations Using Single-Molecule Dielectrophoretic Trapping. *Nat. Commun.* **2016**, *7*, 10217.

(48) Cressiot, B.; Greive, S. J.; Mojtabavi, M.; Antson, A. A.; Wanunu, M. Thermostable Virus Portal Proteins as Reprogrammable Adapters for Solid-State Nanopore Sensors. *Nat. Commun.* **2018**, *9* (1), 4652.

(49) Nadappuram, B. P.; Cadinu, P.; Barik, A.; Ainscough, A. J.; Devine, M. J.; Kang, M.; Gonzalez-Garcia, J.; Kittler, J. T.; Willison, K. R.; Vilar, R.; Actis, P.; Wojciak-Stothard, B.; Oh, S. H.; Ivanov, A. P.; Edel, J. B. Nanoscale Tweezers for Single-Cell Biopsies. *Nat. Nanotechnol.* **2019**, *14* (1), 80–88.

(50) Ying, Y. L.; Li, Y. J.; Mei, J.; Gao, R.; Hu, Y. X.; Long, Y. T.; Tian, H. Manipulating and Visualizing the Dynamic Aggregation-Induced Emission within a Confined Quartz Nanopore. *Nat. Commun.* **2018**.

(51) Cai, S.; Sze, J. Y. Y.; Ivanov, A. P.; Edel, J. B. Small Molecule Electro-Optical Binding Assay Using Nanopores. *Nat. Commun.* **2019**, *10* (1).

(52) Actis, P.; Tokar, S.; Clausmeyer, J.; Babakinejad, B.; Mikhaleva, S.; Cornut, R.; Takahashi, Y.; López Córdoba, A.; Novak, P.; Shevchuck, A. I.; Dougan, J. A.; Kazarian, S. G.; Gorelkin, P. V.; Erofeev, A. S.; Yaminsky, I. V.; Unwin, P. R.; Schuhmann, W.; Klenerman, D.; Rusakov, D. A.; Sviderskaya, E. V.; Korchev, Y. E. Electrochemical Nanoprobes for Single-Cell Analysis. *ACS Nano* **2014**, *8* (1), 875–884.

(53) Momotenko, D.; Byers, J. C.; McKelvey, K.; Kang, M.; Unwin, P. R. High-Speed Electrochemical Imaging. *ACS Nano* **2015**, *9* (9), 8942–8952.

(54) Cadinu, P.; Campolo, G.; Pud, S.; Yang, W.; Edel, J. B.; Dekker, C.; Ivanov, A. P. Double Barrel Nanopores as a New Tool for Controlling Single-Molecule Transport. *Nano Lett.* **2018**, *18* (4), 2738–2745.

(55) Cadinu, P.; Kang, M.; Nadappuram, B. P.; Ivanov, A. P.; Edel, J. B. Individually Addressable Multi-Nanopores for Single-Molecule Targeted Operations. *Nano Lett.* **2020**, *20* (3), 2012–2019.

(56) Tripathi, P.; Shuai, L.; Joshi, H.; Yamazaki, H.; Fowle, W. H.; Aksimentiev, A.; Fenniri, H.; Wanunu, M. Rosette Nanotube Porins as Ion Selective Transporters and Single-Molecule Sensors. *J. Am. Chem. Soc.* **2020**, *142* (4), 1680–1685.

(57) Howorka, S. Building Membrane Nanopores. *Nat. Nanotechnol.* **2017**, *12* (7), 619–630.

(58) Howorka, S. DNA Nanotechnology: Bringing Lipid Bilayers into Shape. *Nat. Chem.* **2017**, *9* (7), 611–613.

(59) Diederichs, T.; Pugh, G.; Dorey, A.; Xing, Y.; Burns, J. R.; Hung Nguyen, Q.; Tornow, M.; Tampé, R.; Howorka, S. Synthetic Protein-Conductive Membrane Nanopores Built with DNA. *Nat. Commun.* **2019**, *10* (1), 1–11.

(60) Hall, A. R.; Scott, A.; Rotem, D.; Mehta, K. K.; Bayley, H.; Dekker, C. Hybrid Pore Formation by Directed Insertion of α-Haemolysin into Solid-State Nanopores. *Nat. Nanotechnol.* **2010**, *5* (12), 874–877.

(61) Bell, N. A. W.; Engst, C. R.; Ablay, M.; Divitini, G.; Ducati, C.; Liedl, T.; Keyser, U. F. DNA Origami Nanopores. *Nano Lett.* **2012**, *12* (1), 512–517.

(62) Wei, R.; Gatterdam, V.; Wieneke, R.; Tampé, R.; Rant, U. Stochastic Sensing of Proteins with Receptor-Modified Solid-State Nanopores. *Nat. Nanotechnol.* **2012**, *7* (4), 257–263.

(63) Fahie, M.; Chisholm, C.; Chen, M. Resolved Single-Molecule Detection of Individual Species within a Mixture of Anti-Biotin Antibodies Using an Engineered Monomeric Nanopore. *ACS Nano* **2015**, *9* (2), 1089–1098.

(64) Wu, H. C.; Bayley, H. Single-Molecule Detection of Nitrogen Mustards by Covalent Reaction within a Protein Nanopore. *J. Am. Chem. Soc.* **2008**, *130* (21), 6813–6819.

(65) Clarke, J.; Wu, H.; Jayasinghe, L.; Patel, A.; Reid, S.; Bayley, H. Continuous Base Identification for Single-Molecule Nanopore DNA Sequencing. *Nat. Nanotechnol.* **2009**, *4* (4), 265–270.

(66) Wang, G. L.; Zhang, B.; Wayment, J. R.; Harris, J. M.; White, H. S. Electrostatic-Gated

Transport in Chemically Modified Glass Nanopore Electrodes. *J. Am. Chem. Soc.* **2006**, *128* (23), 7679–7686.

(67) Fang, X. H.; Tan, W. H. Aptamers Generated from Cell-SELEX for Molecular Medicine: A Chemical Biology Approach. *Acc. Chem. Res.* **2010**, *43* (1), 48–57.

(68) Wilson, D. S.; Szostak, J. W. In Vitro Selection of Functional Nucleic Acids. *Annu. Rev. Biochem.* **1999**, *68*, 611–647.

(69) Bock, L. C.; Griffin, L. C.; Latham, J. A.; Vermaas, E. H.; Toole, J. J. Selection of Single-Stranded DNA Molecules That Bind and Inhibit Human Thrombin. *Nature* **1992**, *355*, 564–566.

(70) Soskine, M.; Biesemans, A.; Moeyaert, B.; Cheley, S.; Bayley, H.; Maglia, G. An Engineered ClyA Nanopore Detects Folded Target Proteins by Selective External Association and Pore Entry. *Nano Lett.* **2012**, *12* (9), 4895–4900.

(71) Gershow, M.; Golovchenko, J. A. Recapturing and Trapping Single Molecules with a Solid-State Nanopore. *Nat. Nanotechnol.* **2007**, *2* (12), 775–779.

(72) Langecker, M.; Pedone, D.; Simmel, F. C.; Rant, U. Electrophoretic Time-of-Flight Measurements of Single DNA Molecules with Two Stacked Nanopores. *Nano Lett.* **2011**, *11* (11), 5002–5007.

(73) Pud, S.; Chao, S. H.; Belkin, M.; Verschueren, D.; Huijben, T.; van Engelenburg, C.; Dekker, C.; Aksimentiev, A. Mechanical Trapping of DNA in a Double-Nanopore System. *Nano Lett.* **2016**, *16* (12), 8021–8028.

(74) Liu, X.; Zhang, Y. N.; Nagel, R.; Reisner, W.; Dunbar, W. B. Controlling DNA Tug-of-War in a Dual Nanopore Device. *Small* **2019**, *15* (30).

(75) Assad, O. N.; Gilboa, T.; Spitzberg, J.; Juhasz, M.; Weinhold, E. Light-Enhancing Plasmonic-Nanopore Biosensor for Superior Single-Molecule Detection. *Adv. Mater.* **2017**, *29*, 1–9.

(76) Huang, S.; Romero-Ruiz, M.; Castell, O. K.; Bayley, H.; Wallace, M. I. High-Throughput Optical Sensing of Nucleic Acids in a Nanopore Array. *Nat. Nanotechnol.* **2015**, *10* (11), 986–997.

(77) Cecchini, M. P.; Wiener, A.; Turek, V. A.; Chon, H.; Lee, S.; Ivanov, A. P.; McComb, D. W.; Choo, J.; Albrecht, T.; Maier, S. A.; Edel, J. B. Rapid Ultrasensitive Single Particle Surface-Enhanced Raman Spectroscopy Using Metallic Nanopores. *Nano Lett.* **2013**, *13*, 4602–4609.

(78) Larkin, J.; Henley, R. Y.; Jadhav, V.; Korlach, J.; Wanunu, M. Length-Independent DNA Packing into Nanopore Zero-Mode Waveguides for Low-Input DNA Sequencing. *Nat. Nanotechnol.* **2017**, No. September, 1–8.

(79) Hu, Y.; Xiang, J.; Liang, G.; Yan, H.; Lieber, C. M. Sub-100 Nanometer Channel Length Ge/Si Nanowire Transistors with Potential for 2 THz Switching Speed. *Nano Lett.* **2008**, *8* (3), 925–930.

(80) Cui, Y.; Wei, Q.; Park, H.; Lieber, C. M. Nanowire Nanosensors for Highly Sensitive and Selective Detection of Biological and Chemical Species. *Science* **2001**, *293* (5533), 1289–1292.

(81) Gao, N.; Gao, T.; Yang, X.; Dai, X.; Zhou, W.; Zhang, A.; Lieber, C. M. Specific Detection of Biomolecules in Physiological Solutions Using Graphene Transistor Biosensors. *Proc Natl Acad Sci U S A* **2016**, *113* (51), 14633–14638.

(82) Chaste, J.; Lechner, L.; Morfin, P.; Feve, G.; Kontos, T.; Berroir, J.-M.; Glattli, D. C.; Happy, H.; Hakonen, P.; Placais, B. Single Carbon Nanotube Transistor at GHz Frequency. *Nano Lett.* **2008**, *8* (2), 525–528.

(83) Nakatsuka, N.; Yang, K.; Abendroth, J. M.; Cheung, K. M.; Xu, X.; Yang, H.; Zhao, C.; Zhu, B.; Rim, Y. S.; Yang, Y.; Weiss, P. S.; Andrews, A. M. Aptamer – Field-Effect Transistors Overcome Debye Length Limitations for Small-Molecule Sensing. **2018**, *324* (October), 319–324.

(84) Elnathan, R.; Kwiat, M.; Pevzner, A.; Engel, Y.; Burstein, L.; Khatchtourints, A.; Lichtenstein, A.; Kantaev, R.; Patolsky, F. Biorecognition Layer Engineering: Overcoming Screening Limitations of Nanowire-Based FET Devices. *Nano Lett.* **2012**, *12* (10), 5245–5254.

(85) Patolsky, F.; Zheng, G.; Hayden, O.; Lakadamyali, M.; Zhuang, X.; Lieber, C. M. Electrical Detection of Single Viruses. *Proc. Natl. Acad. Sci. U. S. A.* **2004**, *101* (39), 14017–14022.

(86) Xue, L.; Cadinu, P.; Paulose Nadappuram, B.; Kang, M.; Ma, Y.; Korchev, Y.; Ivanov, A. P.; Edel, J. B. Gated Single-Molecule Transport in Double-Barreled Nanopores. *ACS Appl. Mater. Interfaces* **2018**, *10* (44), 38621–38629.

(87) Puster, M.; Balan, A.; Rodríguez-Manzo, J. A.; Danda, G.; Ahn, J. H.; Parkin, W.; Drndić, M. Cross-Talk Between Ionic and Nanoribbon Current Signals in Graphene Nanoribbon-Nanopore Sensors for Single-Molecule Detection. *Small* **2015**, *11* (47), 6309–6316.

(88) Traversi, F.; Raillon, C.; Benameur, S. M.; Liu, K.; Khlybov, S.; Tosun, M.; Krasnozhon, D.; Kis, A.; Radenovic, A. Detecting the Translocation of DNA through a Nanopore Using Graphene Nanoribbons. *Nat. Nanotechnol.* **2013**, *8* (12), 939–945.

(89) Heerema, S. J.; Vicarelli, L.; Pud, S.; Schouten, R. N.; Zandbergen, H. W.; Dekker, C. Probing DNA Translocations with Inplane Current Signals in a Graphene Nanoribbon with a Nanopore. *ACS Nano* **2018**, *12* (3), 2623–2633.

(90) Graf, M.; Lihter, M.; Altus, D.; Marion, S.; Radenovic, A. Transverse Detection of DNA Using a MoS 2 Nanopore Supporting Information. *Nano Lett.* **2019**.

(91) Nam, S. W.; Rooks, M. J.; Kim, K. B.; Rossnagel, S. M. Ionic Field Effect Transistors with Sub-10 Nm Multiple Nanopores. *Nano Lett.* **2009**, *9* (5), 2044–2048.

(92) Xue, L.; Ivanov, A. P.; Edel, J. B. Aptamer-Functionalized Nanopore Bio-Transistors for Selective Small Single-Moleculesensing. *Prep.* **2020**.

(93) Xie, P.; Xiong, Q.; Fang, Y.; Qing, Q.; Lieber, C. M. Local Electrical Potential Detection of DNA by Nanowire-Nanopore Sensors. *Nat Nanotechnol* **2011**, *7* (2), 119–125.

(94) Parkin, W. M.; Drndic, M. Signal and Noise in FET-Nanopore Devices. *ACS Sensors* **2018**, *3* (2), 313–319.

Chapter 2

Experimental Methods

Contents

2.1 Introduction 55
2.2 Laser-assisted pulling of nanopipettes 55
2.3 Selective pyrolysis of butane 57
2.4 Electrochemical fabrication of nanopore-FET devices and characterisation 58
2.4.1 Feedback-controlled deposition of gold 58
2.4.2 Characterisation of nanopore-FET devices 60
2.5 Surface functionalisation of deposited gold 60
2.5.1 Functionalisation with small organic molecules 61
2.5.2 Functionalisation with oligonucleotides 61
2.5.3 Electrochemical characterisation 62
2.6 Single-molecule translocation experiments 63
2.6.1 Solutions and reagents 63
2.6.2 Electrochemical configuration 63
2.7 References 68

2.1 Introduction

The fabrication of nanopore-FET sensors consists of laser pulling, pyrolysis of butane, electrochemical deposition of gold and surface functionalisation by thiolated species. Nanopore experiments were conducted using fabricated sensors. This chapter will provide detailed methodologies for sensor fabrication and single-molecule detection using nanopore-FET sensors optimised over the course of this PhD work.

2.2 Laser-assisted pulling of nanopipettes

Quartz nanopipettes are preferred over conventional solid-state nanopores and biological nanopores mainly because of the ease of fabrication. Laser-assisted pulling of quartz capillaries is more efficient and less expensive than e-beam drilling of a solid-state membrane. Moreover, the chemical and physical stability of quartz are advantageous compared to conventional biological nanopores and supported lipid bilayers. Prior to laser pulling, all quartz capillaries were cleaned in a plasma cleaner (Harrick) for half an hour to remove any organic contaminants present on the surface. Similar to fabricating single-barrel nanopipettes, dual-barrel nanopipettes were fabricated from double-barrel theta quartz capillaries (Friedrich & Dimmock, Inc.; 1.2 mm outside diameter × 0.90 mm inside diameter × 100 mm length) using a P-2000 laser puller (Sutter Instruments). Detailed pulling parameters and their definitions are shown below. By using a set of custom-made pulling parameters developed in-house[1–3], the established protocol can be used to fabricate dual-barrel nanopipettes with a diameter ranging from 50 to 100 nm across each barrel. It should be noted that the pulling parameters are device-specific and are sensitive to variations in humidity and temperature.

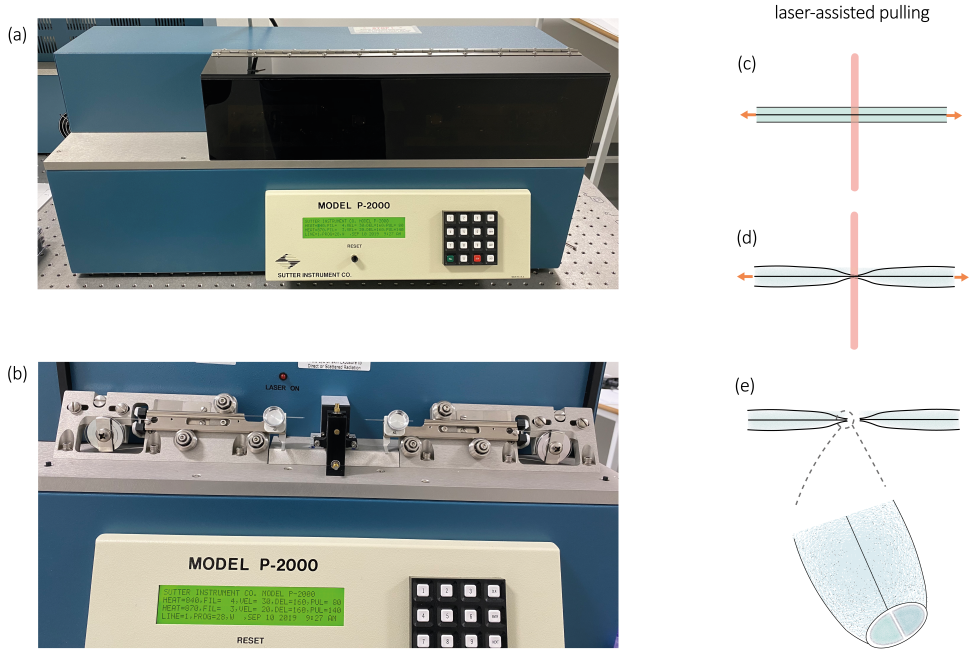


Figure 2-1: Schematic demonstration of laser-assisted pulling processes. (a) Overview of a P-2000 laser puller (Sutter Instruments, USA). (b) After laser-assisted pulling, a pair of nanopipettes were fabricated. Details of the two-line laser pulling protocol: In the first line, (c) the laser beam locally heats the centre of a theta quartz capillary and then deactivates, followed by pulling on both ends to produce (d) a taper in the middle. (e) The second line generates additional heat which melts the taper, and a hard pull results in a pair of dual-barrel nanopipettes.

(1) Heat: output power of the laser used to heat the middle of quartz capillaries. It defines the amount of energy supplied to the middle of the capillary.
(2) Filament: this parameter sets the scanning pattern of the laser, including longitudinal scanning length and rate of scan.
(3) Velocity: the velocity at which the pulling bar must be moving before the hard pull of the capillary to produce a pair of nanopipettes.
(4) Delay: the time interval between the deactivation of the laser and the hard pull.
(5) Pull: the force of the hard pull.

	Heat	Filament	Velocity	Delay	Pull
Line 1	840	4	30	160	80
Line 2	870	3	20	160	140

Table 2-1: Detailed settings for the protocol for pulling dual-barrel nanopipettes. The first line results in a taper in the middle of the capillary, and the second line produces a pair of nanopipettes.

2.3 Selective pyrolysis of butane

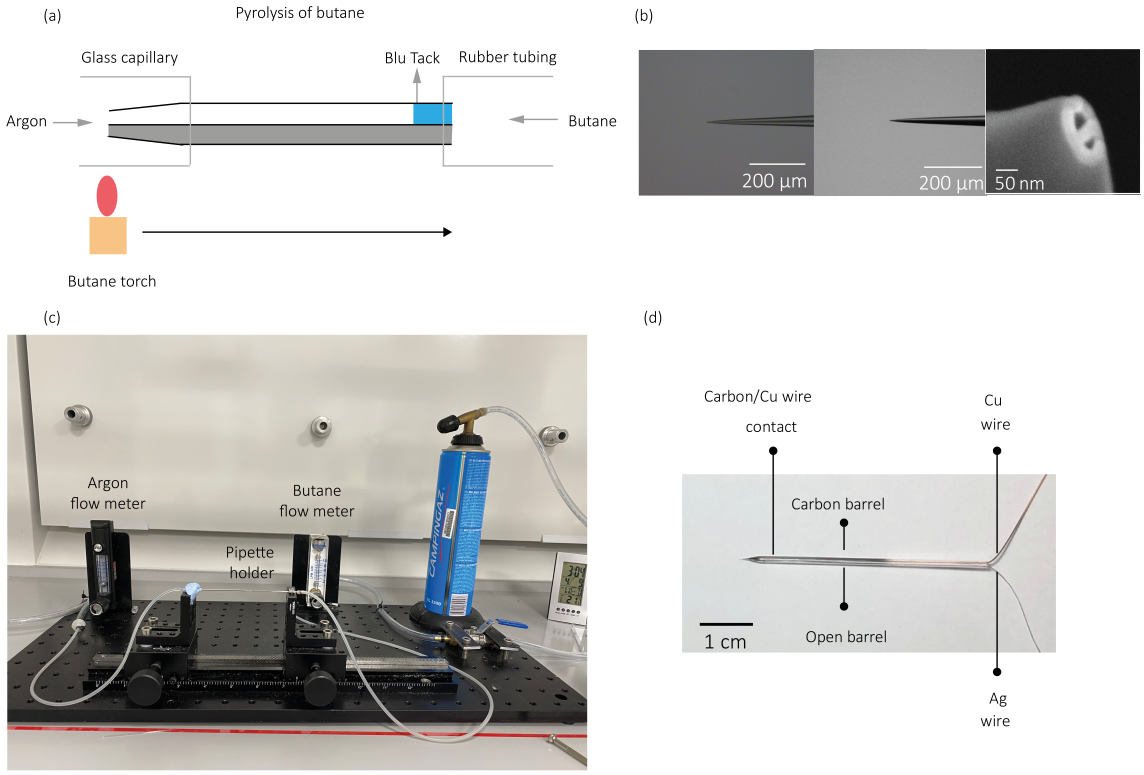


Figure 2-2: Pyrolysis of butane. (a) Schematic illustration of the experimental set-up for pyrolytic deposition of carbon. Butane was passed through one barrel via silicon tubing while the other barrel of the nanopipette was sealed. A butane torch was used to heat the tip of the pipette for pyrolytic deposition of carbon under argon flow to prevent further oxidation of the deposited carbon. A heating time of 35 s was chosen to produce an extensive filament of amorphous carbon through one barrel while leaving the other barrel open. (b) Bright-field micrographs show a change in contrast between a dual-barrel nanopipette before (left) and after (middle) carbon deposition and an SEM image (right) of a dual-barrel nanopipette before carbon deposition. (c) Photo of the set-up for pyrolytic deposition of

carbon. The flowrates of argon and butane were monitored by the two flow meters labelled in the photo. The dual-barrel nanopipette was mounted on the holder first and moved inside the argon tubing to prepare for carbon deposition. (d) Schematic visualisation of the electrical contact in a dual-barrel nanopipette with one barrel filled with carbon. The deposited carbon extends up to ~60% of the length of the nanopipette barrel. However, only the section at the taper of the nanopipette is extensively filled with carbon. The pyrolytic carbon is mostly deposited on the inner walls of the barrel to form a carbon layer. A copper wire was inserted into the carbon barrel so that it is embedded into the bottom section just above the taper directly contacting the deposited carbon.

To selectively deposit carbon in one barrel of the nanopipette while leaving the other barrel open, one barrel of the freshly pulled dual-barrel nanopipettes was filled with Blu Tack (Bostik), and the other barrel remained sealed. Using the set-up shown in Figure 2-2, butane was selectively passed into one barrel only. Pyrolysis was induced by directing the butane flame from the torch. The butane was thermally decomposed to produced amorphous carbon and carbon dioxide. Note that the black colour of the carbon could be visually distinguished immediately upon igniting the flame. Furthermore, the flame temperature of butane is lower than the softening temperature of the quartz so that the nanopore was not closed during pyrolysis.[4,5] All nanopipettes were freshly prepared on the day of the experiments and stored in a sealed petri dish until use.

2.4 Electrochemical fabrication of nanopore-FET devices and characterisation

2.4.1 Feedback-controlled deposition of gold

Controllable gold deposition on a nanoscale is a prerequisite for the electrochemical fabrication of nanopore-FET devices. In contrast to conventional methods for gold deposition using auric chloride or gold cyanide, the electroplating solution (ECF64D, Metalor Technologies) containing gold sulphite (pH ~10) was used here as it is much less toxic and corrosive.[6,7] The electrodeposition of gold on the surface of the electrode occurs as a two-step process via the absorption of the dissociation of the gold (I) complex on the electrode surface and the reduction of the absorbed gold (I).

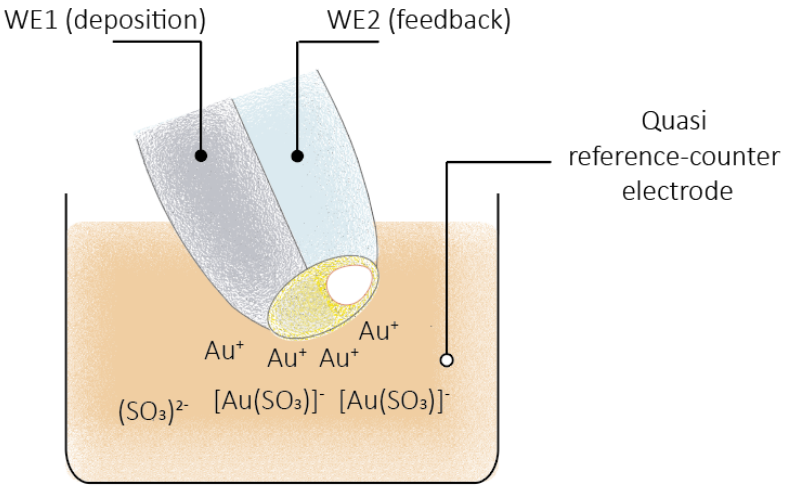


Figure 2-3: Schematic of the electrochemical set-up of feedback-controlled gold deposition. Two working electrodes (WEs) were placed in the carbon barrel and the open barrel, filled with the appropriate supporting electrolyte, with a quasi-reference counter electrode (QRCE) in the plating bath. A reducing potential was held at the first WE. Importantly, a potential difference of -0.1 V between the second WE and QRCE was used as feedback.

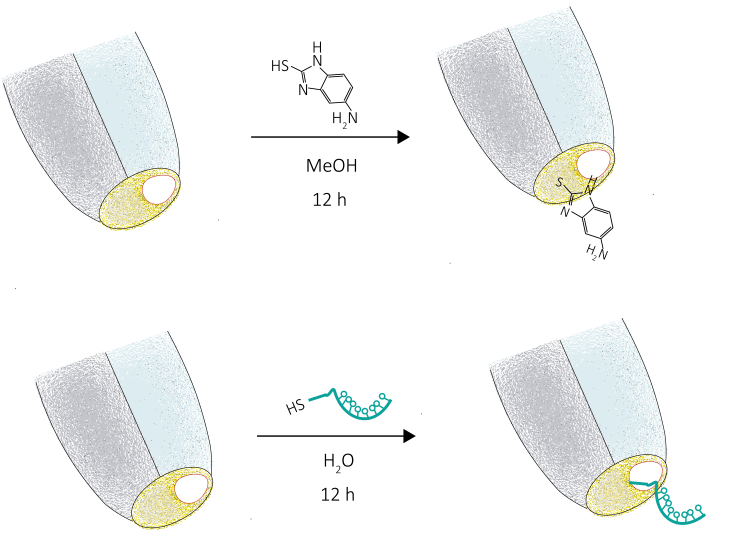
A bipotentiostatic configuration (Figure 2-3) was used to perform electrodeposition of gold on the carbon electrode using a CHI 760 C potentiostat (CH Instruments). A 10-fold diluted ECF64D (Metalor Technologies) plating solution containing 4.4 mM NH_4AuSO_3 in 52 mM $(NH_4)_2SO_3$ was used to fill the plating bath. To establish electrical contact with the carbon electrode, a 0.25 mm diameter copper wire (Goodfellow) was inserted into the carbon barrel. Because of the instability of AgCl in ECF64 (amine complexation), a 0.125 mm diameter Ag wire (Goodfellow) was chosen for both the working electrode inside the open barrel and the quasi-reference counter electrode (QRCE) and verified to be stable in the plating solution by potentiometry measurements. A potential of −0.73 V (vs QRCE) was held at the carbon electrode to reduce the gold from the plating solution. Meanwhile, a potential difference of −0.1 V was applied between the second WE and the QRCE, to monitor in real-time the ionic current flowing through the open barrel filled with 52 mM $(NH_4)_2SO_3$. Notably, a low voltage was chosen to minimise the possible interference with the deposition process.

2.4.2 Characterisation of nanopore-FET devices

Before and after deposition, cyclic voltammetry (−0.5 to 0.5 V, scan rate 0.05 V/s, sampling interval 0.02 V) of the second WE was performed to extract the change of conductance. After deposition, the open barrel was rinsed with water to minimise contamination. To avoid salt crystallisation at the tip, all nanopipettes were stored in a sealed vial filled with deionised water until use.

Capacitance measurements were performed using a three-electrode configuration on a Gamry Reference 600 potentiostat, with deposited gold as the working electrode. An Ag/AgCl electrode was used as the reference electrode. The counter electrode was a Pt wire (Goodfellow). Differential capacitance versus potential curves was obtained by impedance measurements at varying direct current potentials in the presence of a small 10 mV, peak-to-peak alternating current perturbation at a constant frequency of 10 Hz for the gold-deposited electrode and 500 Hz for the amine-functionalised electrode.

2.5 Surface functionalisation of deposited gold



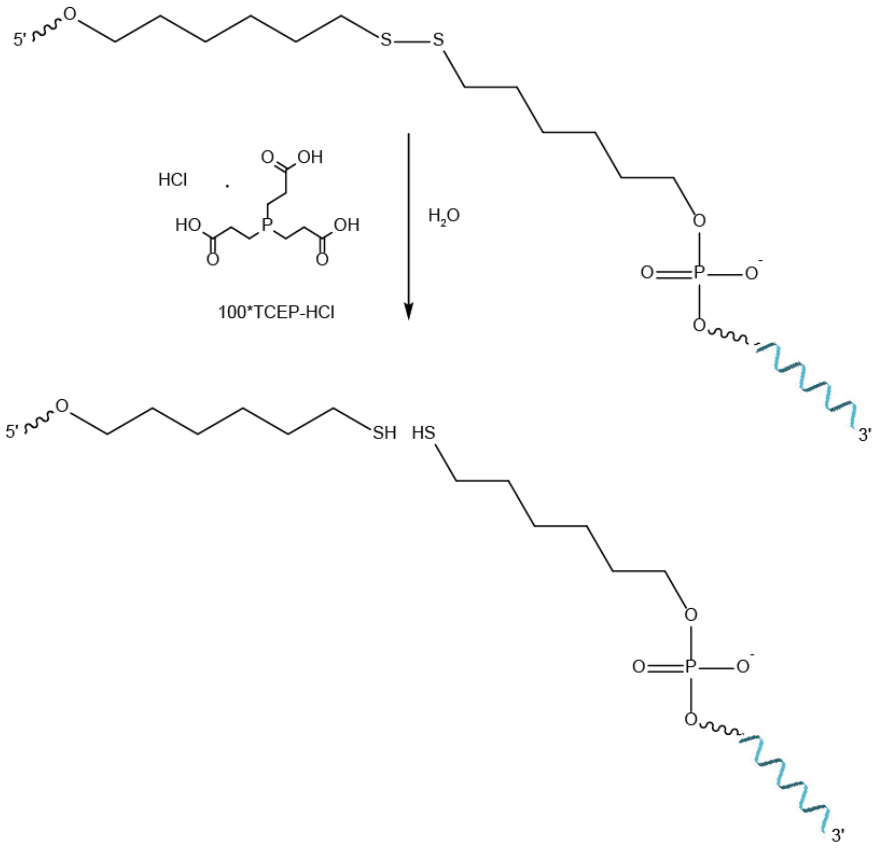
Scheme 2-1: Surface functionalisation of deposited gold. Thiolated small molecules can be attached to the gold surface. Methanol was used as the solvent as it solubilises most organic molecules and simultaneously encourages the wetting of the nanopore surface. Modification with thiolated oligos was performed in DI water because it fully wets the nanopore and solubilises thiol-modified oligos.

2.5.1 Functionalisation with small organic molecules

As gold can easily be functionalised via self-assembly of thiolated species, different types of functionalising agents have been used to modify gold. In this thesis, gold was modified by either small organic molecules possessing different charges or by oligonucleotides. For the modification with small organic molecules, gold-deposited nanopipettes were rinsed with acetone and methanol to remove any surface contaminants from the plating solution. The open barrel was filled with the corresponding solvent during rinsing followed by immersing the pipettes in a 5 mM solution of the functionalising agent in methanol. As the gold-deposited nanopipettes were stored in DI water until functionalisation, methanol was chosen as the solvent because it is miscible with water and solubilises most of the organic molecules. Prior to the DNA translocation experiments, the open barrels of the functionalised nanopipettes were washed with methanol and water to remove any remaining thiol that had diffused into the open barrels during functionalisation. All nanopipettes were freshly functionalised one day before use and used only once for translocation experiments.

2.5.2 Functionalisation with oligonucleotides

In addition to small molecules, gold can be functionalised with oligonucleotides. Thiol-modified oligos were purchased with the addition of the thiol modifier C6 S-S on the 5' end. An aqueous 2 µM solution of thiol-modified oligonucleotides (Integrated DNA Technologies) were treated with a 100-fold excess of tris(2-carboxyethyl)phosphine (TCEP, Thermo Scientific) and gently mixed for three hours before use to deprotect the disulfide bonds (Scheme 2-2). Prior to functionalisation, the open barrels of the gold-deposited pipettes were rinsed with H_2O. The pipettes were then bathed in the resulting solution for 12 h resulting in the attachment of thiol modified oligos to the gold. Before the translocation experiments, the open barrels were rinsed with H_2O to remove any remaining thiols within the pipettes.



Scheme 2-2: Deprotection of disulfide bonds using TCEP. Thiol-modified oligos protected with a C6 S-S modifier were treated with 100-fold molar excess of TCEP to form reactive-thiol oligos that can be attached to the surface of gold through thiol-gold self-assembly. The surface of the gold was modified by the oligonucleotide with a C6 spacer linked in between.

2.5.3 Electrochemical characterisation

To systematically characterise the functionalisation of the gold nanopore, I-clamp measurements were performed to extract the information on nanopore conductance and rectification from the nanopore I-Vs. As nanopores of similar diameter already exhibited ion selectivity[8], I-clamp measurements were completed to reveal the change in nanopore surface charge.

2.6 Single-molecule translocation experiments

2.6.1 Solutions and reagents

Different solutions of analytes were prepared by serial dilution from a known stock concentration (10 kbp DNA, New England Biolabs, 500 µg/mL; human α-thrombin, Invitrogen, RF43100, 6.6 mg/mL, 50% water, 50% glycerol; dopamine, Sigma-Aldrich; serotonin hydrochloride, Fluorochem; acetylcholine chloride, Sigma-Aldrich). All stock solutions were stored in a freezer and freshly prepared before the experiments. Nuclease-free water (Integrated DNA Technologies) was used as the solvent for all solutions.

Electrolyte solutions of different concentrations (1 M, 100 mM, 50 mM and 10 mM KCl) were prepared in 10 mM tris and 1 mM EDTA buffer at pH 8. Before the translocation experiments, all solutions were filtered using a 0.2 µm filter (Millipore, UK) to remove any insoluble impurities that might interfere with the nanopore experiments. The prepared solutions were injected into the nanopipettes using a 0.2 mm Microfil needle (World Precision Instruments).

2.6.2 Electrochemical configuration

As the ionic current flowing through the nanopore under different electrolyte conditions ranges from pA to nA, translocation experiments were recorded using a Multiclamp 700B amplifier (Molecular Devices, USA). The recorded data were digitised using an Axon Digidata 1550B. The experimental data were recorded using the pClamp 10.6 software (Molecular Devices). Freshly chlorodised Ag/AgCl wires were used as working electrodes in the barrels and as the reference/counter electrode in the bath to the ionic currents using the electrochemical reactions specified below:

$$\text{Cathode: } AgCl + e^- \rightarrow Ag + Cl^-$$

$$\text{Anode: } Ag + Cl^- \rightarrow AgCl + e^-$$

Scheme 2-3: Electrochemical reactions on the surface of Ag/AgCl electrodes.

2.6.3 Data analysis

Data analysis was performed using a custom Matlab nanopore app developed in-house by Prof. Joshua Edel. The code enables the identification and analysis of each individual event. Based

on the ionic currents recorded using the Multiclamp amplifier, the baseline current was calculated for every X data points. The baseline threshold was set equal to or higher than six standard deviations. Any peaks above the threshold were identified as translocation events, and the statistics of translocation events were extracted and analysed.[3,9]

Step 1: Data loading, baseline fitting and identification of translocation peaks

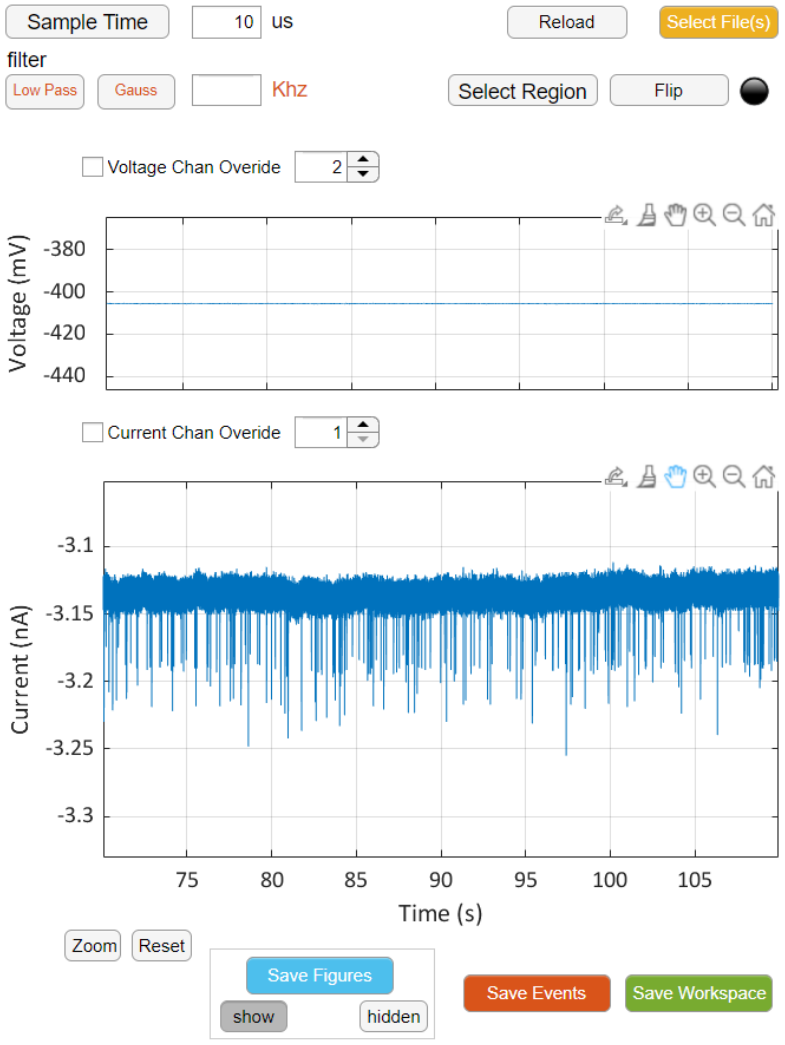


Figure 2-4: User interface for the nanopore app when loading the raw data from Clampfit. After loading the raw data as an ABF file from Clampfit, the output was generated as applied voltage across the nanopore and the resulting ionic current.

Initially, the raw data from Clampfit were loaded into the Nanopore App. The baseline current was then fitted by a moving window average for every X data points. This was defined by steps in the baseline fitting tab. The longer the step, the rougher the fitted baseline is. For current

recordings with more baseline fluctuations and noise, a much longer step, higher poly 1 and lower poly 2 are preferred since these fitting parameters pick up less noise and random fluctuations of the baseline. The current trace was baseline-adjusted with reference to the fitted baseline. Therefore, the all-point histogram of the adjusted trace reveals different current levels that correspond to the baseline, unfolded DNA translocation and folded DNA translocation, respectively. As different current levels are well defined, a standard deviation (std) can be set to ensure all peaks for single-molecule translocations were detected correctly. The baseline current was fitted by a Gaussian distribution as shown in Figure 2-5 to identify the threshold. The std was set to slightly above the threshold in order to recognise all translocation events.

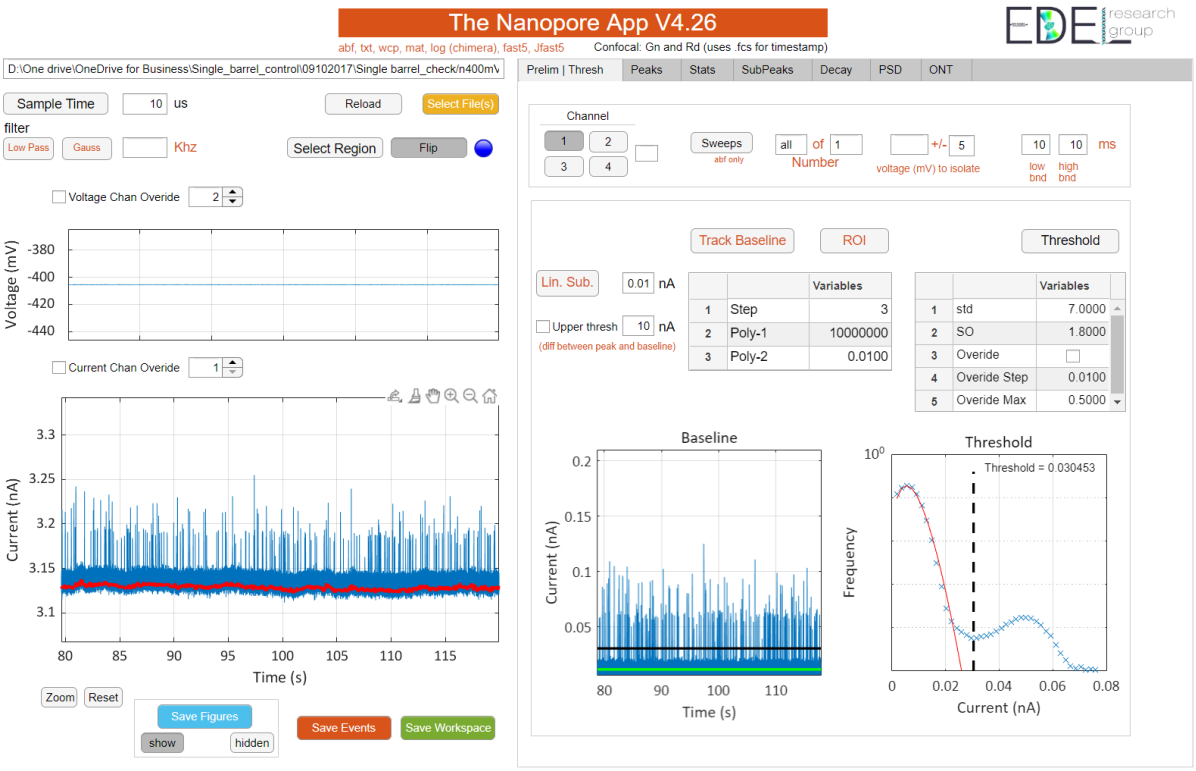


Figure 2-5: Baseline fitting using the Nanopore App. The current trace was flipped and then fitted by a Gaussian distribution function, with adjustable steps and two different polynomial factors. This was followed by defining a standard deviation relative to the fitted baseline. Determining the standard deviation was aided by fitting all points on the histogram of the current trace with a Gaussian function. In this case, three different peaks were found, which correspond to the baseline noise and folded and unfolded single-molecule DNA translocations. Therefore, the standard deviation was set to detect all

translocation peaks correctly by placing it between the boundary of the baseline current and the unfolded translocation peaks.

Step 2: Accumulating single-molecule statistics

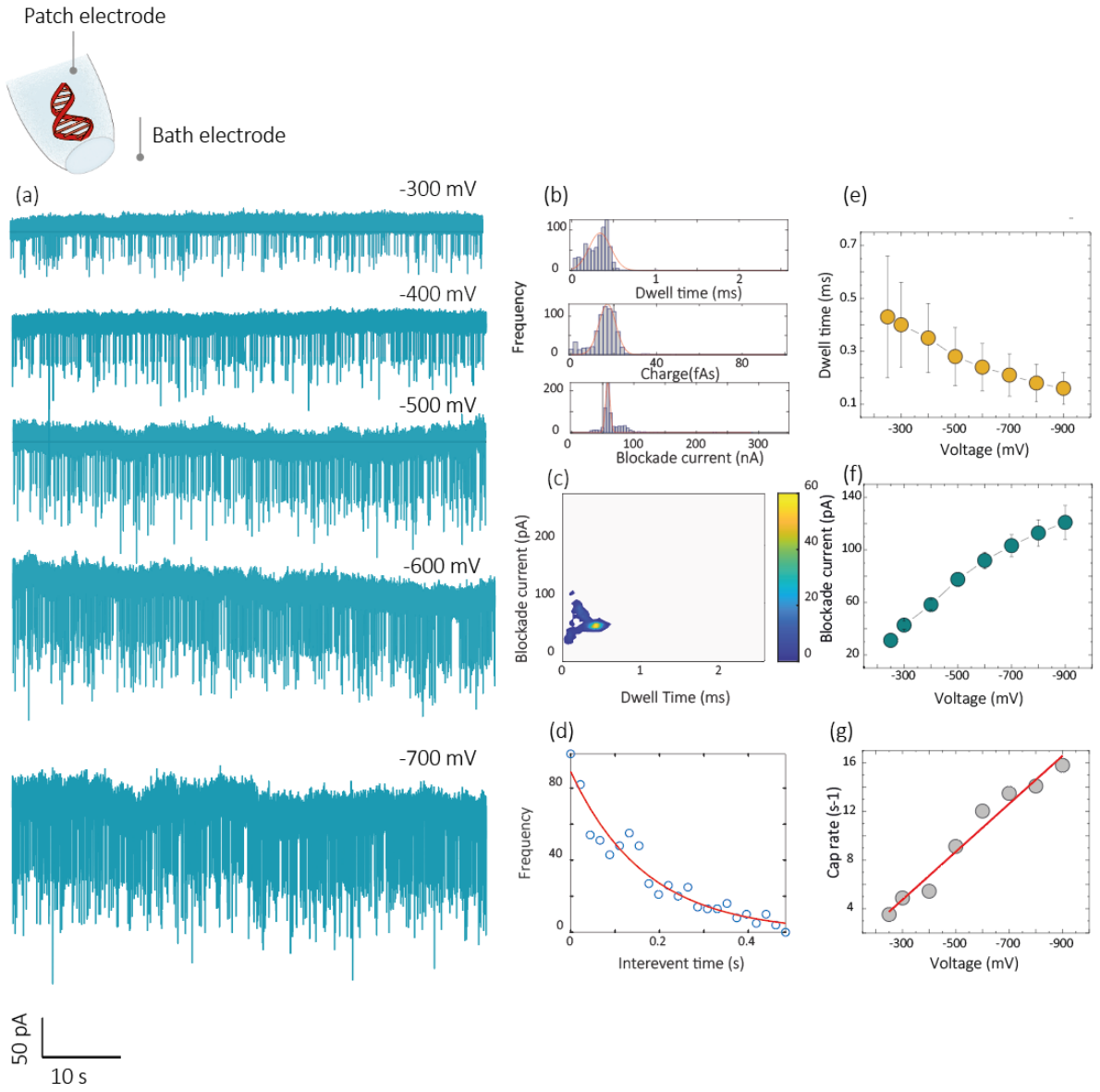


Figure 2-6: Single-molecule detection of 10 kbp DNA using nanopipettes, with the patch electrode (working) in the pipette and the bath electrode (reference/ground) in the KCl bath (100 mM KCl, 10 mM Tris and 1 mM EDTA at pH 8) and 400 pM of 10 kbp DNA added in the nanopipette. (a) Under negative potential, single-molecule translocation of DNA happens from inside the nanopipette to the

KCl bulk solution. The representative current traces are shown from -300 to -700 mV. (b) From the single-molecule statistics extracted and accumulated by the nanopore app, the distribution of dwell time, equivalent charge and blockade current at -400 mV is summarised in the histograms. (c) A 2D heat map demonstrates the distribution of the blockade current versus dwell time. (d) The stochastic nature of single-molecule DNA translocation was confirmed by the exponential fitting of the interevent time, obtaining a 5.94 s^{-1} capture rate. The utility of nanopipettes for single-molecule detection of 10 kbp DNA was established by the voltage dependence of (e) dwell time, (f) blockade current and (g) capture rate. As the single-molecule translocation becomes faster, there is a larger current modulation resulting in more events being captured.

Examples of translocation traces for 10 kbp DNA at -400 mv are shown in Figure 2-6 a. Single-molecule translocation of DNA is revealed as downward spikes for current enhancement. For individual events, representative examples in Figure 2-6 a demonstrate the discrete modulation of ionic current due to the translocation of a single DNA molecule.

To accumulate the statistics at the single-molecule level, the distribution of dwell time and blockade current was fitted by the Nanopore App using a Gaussian distribution (Figure 2-6 b-c). In some cases, a Ling distribution was used with the details shown below:

$$F(t) = \frac{L}{\sqrt{4\pi D t^3}} e^{\frac{-(L-vt)^2}{4Dt}} \qquad \text{Equation 3}$$

In this equation, L is the contour length of DNA, D is the diffusion coefficient, and v is the DNA drift velocity.

In this example of the translocation of 10 kbp DNA across a single-barrel nanopipette at -400 mV, the value of dwell time was fitted as 0.35 ± 0.13 ms, closely matching the literature values for a single-barrel nanopipette with a similar pore diameter as reported by Sze et al. and Gong et al. Assuming a maximum-extended contour length of 3.4 µm for 10 kbp DNA, the translocation velocity was calculated to be 9.7 mm/s, agreeing with the values reported by Li et al.[10] and Gong et al.[11] Note that this model assumes the DNA is fully extended in the electrolyte solution. In reality, hydrogen bonding and hydrophobic effects will cause different base pairs to preferentially stack together.

From the statistics for single-molecule translocation events, the blockade current was obtained as 56.5 ± 8.1 pA; the excluded charge for each translocation event can be calculated by integration with time (17.5 ± 4.0 fAs). Furthermore, a 2D plot of blockade current vs dwell time

is summarised in Figure 2-6 c. Most DNA translocations were occurred in one population centred around the highlighted region.

The single-molecule translocation studies were performed with increasing voltage. As expected, dwell times were found to decrease with voltage while the blockade current increased with more translocation events being captured, meaning that the nanopipette is promising for single-molecule detection of DNA.

2.7 References

(1) Xue, L.; Cadinu, P.; Paulose Nadappuram, B.; Kang, M.; Ma, Y.; Korchev, Y. E.; Ivanov, A. P.; Edel, J. B. Gated Single-Molecule Transport in Double-Barreled Nanopores. *ACS Appl. Mater. Interfaces* **2018**, *10* (44), 38621–38629.

(2) Cadinu, P.; Campolo, G.; Pud, S.; Yang, W.; Edel, J. B.; Dekker, C.; Ivanov, A. P. Double Barrel Nanopores as a New Tool for Controlling Single-Molecule Transport. *Nano Lett.* **2018**, *18* (4), 2738–2745.

(3) Cai, S.; Sze, J. Y. Y.; Ivanov, A. P.; Edel, J. B. Small Molecule Electro-Optical Binding Assay Using Nanopores. *Nat. Commun.* **2019**, *10* (1).

(4) Actis, P.; Tokar, S.; Clausmeyer, J.; Babakinejad, B.; Mikhaleva, S.; Cornut, R.; Takahashi, Y.; López Córdoba, A.; Novak, P.; Shevchuck, A. I.; Dougan, J. A.; Kazarian, S. G.; Gorelkin, P. V.; Erofeev, A. S.; Yaminsky, I. V.; Unwin, P. R.; Schuhmann, W.; Klenerman, D.; Rusakov, D. A.; Sviderskaya, E. V.; Korchev, Y. E. Electrochemical Nanoprobes for Single-Cell Analysis. *ACS Nano* **2014**, *8* (1), 875–884.

(5) Ren, R.; Zhang, Y.; Nadappuram, B. P.; Akpinar, B.; Klenerman, D.; Ivanov, A. P.; Edel, J. B.; Korchev, Y. Nanopore Extended Field-Effect Transistor for Selective Single-Molecule Biosensing. *Nat. Commun.* **2017**, *8* (1), 586.

(6) Osaka, T.; Kato, M.; Sato, J.; Yoshizawa, K.; Homma, T.; Okinaka, Y.; Yoshioka, O. Mechanism of Sulfur Inclusion in Soft Gold Electrodeposited from the Thiosulfate-Sulfite Bath. *J. Electrochem. Soc.* **2001**, *148* (10), C659–C662.

(7) Rutkowska, A.; Freedman, K. J.; Skalkowska, J.; Kim, M. J.; Edel, J. B.; Albrecht, T. Electrodeposition and Bipolar Effects in Metallized Nanopores and Their Use in the Detection of Insulin. *Anal. Chem.* **2015**, *87* (4), 2337–2344.

(8) Rollings, R. C.; Kuan, A. T.; Golovchenko, J. A. Ion Selectivity of Graphene Nanopores. *Nat. Commun.* **2016**, *7*, 11408.

(9) Sze, J. Y. Y.; Ivanov, A. P.; Cass, A. E. G.; Edel, J. B. Single Molecule Multiplexed Nanopore Protein Screening in Human Serum Using Aptamer Modified DNA Carriers. *Nat. Commun.* **2017**, *8* (1), 1552.

(10) Li, J.; Gershow, M.; Stein, D.; Brandin, E.; Golovchenko, J. A. DNA Molecules and Configurations in a Solid-State Nanopore Microscope. *Nat. Mater.* **2003**, *2* (9), 611–615.

(11) Gong, X.; Patil, A. V.; Ivanov, A. P.; Kong, Q.; Gibb, T.; Dogan, F.; Demello, A. J.; Edel, J. B. Label-Free in-Flow Detection of Single DNA Molecules Using Glass Nanopipettes. *Anal. Chem.*

2014, *86* (1), 835–841.

Chapter 3

Controlled Fabrication of nanopore-FET devices

Contents

Abstract 71

3.1 Introduction 72

3.1.1 General background 72

3.1.2 Electrodeposition 73

3.1.3 Cyclic voltammetry 74

3.1.4 Chronoamperometry 75

3.2 Aims and objectives 76

3.3 Results and discussion 77

3.3.1 Deposition mechanism and voltammetry characterisation 77

3.3.2 Real-time ion current feedback 79

3.3.3 Surface characterisation 84

3.4 Conclusion 86

3.5 References 87

Abstract

This chapter presents a novel and straightforward method for the controlled fabrication of nanopore-FET devices, namely feedback-controlled electrochemical deposition of gold. Based on a dual-barrel nanopipette consisting of a carbon-filled barrel and an open barrel, a bipotentiostatic configuration was developed to controllably deposit gold by monitoring the real-time ion current feedback and to address the alignment between the nanopore and FET components. Furthermore, nanopore conductance was demonstrated to be precisely controlled by terminating gold deposition at a pre-set threshold for the feedback current. The fabricated devices were characterised by dark-field microscopy, SEM and TEM.

3.1 Introduction

3.1.1 General background

Fabricating conventional nanopore-FETs based on solid-state nanopores consists of advanced electron beam and lithography techniques, which increase the complexity, time and cost. This is further compounded by the prerequisite that the nanopore and FET components must be precisely aligned.[1,2] In recent years, the emergence of dual-barrel nanopipettes for single-molecule detection has sparked a range of research interests inspired by the pioneering work on scanning ion conductance microscopy and scanning electrochemical microscopy.[3,4] In a dual-barrel nanopipette configuration, two adjacent nanopores can be closely separated by a 20 nm septum. This allows the coupling of two nanopores for synergistic purposes from the advances of nano-fabrication techniques. This chapter explores the integration of nanopores and FET components using a dual-barrel nanopipette platform.

To fabricate nanopore-FETs using dual-barrel nanopipettes, one barrel must act as an electrode to control the single-molecule detection using the other barrel. The basic device design consists of one barrel selectively filled with carbon while leaving the other barrel open. Although promising advances have been made in monitoring pH[5], cellular uptake[6] and even delivery of chemical species into cells[7], the separation between the carbon nanoelectrode and the nanopore by a septum of 20 nm is still a limitation for nanopore-FET functionality in near-physiological conditions. Ideally, the controlling component in the nanopore-FET (i.e. the gate electrode) must be present in or around the nanopore to facilitate the voltage gating. Different surface modification strategies can be used to incorporate the controlling component closer to the nanopore opening. Electrodeposition of metal is preferred because of the ease of operation using a potentiostat. More importantly, the presence of the open barrel next to the carbon nanoelectrode allows for the monitoring of the metal deposition using the deposition current from the nanoelectrode and the ion current flowing through the nanopore simultaneously.

3.1.2 Electrodeposition

Electrodeposition is a technique that uses an electrical current on the surface of an electrode to reduce metal cations in the electrolyte. This is a versatile method used in semiconductor industries, nanotechnology and corrosion protection.[8,9] Compared with other methods to fabricate nanopore field-effect transistors using electron-beam lithography that require cleanroom facilities, electrodeposition can be performed at room temperature using an electrochemical workstation enabling easier and more efficient operation.

The detailed mechanism of electrodeposition is shown in Figure 3-1. Metal ions in the bulk plating electrolyte migrate towards the surface of the electrode under a reducing potential relative to the counter/reference electrode in the plating bath. Once the metal ions have diffused into the electrical double layer, the hydration layer around the metal cations is partially detached to enable absorption onto the electrode surface. Electron transfer from the electrode to the metal cations occurs for the reducing metal cations. Overall, the metal deposition on the surface of the electrode can be classified into two different phases, nucleation and outward growth.

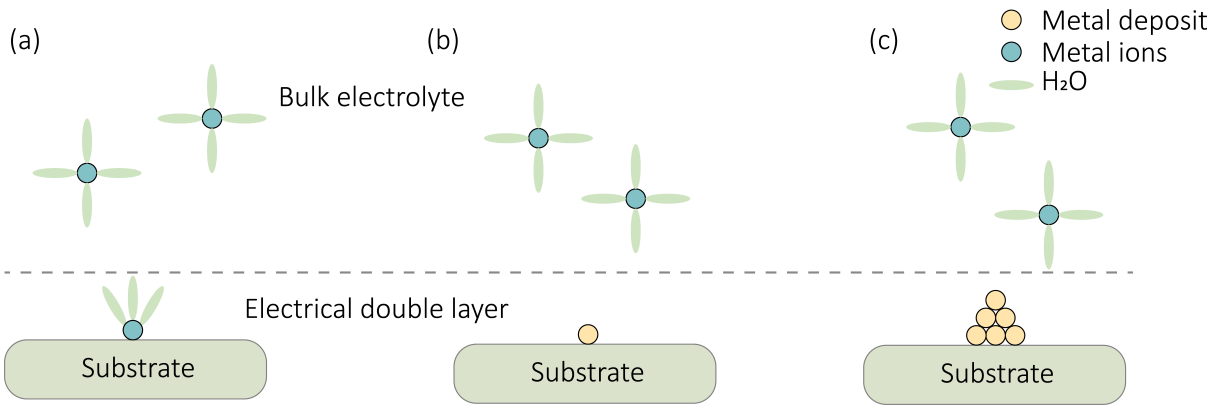


Figure 3-1: Schematic demonstration of electrodeposition. A reducing potential is applied to the substrate. (a) The hydrated metal ions migrate from the bulk electrolyte into the electrical double layer and absorb onto the surface of the electrode with a partial detachment of the hydration layer. (b) Electron transfer from the substrate onto the absorbed metal ions occurs to reduce the metal cations with a positive valency to a zero valency. This process is repeated to form the seed on the surface of the electrode (i.e. nucleation). (c) The deposition of metal can be accelerated based on the nucleated metal deposit, which increases the active electrode area.

3.1.3 Cyclic voltammetry

Among the different methods to investigate electrochemical phenomena on electrode surfaces, cyclic voltammetry is a widely used technique in which the potential of the electrode is swept between a cathodic potential (E_c) and an anodic potential (E_a) at a constant scan rate. The resultant faradic current is produced by different electrode processes including reduction and oxidation on the surface of electrode. As such, cyclic voltammetry is a useful tool to explore the reduction and oxidation of the molecular species on the electrode. Particularly for electrodeposition, the range of potentials used for depositing metals can be determined based on the characteristics of the electrochemical currents.[10,11]

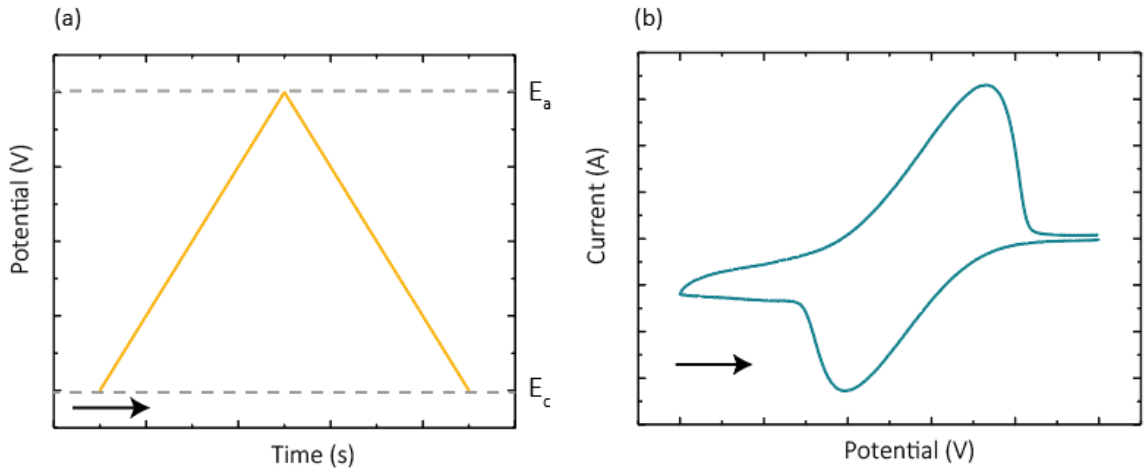


Figure 3-2: Schematic demonstration of cyclic voltammetry. (a) The potential is swept between the anodic potential (E_a) and cathodic potential (E_c) at a constant scan rate. (b) The resulting voltammogram shows peaks in the positive and negative scan directions, corresponding to oxidation and reduction of the electroactive species, respectively. For a reversible electrochemical process, the middle point of the two redox peaks is the equilibrium potential. In both figures, black arrow indicates the initial scan direction.

The typical shape of a cyclic voltammogram results from an interplay of electrode reactions and diffusion-controlled processes. Considering the electrochemical reduction of $O + e^- \rightarrow R$, if the rate of consumption for *O* at the electrode surface is always greater than the diffusion rate of *O* from the bulk solution into the electrical double layer; this process is diffusion-controlled. Moreover, there is a linear concentration gradient of *O* within the electrical double layer compared to the bulk solution.

Upon sweeping in the cathodic direction, the potential at which *O* is reduced, the surface concentration of *O* is reduced. The concentration gradient of *O* is increased, and thus the current measured from the electrode, which is proportional to the flow of *O* towards the electrode surface. Further sweeping of the potential decreases the surface concentration of *O* to zero. At this point, the reduction of product *R* starts to build up, causing a decrease of the electrochemical current. This 'consumption-build-up' process gives rise to the shape of the peaks on cyclic voltammograms. A backward sweep in the anodic direction produces a similar shape as in the forward case. However, the shape of the electrode can influence the peaks on cyclic voltammograms as well.

3.1.4 Chronoamperometry

Chronoamperometry is an electrochemical method in which a step change of potential is applied to the electrode. The response of the electrode is recorded as current plotted against time. Compared to cyclic voltammetry, this method is more straightforward for quantifying and monitoring metal deposition processes, as the working potential is constant during the experiments.

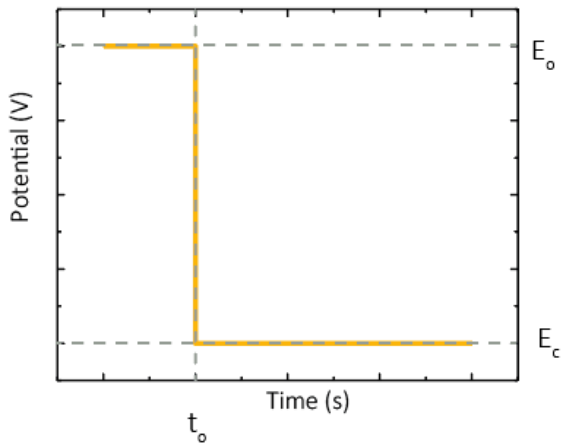


Figure 3-3: Schematic demonstration of chronoamperometry. A constant potential of E_0 is held at the electrode until the start of the experiment at time t_0. The voltage is switched to a constant value (E_c) and held constant over time. The typical response of the chronoamperometric current is not listed in this figure as it depends on multiple parameters.

Initially, the electrode is held at a constant potential (E_0). At t=0, the potential is switched to a constant value of E_c. The response of the electrode can be divided into two different aspects,

the capacitance due to the charging of the electrical double layer and the electron transfer reaction for the reduction or oxidation of electroactive species. This can be partially interpreted by the Cottrell equation shown below for an ideal planar electrode:

$$i = \frac{nFAC\sqrt{D}}{\sqrt{t\pi}} \qquad \text{(Equation 3.1)}$$

In this equation, i is the current, t is the time, F is the Faraday constant, A is the electrochemically active area of the electrode, C is the initial concentration of the electroactive analyte and D is its diffusion coefficient.

In addition to the above equation for electron transfer, the capacitive component of the current is described below:

$$i = \frac{E}{R} e^{-\frac{t}{RC}} \quad \text{(Equation 3.2)}$$

Here R is the resistance, E is the potential applied, C is the capacitance and t is time. The capacitive component for the chronoamperometric current follows an exponential decay with a time constant of RC.

Overall, the electrochemical currents from chronoamperometry measurements vary with time, depending on a number of parameters shown in Equations 3.1 and 3.2. For metal deposition, this can be correlated to the surface area of the electrode, the concentration of the plating solution and the resistance and capacitance of the system.

3.2 Aims and objectives

The experimental aim of this chapter is to establish a reliable and reproducible fabrication protocol for nanopore-FET devices based on dual-barrel nanopipettes using electrochemistry. Initially, the formulation of the plating solution and its electrochemical effect on the carbon nanoelectrode was investigated, followed by determining the electrochemical conditions for controlled nanopore-FET device fabrication.

- Exploring the electrochemical conditions for gold deposition on the surface of a carbon nanoelectrode.

- Choosing a suitable gold plating method for controllable deposition on a nanoscale.
- Determining the electrochemical behaviour of the chosen plating solution.

➢ Establishing a feedback-controlled fabrication protocol to integrate the nanopore with the FET using optimised electrochemical conditions.

- Establishing the use of the open barrel as a feedback channel to monitor the gold deposition on the carbon nanoelectrode, as well as the growth of gold around the nanopore opening.
- Verifying the reproducibility and reliability of the feedback-controlled deposition of gold and controlling nanopore conductance by a feedback mechanism.

3.3 Results and discussion

3.3.1 Deposition mechanism and voltammetry characterisation

Gold was chosen as the deposition material mainly because of its robustness, resistance to corrosion and, more importantly, versatile surface functionalisation by thiolated species. An alkaline gold sulphite plating solution (ECF64, Metalor Technologies) was used in place of the conventional auric chloride or gold cyanide method as it is much less toxic and offers more control of plating at nanoscale. At a reducing potential on the surface of the electrode, the gold deposition occurs via a two-step process[12]:

$$[Au\,(SO_3)]^- \rightleftharpoons Au_{ads}^{+} + (SO_3)^{2-}$$

$$Au_{ads}^{+} + e^- \longrightarrow Au$$

Scheme 3-1: Electrochemical deposition of gold using ECF64 plating solution containing gold sulphite.
The deposition mechanism proceeds via absorption of the gold (I) complex followed by electron transfer to reduce the absorbed gold (I).

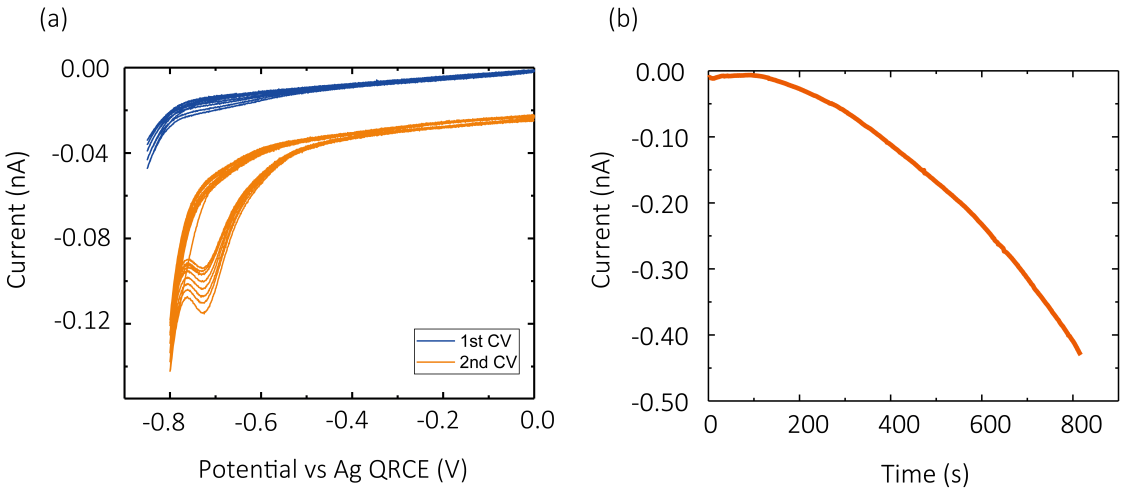


Figure 3-4: Comparison between (a) cyclic voltammetry and (b) chronoamperometry for electrodeposition of gold using 10-fold diluted ECF64 plating solution. (a) Cyclic voltammetry was performed with a scan rate of 0.02 V/s. The first set of CVs exhibited a small increase in electrochemical current and deposition peaks, meaning that gold is only minimally reduced from the plating solution. To investigate the precise location of the gold reduction peak on the carbon nanoelectrode, the resulting electrode was held at -0.7 V for 200 s to stimulate the nucleation of gold. The second set of CVs revealed a significant reduction peak at around -0.73 V. (b) Amperometric deposition of gold at a constant potential of -0.73 V exhibited an initial deposition current at roughly 0.01 nA for the first 100 s. This was followed by a gradual increase with the slope becoming steeper over time, indicating faster deposition. A carbon nanoelectrode was used as the working electrode, with a quasi-reference counter electrode in the plating solution.

To achieve controllable deposition on a nanoscale, it is crucial to determine the electrochemical window of the gold plating solution. The literature suggests that the deposition occurs at around -0.7 V.[13,14] From the cyclic voltammograms of the carbon nanoelectrode in ECF 64 solution, the first set of CV measurements revealed no obvious peaks apart from the increase of electrochemical currents at around -0.8 V because of oxygen reduction. This likely correlated with the initial nucleation stage of gold deposition.

Further confirmation of gold deposition can be obtained by a second round of cyclic voltammetry on the same electrode, but after the amperometric treatment at -0.73 V for 200 s. The three-fold enhancement of reduction current upon cathodic polarisation confirms the increase in the electrochemical area of the gold deposited electrode, as seen by the increase of the reduction current peak at -0.73 V after each cycle, in good agreement with the literature value. The results from cyclic voltammetry also correlated with the chronoamperometry

experiments at a constant potential of -0.73 V. In this case, holding the electrode at a constant reducing potential caused a small enhancement of the current in the first 100 s. This was followed by a significant increase with the slope becoming steeper over time, suggesting that the deposition rate was increasing. The above electrochemical results confirmed that the electrochemical deposition occurred via nucleation on the surface of the electrode, followed by outward expansion as the deposition proceeded to more electrochemically active areas.

3.3.2 Real-time ion current feedback

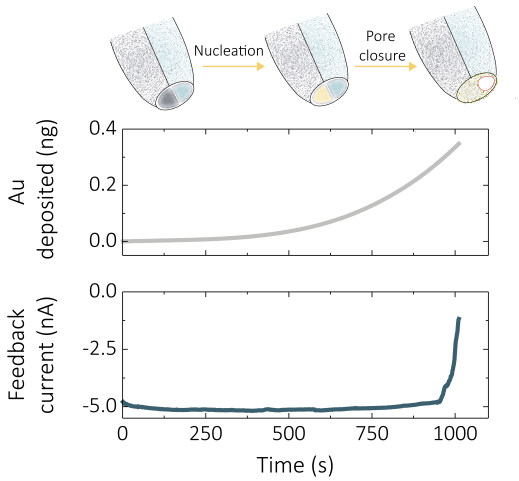


Figure 3-5: Representative examples for the feedback-controlled deposition of gold. Gold deposition was simultaneously performed using a bipotentiostatic configuration with two working electrodes inside the carbon barrel and the open barrel, respectively, where $V_{depositon}$ = -0.73 V and $V_{feedback}$ = -0.1 V. The deposition current exhibited no significant difference compared with experiments that did not incorporate the feedback (Figure 3-4). The feedback current remained roughly constant and then decreased rapidly. As the ionic current flowing through the open barrel is a function of pore conductance, the sharp decrease in feedback current undoubtedly suggests rapid pore shrinking within this sharp transition regime.

Nanoscale separation of the carbon nanoelectrode and the nanopore on the dual-barrel nanopipette platform provides a viable way to deposit gold around the nanopore using electrochemistry. Based on the electrochemical characterisation of the gold deposition in Section 3.2.1, dual-chronoamperometry was used to deposit gold while monitoring the real-

time ion current flowing through the nanopore. This was achieved through a bipotentiostatic configuration where two working electrodes were placed in the carbon barrel and the open barrel, respectively, and a quasi-reference counter electrode (QRCE) in the plating bath. A reducing potential of -0.73 V was held at the carbon barrel to reduce the gold from the plating solution, and a potential difference of -0.1 V was applied between the working electrode inside the open barrel and the QRCE to produce a real-time ion current flowing through the nanopore.

The dual-chronoamperometry data on the carbon nanoelectrode and the nanopore are shown in Figure 3-5. The amount of gold deposited on the carbon nanoelectrode can be calculated using the equation shown below, assuming the only faradic process occurring on the carbon nanoelectrode is gold deposition:

$$m_{gold} = \frac{\int I_{dep} dt}{F} \times M_{gold} \qquad \text{(Equation 3.3)}$$

In this equation, m_{gold} is the total mass of deposited gold, I_{dep} is the deposition current measured from carbon nanoelectrode, F is the Faraday constant and M_{gold} is the molar mass of gold.

The trend of gold deposition on the carbon nanoelectrode with open barrel as a feedback was similar to the amount for the single electrode, indicating the introduction of ion current feedback caused little difference in gold deposition. Simultaneously monitoring the nanopore ion current reveals an interesting phenomenon. The feedback current initially remained roughly constant and then suddenly decreased. The initial stage where feedback current is constant corresponds to the nucleation of gold and the deposition before the nanopore is closed. The sudden decrease of feedback current means the nanopore is being reduced in size by electrodeposition.

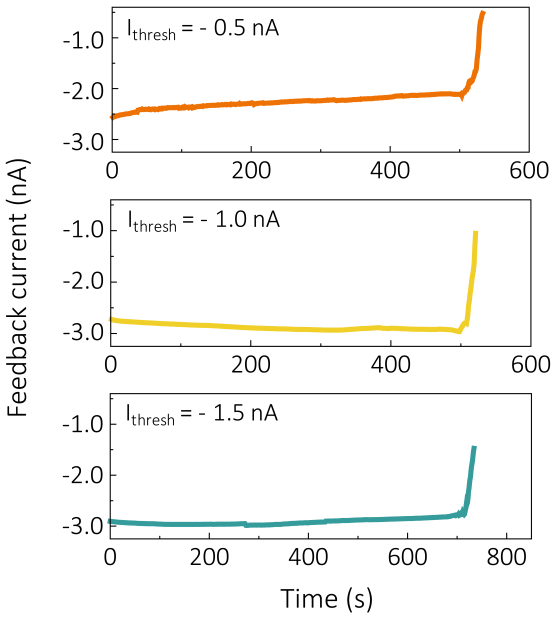


Figure 3-6: Examples demonstrating the reproducibility of the sharp decrease of feedback current. Although the time taken to reach the sharp transition varies for different pipettes, the sharp decrease of feedback current is reproducible. As a result, precise tailoring of nanopore conductance is feasible by terminating deposition processes at different currents. The data were obtained from 3 independent nanopores.

The reproducibility of this approach was verified by repeating the experiments using different nanopipettes. As shown in Figure 3-6, although the time taken to reach this sharp transition varied from pipette to pipette, the sudden decrease of feedback current is highly reproducible. Almost 90% of all pipettes analysed (N=767) exhibited this type of behaviour. Note that the overgrowth of deposited gold can be inhibited by stopping the deposition at a pre-set threshold of feedback current. Therefore, the nanopore is not fully closed but is fabricated with conductance defined by the feedback current.

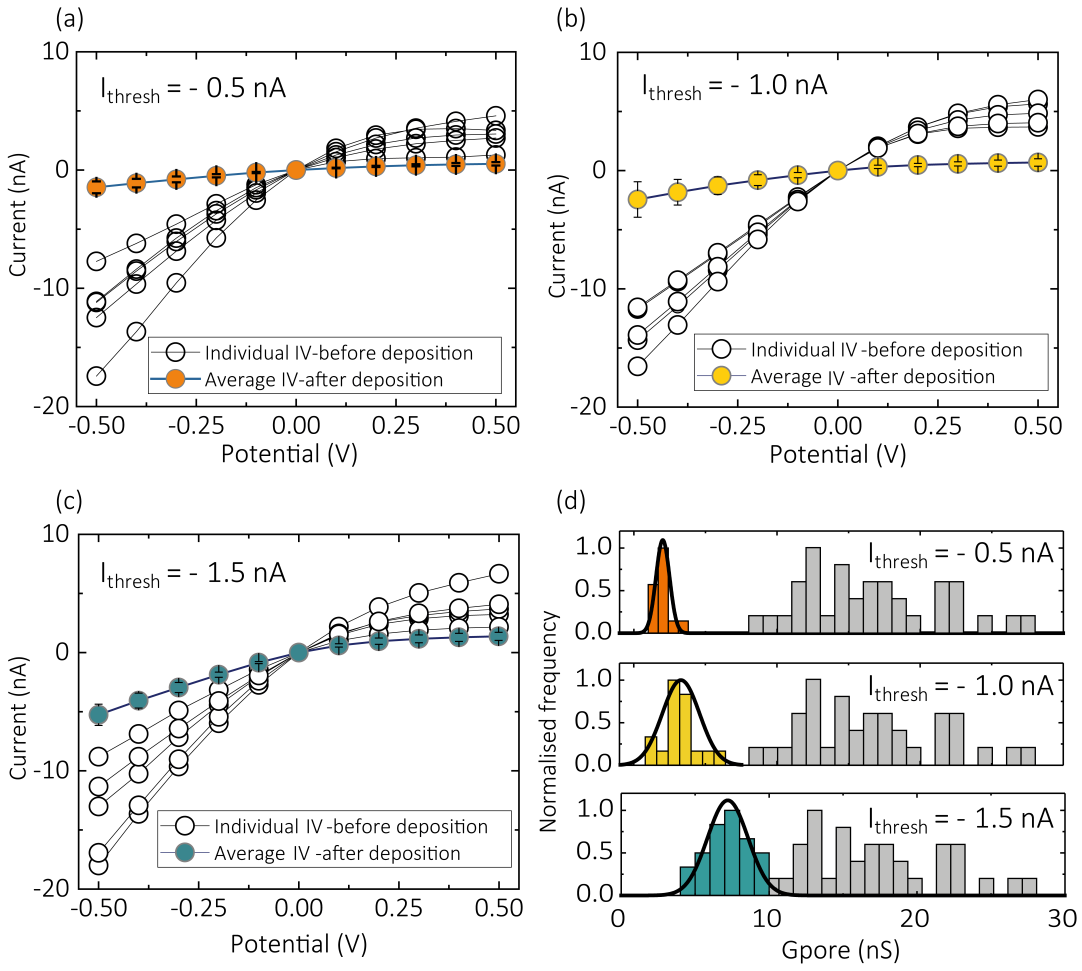


Figure 3-7: Controlling nanopore conductance by feedback-controlled deposition of gold. I-Vs for carbon-only nanopipettes and gold-deposited pipettes with a threshold feedback current of (a) -1.5 nA, (b) -1.0 nA and (c) -0.5 nA. (d) Detailed histograms show a large device-to-device variation (17.3 ± 6.4 nS) before gold deposition. However, the nanopore conductance was precisely tailored after feedback-controlled deposition (7.2 ± 1.4 nS for $I_{threshold}$ = -1.5 nA, 3.5 ± 1.9 nS for $I_{threshold}$ = -1.0 nA, 2.0 ± 0.4 nS for $I_{threshold}$ = -1.5 nA). The data were obtained from 90 independent nanopores.

Precise control of nanopore conductance is important for tailoring nanopores to be used for different purposes, including sensing analytes of different sizes and serving as a tuneable platform for surface functionalisation by different thiolated species. Based on the reproducibility of feedback-controlled deposition, gold deposition can be terminated at different feedback currents to fine-tune nanopore conductance (Figure 3-7). Before deposition, carbon-only devices have a relatively broad distribution of conductance with a large device-to-

device variation. By stopping the deposition at a final feedback current of -1.5, -1.0 and -0.5 nA, respectively, the nanopore conductance can be controlled precisely with a narrower distribution. However, the actual size of the nanopore was not estimated here as the pore geometry and surface charge can change after gold deposition. Currently, the models to calculate nanopore size from conductance are based on established geometry and surface charge.

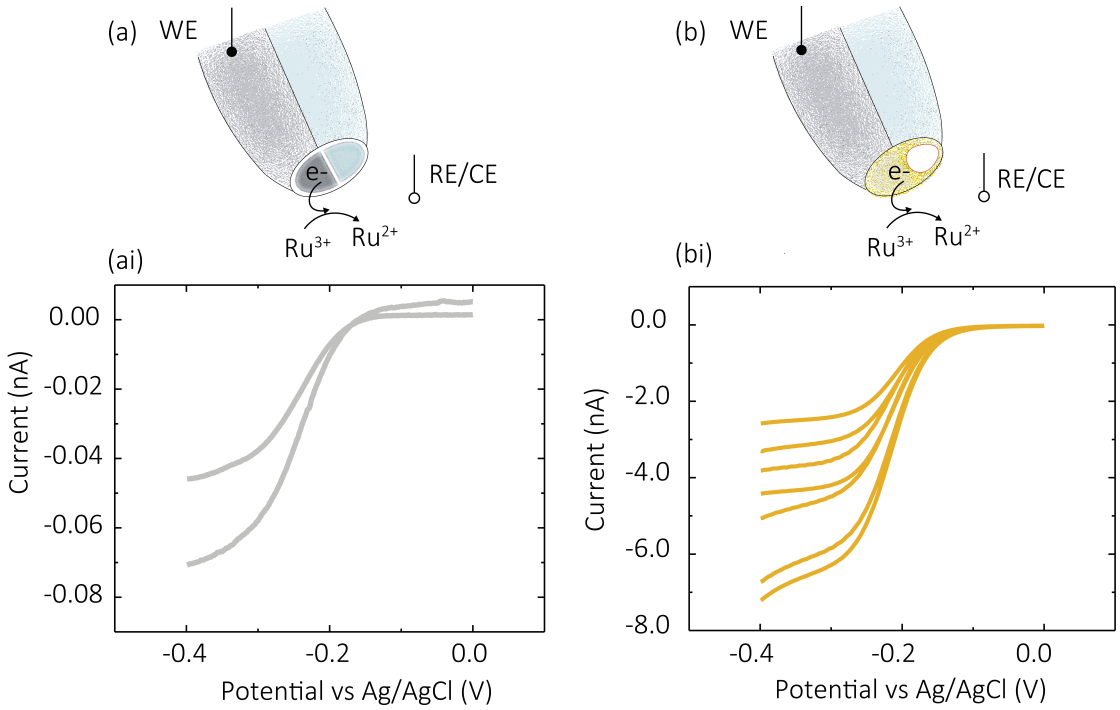


Figure 3-8: Characterisation of the electrochemically active area using the redox probe for carbon-only and gold-deposited devices. The electrochemistry is based on the cathodic polarisation of either (a) the carbon nanoelectrode or (b) the gold-deposited electrode. As a result, Ru^{3+} is reduced to $Ru^{2+,}$ giving rise to diffusion-limited currents, which are indicative of an electrochemically active area.

Apart from nanopore conductance, which is indicative of pore diameter, trials were performed to characterise the enhancement of the electrode area after gold deposition using $Ru(NH_3)_6Cl_3$ as the redox probe (Figure 3-8).

The diameter of the carbon nanoelectrode can be estimated from the steady-state diffusion-limited current using the equation below, assuming a disk-shaped electrode:

$$r = \frac{I_{steady\ state}}{4.64nFCD} \quad \text{(Equation 3.2)}$$

In this equation, r is the radius of the electrode, n is the number of electrons involved in the redox process (i.e. 1-electron reduction), F is the faraday constant, C is the concentration of the redox mediator (1 mM $Ru(NH_3)_6Cl_3$) and D is the diffusion coefficient of $Ru(NH_3)_6Cl_3$ in the electrolyte solution (6.3×10^{-6} cm^2/s). The size of the carbon nanoelectrode was determined to be 50 ± 11 nm from the steady-state currents.

Significant enhancement of diffusion-limited currents was obtained, confirming a more active electrode area after gold deposition, consistent with the results presented in Figures 3-4 and 3-5. As the shape of the electrode was changed after gold deposition, a rough estimation revealed that the deposited gold is in the micron range. Although the electrochemical method for nanopore-FET device fabrication is robust, the detailed local structure of deposited gold must still be investigated using optical and electron microscopy characterisation techniques.

3.3.3 Surface characterisation

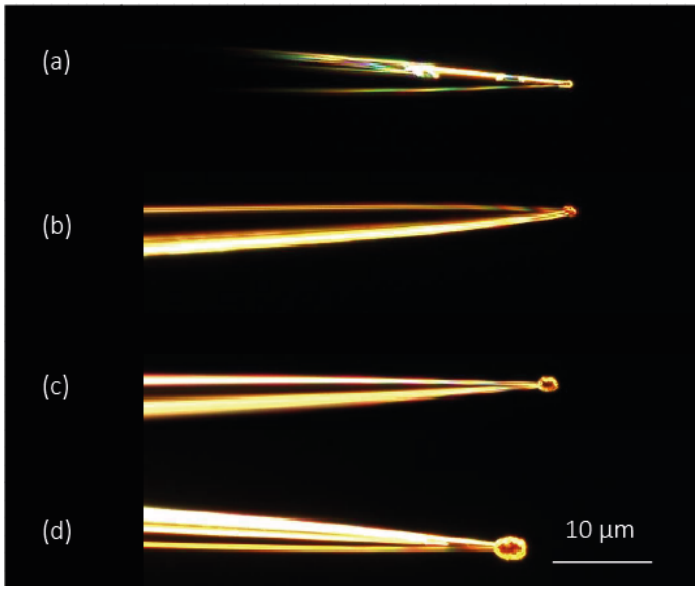


Figure 3-9: Characterisation of deposited gold using dark-field microscopy. Dark-field images taken at (a) 700 s, (b) 1000 s, (c) 2000 s and (d) 3000 s during the deposition process show the gradual expansion of a gold blob. The data were obtained from 4 independent nanopores.

Systematically characterising gold deposition and deposited pipettes using different surface characterisation techniques is necessary to investigate the growth pattern of gold around the nanopore. Resolving deposited gold optically using bright-field microscopy confirmed the additional presence of deposited material around the nanopore. Compared to quartz and

carbon, gold possesses an enhanced ability to scatter incident light. Dark-field microscopy was used to selectively visualise the deposited gold. As expected, the presence of gold at the end of the nanopipette was visualised, and importantly, the electrodeposition of gold showed outward expansion over time (Figure 3-9). This is consistent with the results from cyclic voltammetry and chronoamperometry of gold deposition. The lateral views of the optical characterisation confirmed the successful deposition of gold at the nanopipette tip but did not have enough spatial resolution to resolve the nanopore.

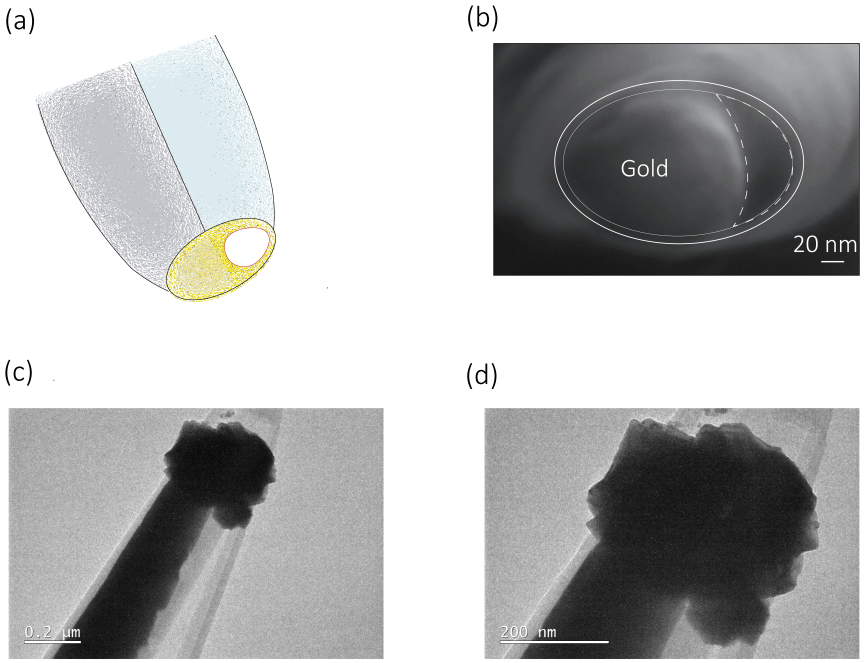


Figure 3-10: SEM and TEM characterisation of nanopore-FET devices. (a) Schematic illustrating the device configuration of gold deposited nanopipettes. (b) An SEM image of the top view shows the pore closure from the feedback-controlled deposition of gold and is confirmed by TEM images (c-d) showing the accurate deposition of gold at the tip. SEM and TEM were obtained from two independent nanopores.

Electron microscopy techniques allow for the characterisation of gold deposition on a nanoscale. SEM and TEM were both used here. The lateral view TEM clearly shows the accurate deposition of gold around the nanopore, while the SEM image demonstrates that the nanopore is being closed by the growth of gold (Figure 3-10).

Overall, the optical characterisation visualised the successful electrodeposition of gold (Figure 3-9), consistent with the TEM image verifying the accurate location of gold around the nanopore opening (Figure 3-10). The SEM image captured the nanopore being closed by gold deposition (Figure 3-10), as had been shown by feedback-controlled electrodeposition of gold in which the sudden decrease of feedback current was highly reproducible.

3.4 Conclusion

In this chapter, a reproducible fabrication protocol for nanopore-FET devices was established by feedback-controlled electrodeposition. According to the measured electrochemical window and the deposition potential of the gold plating solution, the use of the bipotentiostatic configuration simultaneously deposited gold and incorporated a feedback mechanism to monitor the growth of gold around the nanopore using a real-time ionic current from the open barrel. Based on the optimised plating formulation and electrochemical conditions, a novel and straightforward method for fabricating gold nanopores was presented. A sharp transition regime, where nanopore feedback current suddenly decreased, was reproducibly demonstrated for different devices with a relatively large device-to-device variation. The reliability of feedback-controlled deposition was verified by precisely controlling the nanopore conductance through terminating deposition at a pre-determined threshold. Moreover, the fabricated devices were successfully characterised by a range of optical microscopy and electron microscopy techniques. The most important experimental objective of accurately depositing gold around the nanopore opening was shown to be feasible. The integration of the nanopore with a FET component was made possible using this fabrication method.

However, using an electrochemical method to fabricate nanopore-FET devices presents several limitations. Although nanopore conductance and possibly the size can be precisely defined using a feedback current threshold, the fabrication of a gold nanopore with controlled geometry is challenging using electrodeposition because the nucleation of gold on the surface of the electrode is a stochastic process. Using an electrochemical approach, the surface morphology of the gold nanopore in the sensing region might vary even though the nanopore conductance remains the same.

On the other hand, combining nanopipettes with electrodeposition advances the field of nanopore-FET fabrication by increasing yields, improving efficiency and reducing costs as compared to advanced lithography techniques for solid-state nanopores. It has been shown that integrating graphene with solid-state nanopores is exceptionally challenging, particularly with a low yield[15,16], and is further compounded by more complicated fabrication by e-beam lithography.[1,2,17] Even though the surface morphology can vary from a pipette to pipette, perfect alignment between the nanopore and the FET electrode has been achieved using a feedback-controlled mechanism. Further research opportunities are possible at this stage because of the alignment between nanopore and deposited gold.

3.5 References

(1) Xie, P.; Xiong, Q.; Fang, Y.; Qing, Q.; Lieber, C. M. Local Electrical Potential Detection of DNA by Nanowire–Nanopore Sensors. *Nat. Nanotechnol.* **2011**, *7* (2), 119–125.

(2) Traversi, F.; Raillon, C.; Benameur, S. M.; Liu, K.; Khlybov, S.; Tosun, M.; Krasnozhon, D.; Kis, A.; Radenovic, A. Detecting the Translocation of DNA through a Nanopore Using Graphene Nanoribbons. *Nat. Nanotechnol.* **2013**, *8* (12), 939–945.

(3) Takahashi, Y.; Shevchuk, A. I.; Novak, P.; Zhang, Y.; Ebejer, N.; MacPherson, J. V.; Unwin, P. R.; Pollard, A. J.; Roy, D.; Clifford, C. A.; Shiku, H.; Matsue, T.; Klenerman, D.; Korchev, Y. E. Multifunctional Nanoprobes for Nanoscale Chemical Imaging and Localized Chemical Delivery at Surfaces and Interfaces. *Angew. Chemie - Int. Ed.* **2011**, *50* (41), 9638–9642.

(4) Actis, P.; Tokar, S.; Clausmeyer, J.; Babakinejad, B.; Mikhaleva, S.; Cornut, R.; Takahashi, Y.; López Córdoba, A.; Novak, P.; Shevchuck, A. I.; Dougan, J. A.; Kazarian, S. G.; Gorelkin, P. V.; Erofeev, A. S.; Yaminsky, I. V.; Unwin, P. R.; Schuhmann, W.; Klenerman, D.; Rusakov, D. A.; Sviderskaya, E. V.; Korchev, Y. E. Electrochemical Nanoprobes for Single-Cell Analysis. *ACS Nano* **2014**, *8* (1), 875–884.

(5) Zhang, Y.; Takahashi, Y.; Hong, S. P.; Liu, F.; Bednarska, J.; Goff, P. S.; Novak, P.; Shevchuk, A.; Gopal, S.; Barozzi, I.; Magnani, L.; Sakai, H.; Suguru, Y.; Fujii, T.; Erofeev, A.; Gorelkin, P.; Majouga, A.; Weiss, D. J.; Edwards, C.; Ivanov, A. P.; Klenerman, D.; Sviderskaya, E. V.; Edel, J. B.; Korchev, Y. High-Resolution Label-Free 3D Mapping of Extracellular PH of Single Living Cells. *Nat. Commun.* **2019**, *10*, 5610.

(6) Page, A.; Kang, M.; Armitstead, A.; Perry, D.; Unwin, P. R. Quantitative Visualization of Molecular Delivery and Uptake at Living Cells with Self-Referencing Scanning Ion Conductance Microscopy-Scanning Electrochemical Microscopy. *Anal. Chem.* **2017**, *89* (5), 3021–3028.

(7) Babakinejad, B.; Jönsson, P.; López Córdoba, A.; Actis, P.; Novak, P.; Takahashi, Y.; Shevchuk, A.; Anand, U.; Anand, P.; Drews, A.; Ferrer-Montiel, A.; Klenerman, D.; Korchev, Y. E. Local Delivery of Molecules from a Nanopipette for Quantitative Receptor Mapping on Live Cells. *Anal. Chem.* **2013**, *85* (19), 9333–9342.

(8) Gurrappa, I.; Binder, L. Electrodeposition of Nanostructured Coatings and Their

Characterization - A Review. *Sci. Technol. Adv. Mater.* **2008**, *9* (4), 043001.

(9) Elias, J.; Gizowska, M.; Brodard, P.; Widmer, R.; Dehazan, Y.; Graule, T.; Michler, J.; Philippe, L. Electrodeposition of Gold Thin Films with Controlled Morphologies and Their Applications in Electrocatalysis and SERS. *Nanotechnology* **2012**, *23* (25).

(10) Bard, A. J.; Faulkner, L. R. *Electrochemical Methods: Fundamentals and Applications, 2nd Edition*; 2001, 239-243.

(11) Compton, R. G.; Banks, C. E. *Understanding Voltammetry*; 2007, 107-155.

(12) Osaka, T.; Kato, M.; Sato, J.; Yoshizawa, K.; Homma, T.; Okinaka, Y.; Yoshioka, O. Mechanism of Sulfur Inclusion in Soft Gold Electrodeposited from the Thiosulfate-Sulfite Bath. *J. Electrochem. Soc.* **2001**, *148* (10), C659–C662.

(13) Rutkowska, A.; Freedman, K. J.; Skalkowska, J.; Kim, M. J.; Edel, J. B.; Albrecht, T. Electrodeposition and Bipolar Effects in Metallized Nanopores and Their Use in the Detection of Insulin. *Anal. Chem.* **2015**, *87* (4), 2337–2344.

(14) Gao, R.; Ying, Y. L.; Li, Y. J.; Hu, Y. X.; Yu, R. J.; Lin, Y.; Long, Y. T. A 30 Nm Nanopore Electrode: Facile Fabrication and Direct Insights into the Intrinsic Feature of Single Nanoparticle Collisions. *Angew. Chemie - Int. Ed.* **2018**, *57* (4), 1011–1015.

(15) Heerema, S. J.; Dekker, C. Graphene Nanodevices for DNA Sequencing. *Nat. Nanotechnol.* **2016**, *11* (2), 127–136.

(16) Heerema, S. J.; Vicarelli, L.; Pud, S.; Schouten, R. N.; Zandbergen, H. W.; Dekker, C. Probing DNA Translocations with Inplane Current Signals in a Graphene Nanoribbon with a Nanopore. *ACS Nano* **2018**, *12* (3), 2623–2633.

(17) Puster, M.; Balan, A.; Rodríguez-Manzo, J. A.; Danda, G.; Ahn, J. H.; Parkin, W.; Drndić, M. Cross-Talk Between Ionic and Nanoribbon Current Signals in Graphene Nanoribbon-Nanopore Sensors for Single-Molecule Detection. *Small* **2015**, *11* (47), 6309–6316.

Chapter 4

Chemically-modified nanopore field-effect transistors for controlling single-molecule transport

Contents

Abstract 90
4.1 Introduction 91
4.2 Single-molecule detection of DNA using gold-deposited nanopore-FET 92
4.3 Controlling DNA transport using gold-deposited nanopore-FET 94
4.4 Chemical modification of nanopore-FET 97
4.5 Fine-tuning single-molecule transport using amine-modified nanopore-FET 103
4.6 Conclusion and future work 106
4.7 References 107

Abstract

Building on the fabrication methodology used for the nanopore-FET sensing platform, the distinctiveness of two-barrel architecture makes it possible to align gold with nanopores at the nanoscale. Controlling the transport of single molecules can be achieved by switching on/off single-molecule translocations. To introduce more active control to the transport of single molecules, a generalised functionalisation protocol was developed for the attachment of small molecules with different charges. Finally, nanopore-FETs modified by a positively charged amine can be used to control molecular transport across nanopores by orders of magnitude, including capture rates and translocation velocities.

4.1 Introduction

The development of new analytical methods is currently at the forefront of healthcare research due to the need for improved performance compared to what is now considered state-of-the-art. This is especially true for applications such as early-stage disease diagnosis and treatment.[1,2] To that end, different techniques including fluorescence[3–5] and optical[6] and magnetic tweezers[7,8] have been reported with sensitivities reaching the single-molecule limit. Even though such techniques could provide the sensitivity to detect and manipulate molecules one at a time, their broader application in a clinical setting is impeded by the complexities associated with sample preparation and processing. Therefore, the development of 'single-pot' label-free approaches remains one of the most attractive avenues for single-molecule sensors. Among different label-free techniques, nanopores and field-effect transistors (FET) have emerged as exceptionally promising methods due to their inherent sensitivity and aptitude for multiplexed detection.[9–13]

Nanopores operate by driving analytes electrokinetically across a nanoscale pore, allowing single-molecule identification by measuring characteristic modulations in the ionic current. By extracting the magnitude and duration of individual translocation events, one can obtain information such as molecular dimensions, concentration and in some cases, even charge and conformation.[10,11,14] Although numerous advances have been made,[10,11,15–18] fast analyte transport and analyte selectivity still represent a substantial challenge.[10,19–23] To this end, different strategies have recently been investigated, including the use of FET-coupled nanopores. Nanoscale FETs are capable of label-free sensing of biological analytes in real time,[12,24] and the sensing principle is based on monitoring the change of conductance between the drain-source upon the binding of biomolecules to the gate electrode. However, the sensing area is governed by the Debye screening length, which is relatively short under physiological conditions (~1 nm).[13] Unlike nanopores, this limits the possibility of actively transporting analytes to the sensing region and controlling throughput.

It is no surprise that due to the distinct advantages offered by the two techniques, the development of combined nanopore-FET platforms has attracted an increasing amount of interest, both experimentally[17,25–28] and theoretically[29–31]. In a hybrid nanopore-FET design, the nanopore can be viewed as a drain-source channel for single-molecule translocation, while the

FET is integrated by placing a gate electrode near the nanopore aperture. A distinctive advantage of such a platform lies in its ability to control the surface charge near the nanopore by varying the potential applied to the gate electrode, which in turn allows for manipulation of the transport of single molecules across the nanopore. Furthermore, the possibility of simultaneously detecting the ionic current (drain-source) and gate channels can offer an additional sensing channel and enrich the obtained single-molecule information. Previous work demonstrated simultaneous dual-channel, single-molecule DNA detection by incorporating a solid-state nanopore with a silicon nanowire[27] or graphene nanoribbon.[17,32,33] More recently, Panday et al.[34] proposed the integration of a carbon nanoelectrode within relatively large nanopores for the detection of 40 nm nanoparticles. Additionally, different approaches have been proposed and developed to control transport, including programming voltage pulses,[35,36] tuning the viscosity of solvents,[37] changing the local temperature,[38] and voltage gating.[22] The variation of nanopore surface charge with gating potential is expected to play a key role in the manipulation of single-molecule translocation,[30,31,39] thereby improving or supplementing existing strategies for controlling single-molecule transport.

Building upon these advances, I presented a new fabrication strategy in Chapter 3 for the facile design and alignment of a sub-30-nm nanopore to the gate electrode in order to control molecular transport at the single-molecule level. Rapid fabrication was achieved by controlled electrodeposition of gold onto a nanoscale carbon electrode formed inside one of the barrels of a double-barrelled nanopore/nanopipette. Ion current feedback was used to fabricate the gold gate electrode, localised at the nanopore opening while monitoring and tuning the pore conductance in real-time. In this chapter, voltage gating and surface functionalisation can be used to tune the nanopore surface charge and, in turn, switch on/off or accurately control the rate of single-molecule transport. The results demonstrate that these hybrid nanopore–FET devices can be readily used to control molecular transport by tuning nanopore charge both electrically and chemically.

4.2 Single-molecule detection of DNA using gold-deposited nanopore-FET

After feedback-controlled deposition of gold, the nanopore was decreased to ~20 nm surrounded by very localised gold. Two very important parameters for nanopore sensing – size

and surface – were changed because of the gold deposition. Thus, it is important to explore changes in single-molecule translocation behaviour. Initially, the single-molecule sensitivity was confirmed using plain quartz/carbon devices without gold electrodeposition. To this end, 400 pM of 10 kbp ds DNA in 100 mM KCl was added to the nanopore barrel of the pipette. In this configuration, under applied negative voltage, translocations occurred from the inside of the nanopipette (cis) to the bath (trans), resulting in an overall increase in conductance when using 100 mM KCl at pH 8. Across all devices, we found dwell times and peak currents for 10 kbp ds DNA to be in agreement with those in previous studies using unmodified (bare quartz) single-barrel nanopipettes,[40–42] indicating that the incorporation of a carbon nanoelectrode adjacent to a quartz nanopore caused a negligible effect on single-molecule DNA translocation (Figure 4-1).

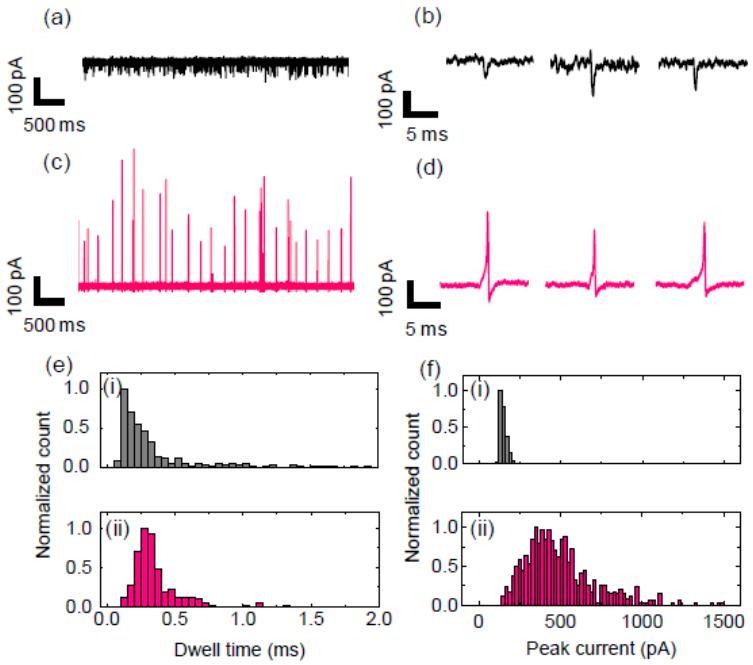


Figure 4-1: Validation of single-molecule functionality for the nanopore-FET devices. Representative It traces and individual translocation events recorded at the nanopore channel before (a,b) and after (c,d) feedback-controlled deposition of gold, showing a slight increase in dwell time from (ei) 0.13 ± 0.06 ms to (eii) 0.35 ± 0.17 ms, a significant increase in peak current from (fi) 149 ± 25 pA to (fii) 510 ± 252 pA, and a reduction of capture rate from 17 ± 3 s^{-1} to 7 ± 1 s^{-1} . This was attributed to the smaller opening of the gold-coated nanopore, which induced enhanced interactions between DNA and the nanopore

surface. Vpore = −700 mV, Vgate = 0 mV. 10 kbp DNA was added in the nanopipette and translocation occurred from in to out.

After gold electrodeposition, we observed a substantial (up to 200%) increase in the mean peak current, as can be seen in Figure 4-1. Smaller Au-coated nanopores likely resulted in enhanced interactions between DNA and the nanopore surface, leading to larger peak currents, longer dwell times, and lower capture rates. Furthermore, due to the change of nanopore surface charge after gold deposition, the direction of the nanopore current changed at 100 mM KCl; current enhancement was observed with carbon-/glass-coated nanopipettes, while the current blockade was recorded with gold-coated ones.

Before gold deposition, single-molecule translocation of DNA across quartz/carbon nanopipettes, causing current enhancement, as a large number of DNA counterions are introduced into the nanopore sensing region which increases nanopore conductance. Interestingly, the current blockade was observed after gold deposition. It is known that chloride anions have a high surface affinity towards gold.[43,44] Moreover, the current blockade of single-molecule DNA translocation was caused by the hindered access of ions across the nanopore.[45] In this case, perhaps the dragging force between absorbed chloride and counterions of DNA (K^+) induced the current blockade of 10 kbp ds-DNA translocation.

4.3 Controlling DNA transport using gold-deposited nanopore-FET

As stated previously, the presence of gold around the nanopore opening made it possible to use it as a controlling component in single-molecule DNA translocation. As for conventional FET devices, voltage gating was established in this system by electrical contacts and charge mirroring between the carbon electrode and deposited gold.

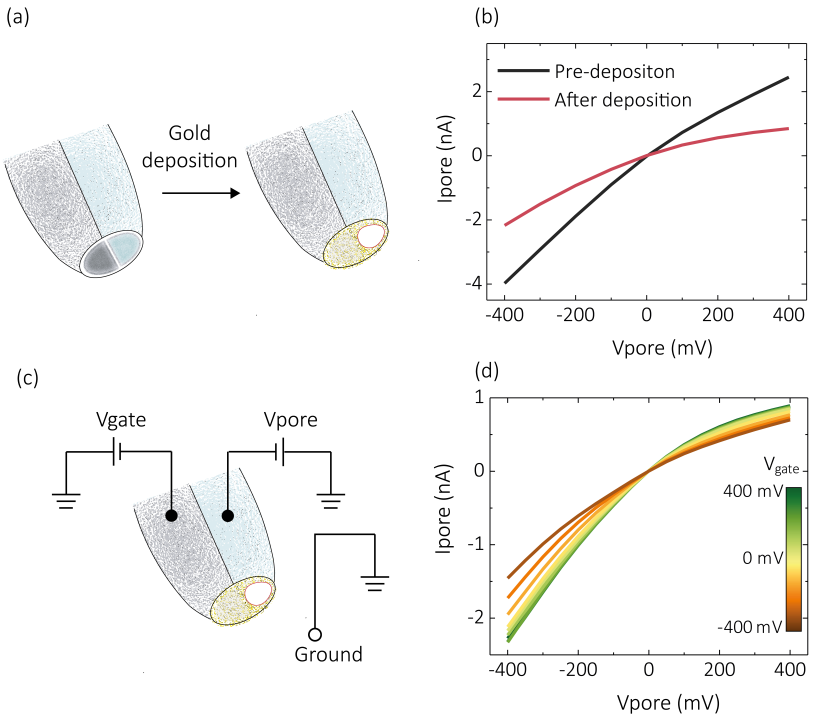


Figure 4-2: Voltage gating of the nanopore, (a,b) I-V characterisation of the nanopore-FET before and after gold deposition, and (c,d) after gold deposition at varying V_{gate}.

To control single-molecule transport by voltage gating, it is important to determine the ideal 'gating window' in which (1) no electrochemical reactions happen and (2) the charge of the gating electrode varies significantly with different applied potentials. Ionic transport across the nanopore was the preliminary aim of investigation. A range of gating potentials wherein no electrochemical reactions occurred (-400 mV, 400 mV) was verified for the gold electrode. Beyond this potential range, oxygen reduction or gold oxidation would occur, both of which are detrimental to the device's stability. Within this potential range, the I-Vs at different V_{gate} were obtained where only negative potentials were able to cause the modulation of ionic transport. To rationalise this, the correlation between the charge of double-layer and applied V_{gate} was extracted by differential capacitance measurements. The minimum of the capacitance versus V_{gate} was attributed to the potential of zero charge (-90 ± 10 mV), where the charge of the double-layer was neutral. This accords well with the value given in the literature,[46] confirming that the gating electrode was negatively charged at potentials below pzc and positively charged at the potentials above pzc (Figure 4-3 a). However, it should be

noted that the differential capacitance of the gate was challenging to measure due of MΩ resistance. Instead, an ultramicron gold-deposited electrode was used here.

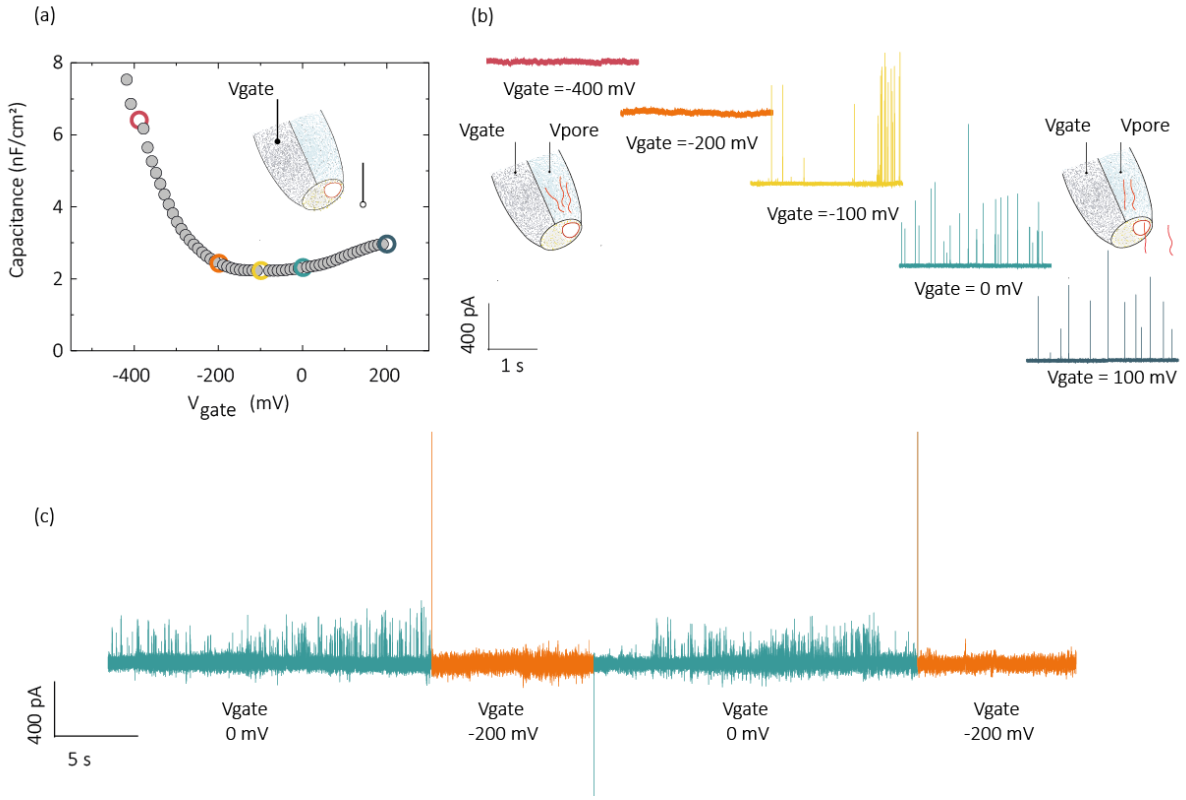


Figure 4-3: Voltage gating of DNA translocation. (a) The variation of nanopore surface charge with gating potentials (V_{gate}) was probed by differential capacitance measurements on an ultramicron gold-deposited electrode, showing a capacitance minimum at −100 mV, which was attributed to the potential of zero charge (pzc). (b) This correlates well with the gating of 10 kbp DNA in 100 mM KCl, 10 mM Tris-HCl and 1 mM EDTA buffer at pH 8. DNA transport could be switched off or turned on depending on whether the potential applied to V_{gate} was above or below the pzc. By controlling the gate potential, translocations could be switched on and off in real time as shown in (c). Vpore = −700 mV. 10 kbp DNA was added in the nanopipette and translocation occurred from in to out.

Established by the behaviour of electrical double-layer at varying V_{gate}, controlling single-molecule transport by voltage gating was achieved by applying different V_{gate} along the differential capacitance curve on both sides of the pzc (Figure 4-3). At V_{gate} −200 and −400 mV, the single-molecule transport was switched off. Switching the single-molecule transport back on was done at the potential, very close to (V_{gate} = −100 mV) and above the pzc (V_{gate} = 0 mV and V_{gate} = 200 mV). As the results from voltage gating correlated very well with differential

capacitance measurements, electrostatic repulsion was verified as the dominant reason, confirmed by supplementary experiments showing the disappearance of on/off behaviour for 200 and 50 bp ds DNA. On the other hand, electroosmotic flow in the direction opposed to electrophoresis also synergistically helped the switch-off of single-molecule DNA transport[47] (Figure 4-3).

Although the establishment of on/off switching provides a leap forward in controlling single-molecule transport, more active control of molecular transport is needed to fine-tune transport properties. One possible way to achieve this is to functionalise the gold surface with different thiolated species to disturb the double-layer and overcome the issue of Debye screening.

4.4 Chemical modification of nanopore-FET

From what has been characterised by dark-field, SEM, and TEM, the localised gold around nanopore openings unlocks the possibility for the chemical modification via thiol–gold self-assembly. Initially, as a proof of concept, thiolated molecules with different charges were chosen with the aim of establishing a functionalisation protocol and formulation.

The charge of the nanopore surface plays an important role in terms of ionic transport and current rectification. Herein, two thiolated molecules (1-dodecanethiol and 5-amino-2-mercaptobenzimidazole) bearing different charges at pH 8 were chosen to modify the surface of gold. It was shown previously that nanopore field-effect transistors are exceptionally challenging to fabricate. With one more step to surface functionalisation, protocol and formulation must be established and optimised carefully to allow a reasonable yield for use in the subsequent steps.

As with all surface modifications, the choice of solvent has important implications on yield and success rate. This is especially true for the chemical modification of our nanopore field-effect transistors. Considering the device configuration, the functionalising agent must ideally be able to diffuse into the nanopore sensing region and also ensure that there is not an excess of unattached thiols present that may cause interference with single-molecule detection. Therefore, the choice of the solvent, or solvent combination, used in the chemical modification and purification will be discussed in the following paragraph.

After gold deposition, the residues of plating solution are likely to remain on the gold's surface and within the open barrel. To achieve the maximum possible purification, the open barrel was rinsed with DI H_2O using a Microfil needle. Also, the fabricated devices were left in DI H_2O until use, so as to remove the residues on the deposited gold.

The solution-based functionalisation involved immersing the tips of gold deposited pipettes in the solvent. To ensure thiols could attach to the gold surface in the nanopore sensing region, the open barrel and the bath were both filled with solvents. Considering that nanopore-FET devices are composed of both quartz and gold, the wetting between nanopore surfaces and the solvent is a critical factor. As the devices were left in DI H_2O until functionalisation, methanol was chosen as the solvent for functionalisation, as it is miscible with H_2O and has reasonable wetting with quartz and gold, and it simultaneously solubilises most organic molecules. Attempts to functionalise the gold using other solvents, such as ethanol, acetone, and hexane, were not successful – either the change of nanopore I-V was not observable, or the gold was detached after functionalisation. Moreover, the presence of an H_2O layer around the nanopore, forming a meniscus as observed by other studies on dual-barrel nanopipettes, was possibly the reason for the failure of functionalisation.

Importantly, a high concentration of thiolated molecules (5 mM) was added to the solvent bath only, and no thiols were present in the solvent that was used to fill the open barrel. As a result of conical geometry, adding thiols inside of an open barrel is likely to cause an excess amount accumulating at the tip, making them difficult to rinse out, as well as the possibility of interfering with electrical characterisation and translocation experiments. Therefore, thiols were only added in the bath, while only solvent was filled in the open barrel. In this case, thiols could be attached to the gold if they could diffuse inside the nanopore sensing region while minimising the amount of thiols in the open barrel. Notably, at lower concentrations, a reduction in the yield of functionalised devices was observed.

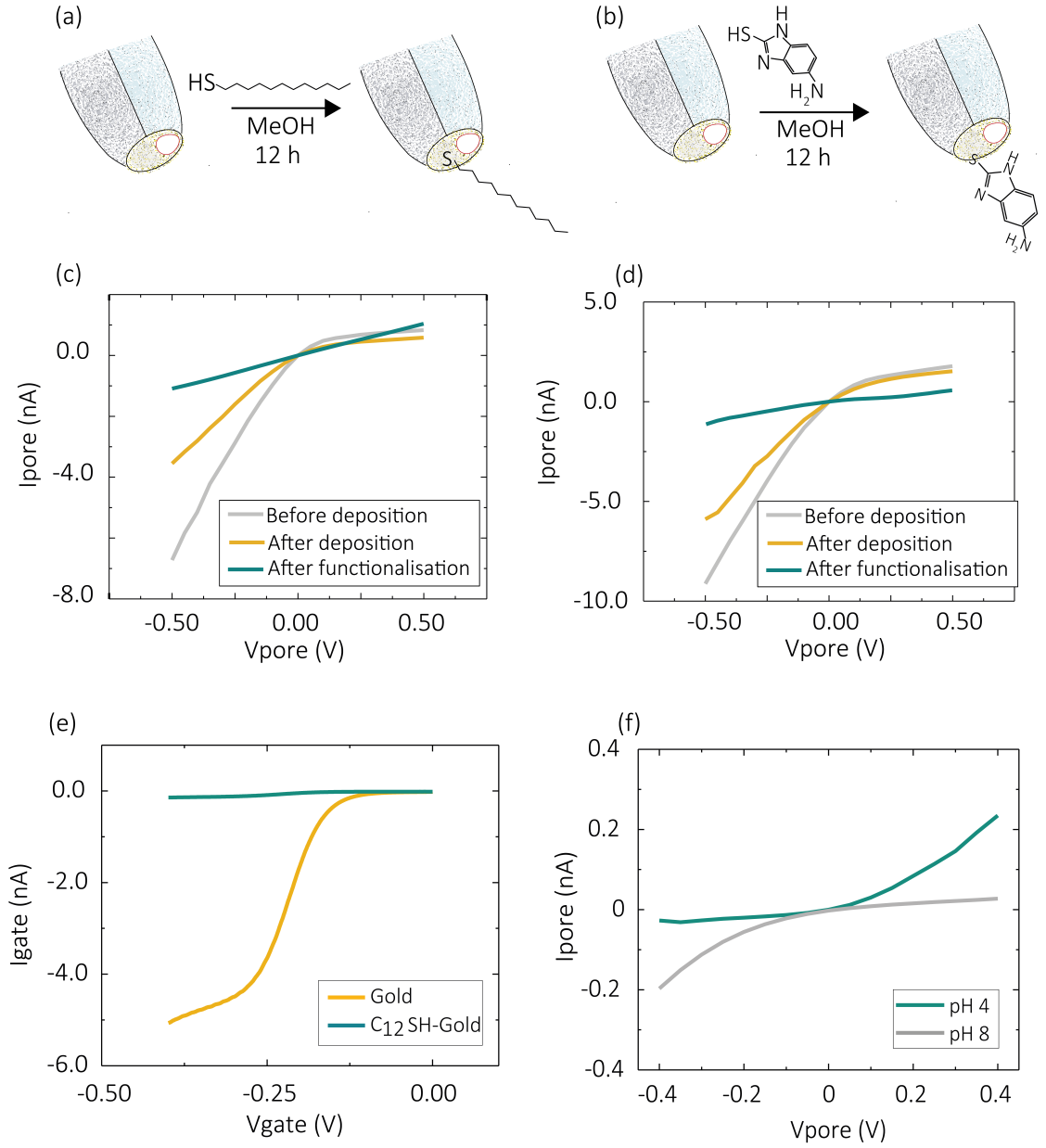


Figure 4-4: Surface functionalisation of gold-deposited nanopores with (a) 1-dodecanethiol and (b) 5-amino-2-mercaptobenzimidazole. For each case, (c,d) successful functionalisation was seen from the consecutive change of I-V with respect to the fabrication workflow of nanopore-FET devices. Electrolyte: 52 mM $(NH_4)_2SO_3$. This was further confirmed by (e) the suppression of the electrochemically active area for the gold gate functionalised by 1-dodecanethiol, the electrochemical characterisation was performed with 1 mM $Ru(NH_3)_6Cl_3$ in 100 mM KCl. (f) The inversion of I-V from negative rectification to positive rectification for gold gate functionalised by 5-amino-2-mercaptobenzimidazole in 100 mM KCl. The data were obtained from the measurements of 4 independent nanopores.

Based on the established protocol and formulation, different small organic molecules were successfully functionalised onto the gold, as presented in Figure 4-4. With respect to the fabrication workflow, consecutive change of I-Vs in both cases definitely suggested the attachment of thiols inside the nanopore. Interestingly, the self-assembly of very hydrophobic 1-Dodecanethiol onto gold caused a linear I-V, hardly with any rectification because of the neutral charge of dodecane. Perhaps this can be attributed to the closely packed dodecane perpendicular to the surface of gold, as facilitated by interchain Van der Waals interactions. Further characterisation was made using a Ruthenium (III) redox probe; more than a 100x reduction of the limiting current was obtained as a result of blocking diffusive flux for the redox mediator towards the surface of gold.

Functionalisation of gold nanopores with 5-amino-2-mercaptobenzimidazole, being positively charged at pH 8,[48] gave rise to yet more interesting phenomena. Apart from the change of I-V, the presence of heteroatoms allowed the tuning of molecular charge via protonation/deprotonation by changing the pH. By lowering the pH from 8 to 4, the rectification was inverted from negative to positive with a 98% change of the rectification ratio ($r = |I_{-400\ mV}/I_{400\ mV}|$) from 4.41 ± 0.17 to 0.11 ± 0.01. In contrast, in gold-coated pipettes, the change of rectification was much less (4.84 ± 0.14 to 2.02 ± 0.09).

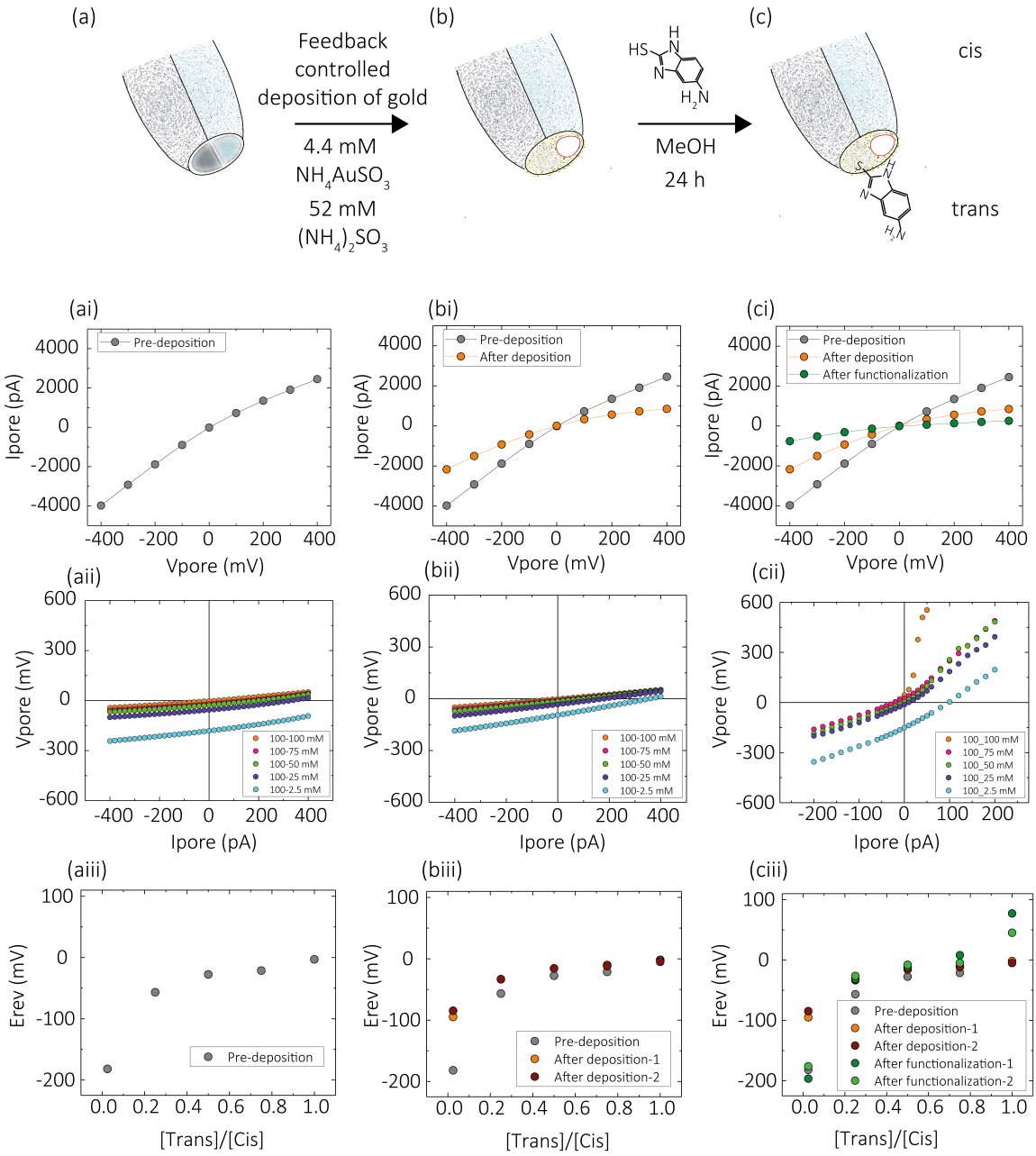


Figure 4-5: Fabrication process of the nanopore-FET device, starting from (a) unmodified (carbon only) pipettes, to (b) gold modified pipettes, and then (c) functionalised pipettes, with the corresponding (i) I-V characterisation after each stage of fabrication. Conductance values in 100 mM KCl were 8.13 ± 0.43 nS before deposition, 3.79 ± 0.30 nS after deposition, and 1.00 ± 0.15 nS after functionalisation. Considering the change of the nanopore surface charge after amine functionalisation, the I-V response across the nanopore revealed a significant change, from negative to positive rectification by tuning the pH from 8 to 4 in 10 mM KCl (inset, ciii). (ii) Ion selectivity measurements across nanopores after each stage of fabrication by using current-clamp mode of a Multiclapm 700B amplifier. Potential–current (Iclamp) measurements for nanopore-FET devices (a) before deposition, (b) after deposition and (c)

after functionalisation at different KCl concentration gradients. The concentration of KCl was only diluted by DI water outside of the nanopore to 75 mM, 50 mM, 25 mM, 2.5 mM, while the inside remained the same (100 mM KCl, 10 mM Tris-HCl and 1 mM EDTA buffer at pH 8). (iii) The potential at which the current is set to zero is represented as the reversal potential (E_{rev}). Before deposition, the nanopores exhibited cationic selectivity, indicated by (aiii) more negative reversal potentials as the concentration of the trans side was diluted. (biii) After deposition, the reversal potentials became less negative due to the reduction of surface charge. (ciii) The appearance of more positive reversal potentials after amine functionalisation indicated more positive nanopore surface charge. Ion-selectivity measurements showed a gradual tuning of nanopore surface charge. In all cases, the gate electrode was left floating. Potentials quoted here are relative to Ag/AgCl reference electrode in KCl bath.

Aside from the change of conductance and rectification, the incorporation of quartz, carbon, gold, and functionalised layers onto this nanopore-FET sensing platform resulted in the tuning of surface charge in solution. As the surface charge was tuned during the fabrication processes, cations and anions in the electrolyte had different tendencies to transport across the nanopore. To extract the information regarding the selectivity of ionic transport across the nanopore, I-clamp measurements were taken by setting up a constant transmembrane current that generated the potential difference between cis and trans chamber. The potential difference at which nanopore current became zero was defined as the reversal potential (Erev). With the working electrode inside the open barrel and the ground electrode in the bath, the preferential transport of cations gave a negative Erev, and vice versa. Most measurements were performed with a salt gradient between cis and trans to induce ion diffusion.

Ion selectivity characterisation in Figure 4-5 indicated that the nanopore possessed less negative charge after gold deposition as a result of positively charged gold, as shown by its pzc in Figure 4-3. As expected, functionalisation with positively charged amine was able to tune the surface charge more positive. Interestingly, the positively charged amine coating even induced a very positive Erev without any salt gradient. Due to the strong charge of the amine coating, we decided to proceed with the DNA translocation experiments with the aim of slowing down and fine-tuning single-molecule transport through voltage gating.

4.5 Fine-tuning single-molecule transport using amine-modified nanopore-FET

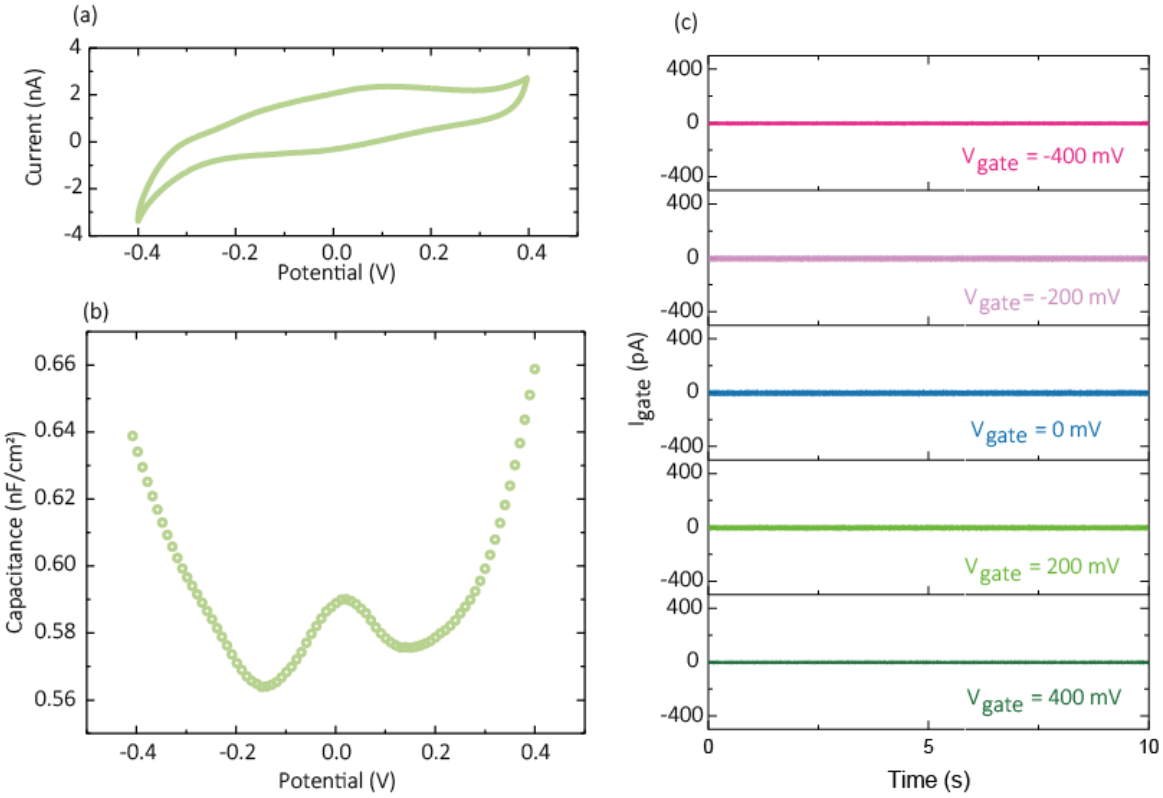


Figure 4-6: Electrochemical characterisation of an amine-modified gate. (a) Cyclic voltammetry from −0.4 to 0.4 V showed minimal faradaic currents within the range of V_{gate}, scan rate = 0.2 V/s. (b) Differential capacitance measurements of an amine-modified electrode showed a secondary capacitance minimum at 0.15 V. Effective charge tuning at the electrode-electrolyte interface was obtained for the functionalised system, as seen from the pronounced change of capacitance at both sides of the pzc; Using an amine-functionalised nanopore-FET, (c) I-t traces recorded from the amine functionalised gate showed that the magnitude of current remained at 0 pA, indicating that was unlikely that Faradaic processes took place on the functionalised gate electrode in the potential window V_{gate} = -400 to V_{gate} = 400 mV. All characterisation was performed in 100 mM KCl, 10 mM Tris-HCl and 1 mM EDTA buffer at pH 8.

Translocations with these surface-modified nanopores were performed using 200 pM 10 kbp DNA in 100 mM KCl at pH 8. Similar to using gold-deposited devices for voltage gating, an operating range V_{gate} = (−400, 400 mV) was selected to minimise Faradaic processes at the

functionalised surface (Figure 4-6), verified through cyclic voltammetry on a functionalised ultramicroelectrode, with the zero-current recorded on the gate electrode at different applied potentials. Therefore, the SAM coating was stable enough under the experimental conditions outlined above.

Based on the stability of the amine coating within the potential range, the voltage-responsive behaviour of the double-layer was measured using differential capacitance. Previously, it was shown that the charge of functional groups on the modified gold electrode had a significant effect on the potential of zero charge, with pzc being shifted according to the charge of functional groups.[49,50] In this case, the functionalised electrode exhibited an additional capacitance minimum at a more positive potential of 150 mV. (Figure 4-6)

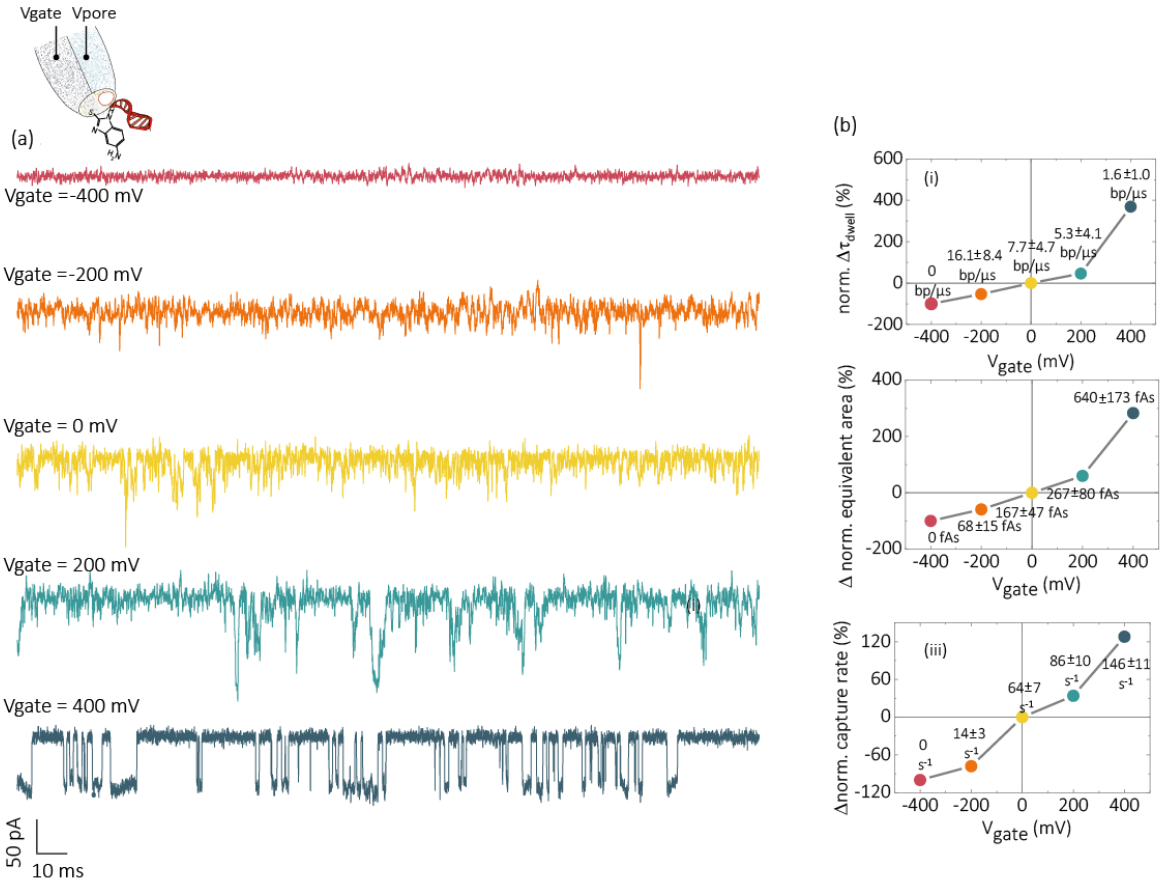


Figure 4-7: Voltage gating of an amine-modified nanopore-FET. Voltage gating was achieved via a stepwise increase of V_{gate} from −400 mV to 400 mV at 200 mV intervals. (a) Current–time traces showing the gating control of 10 kbp DNA translocation at an applied V_{gate} of −400 mV, −200 mV, 0 mV, 200 mV, and 400 mV. (b) The dependence on (i) dwell time, (ii) equivalent area, and (iii) event frequency is shown as a function of the gating potentials. All data were expressed as percentage change with respect

to V_{gate} = 0 mV, and in all cases, V_{pore} = −500 mV. 10 kbp DNA was added in the nanopipette and translocation occurred from in to out.

By increasing V_{gate} from −400 to 400 mV, translocations across the functionalised nanopore could be switched on/off and, more importantly, the translocation velocity and frequency could be controlled. A decrease in mean translocation velocity (Figure 4-7 a) from 16.1 to 1.6 bp/µs and a controllable increase in event frequency (Figure 4-7 b) from 0 to 147 ± 29 s^{-1} were achieved via stepwise tuning of V_{gate} from −400 to 400 mV. The reproducibility of gating control was verified by repeating the experiment using different functionalised nanopipettes (Figure 4-8). It is also possible that irreversible binding between DNA and positively charged surface occurred but at all gating potentials the currents recorded on the gate remained at zero, excluding the possibility of significant surface absorption.

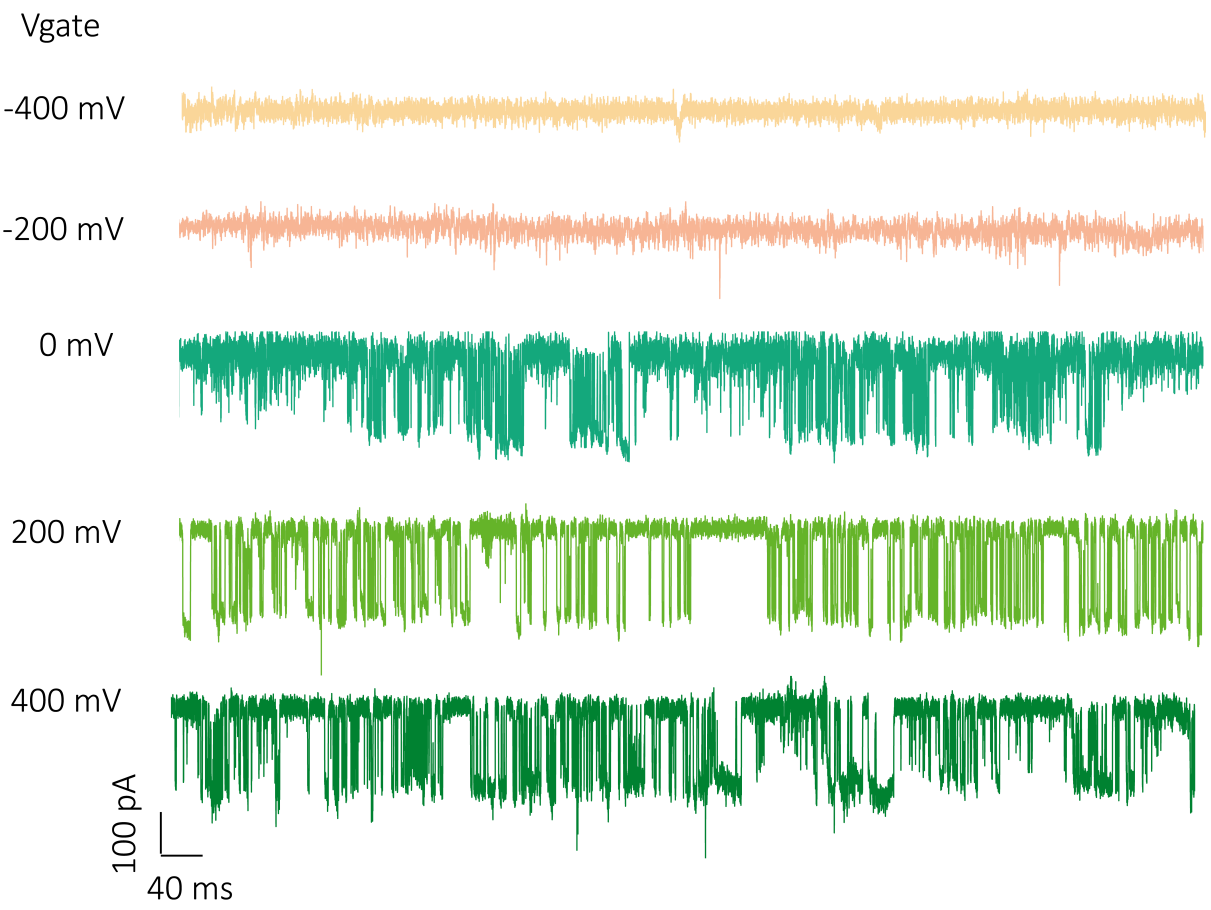


Figure 4-8: Supplementary traces of 10 kbp DNA confirming the reproducibility of voltage gating with amine-functionalised nanopore-FETs. V_{pore} = −500 mV. V_{gate} was tuned between −400 and 400 mV. 10 kbp DNA was added in the nanopipette and translocation occurred from in to out.

4.6 Conclusion and future work

In this chapter, I demonstrated a new class of nanopore–FETs for gating manipulation of single molecules. Voltage gating was implemented into this system by tuning both electrophoretic and electroosmotic flow as well as electrostatic interactions with analytes, allowing DNA transport to be switched on/off in real-time. This platform allowed for easy surface functionalisation, which permitted us to further tune molecular gate transport through the nanopore, including dwell time and capture rates. The performance of the nanopore–FET devices presented in this article has implications for the enhancement of the controllability, sensitivity, and selectivity of nanopore sensing.

More importantly, facile chemical functionalisation of gate electrodes opens up the possibility of using this platform to detect and manipulate a wide range of biological analytes with improved sensitivity and selectivity. As the functionalisation has been verified to be entirely possible for small organic molecules, an extension can be made towards functionalising nanopores with recognition elements to combine the advantages of molecular recognition, nanopores, and field-effect transistors.

4.7 References

(1) Turner, A. P. F. Biosensors: Sense and Sensibility. *Chem. Soc. Rev.* **2013**, *42* (8), 3184–3196.

(2) Newman, J. D.; Turner, A. P. F. Home Blood Glucose Biosensors: A Commercial Perspective. *Biosens. Bioelectron.* **2005**, *20* (12), 2435–2453.

(3) Eid, J.; Fehr, A.; Gray, J.; Luong, K.; Lyle, J.; Otto, G.; Peluso, P.; Rank, D.; Baybayan, P.; Bettman, B.; Bibillo, A.; Bjornson, K.; Chaudhuri, B.; Christians, F.; Cicero, R.; Clark, S.; Dalal, R.; DeWinter, A.; Dixon, J.; Foquet, M.; Gaertner, A.; Hardenbol, P.; Heiner, C.; Hester, K.; Holden, D.; Kearns, G.; Kong, X.; Kuse, R.; Lacroix, Y.; Lin, S.; Lundquist, P.; Ma, C.; Marks, P.; Maxham, M.; Murphy, D.; Park, I.; Pham, T.; Phillips, M.; Roy, J.; Sebra, R.; Shen, G.; Sorenson, J.; Tomaney, A.; Travers, K.; Trulson, M.; Vieceli, J.; Wegener, J.; Wu, D.; Yang, A.; Zaccarin, D.; Zhao, P.; Zhong, F.; Korlach, J.; Turner, S. Real-Time DNA Sequencing from Single Polymerase Molecules. *Science* **2009**, *323* (5910), 133–138.

(4) Juette, M. F.; Terry, D. S.; Wasserman, M. R.; Zhou, Z.; Altman, R. B.; Zheng, Q.; Blanchard, S. C. The Bright Future of Single-Molecule Fluorescence Imaging. *Curr. Opin. Chem. Biol.* **2014**, *20* (1), 103–111.

(5) Huang, S.; Romero-Ruiz, M.; Castell, O. K.; Bayley, H.; Wallace, M. I. High-Throughput Optical Sensing of Nucleic Acids in a Nanopore Array. *Nat. Nanotechnol.* **2015**, *10* (11), 986–997.

(6) Bulushev, R. D.; Marion, S.; Petrova, E.; Davis, S. J.; Maerkl, S. J.; Radenovic, A. Single Molecule Localization and Discrimination of DNA-Protein Complexes by Controlled Translocation Through Nanocapillaries. *Nano Lett.* **2016**, *16* (12), 7882–7890.

(7) Peng, H.; Ling, X. S. Reverse DNA Translocation through a Solid-State Nanopore by Magnetic Tweezers. *Nanotechnology* **2009**, *20* (18), 185101.

(8) Neuman, K. C.; Nagy, a. Single-Molecule Force Spectroscopy: Optical Tweezers, Magnetic Tweezers and Atomic Force Microscopy. *Nat. Methods* **2008**, *5* (6), 491–505.

(9) Wanunu, M.; Meller, A. Chemically Modified Solid-State Nanopores. *Nano Lett.* **2007**, *7* (6), 1580–1585.

(10) Miles, B. N.; Ivanov, A. P.; Wilson, K. a; Doğan, F.; Japrung, D.; Edel, J. B. Single Molecule Sensing with Solid-State Nanopores: Novel Materials, Methods, and Applications. *Chem. Soc. Rev.* **2013**, *42* (1), 15–28.

(11) Venkatesan, B. M.; Bashir, R. Nanopore Sensors for Nucleic Acid Analysis. *Nat. Nanotechnol.* **2011**, *6* (10), 615–624.

(12) Cui, Y.; Wei, Q.; Park, H.; Lieber, C. M. Nanowire Nanosensors for Highly Sensitive and Selective Detection of Biological and Chemical Species. *Science* **2001**, *293* (5533), 1289–1292.

(13) Zhang, A.; Lieber, C. M. Nano-Bioelectronics. *Chem. Rev.* **2016**, *116*, 215–257.

(14) Cao, C.; Li, M.-Y.; Cirauqui, N.; Wang, Y.-Q.; Dal Peraro, M.; Tian, H.; Long, Y.-T. Mapping the Sensing Spots of Aerolysin for Single Oligonucleotides Analysis. *Nat. Commun.* **2018**, *9* (1), 2823.

(15) Freedman, K. J.; Otto, L. M.; Ivanov, A. P.; Barik, A.; Oh, S.-H.; Edel, J. B. Nanopore Sensing at Ultra-Low Concentrations Using Single-Molecule Dielectrophoretic Trapping. *Nat. Commun.* **2016**, *7*, 10217.

(16) Clarke, J.; Wu, H.; Jayasinghe, L.; Patel, A.; Reid, S.; Bayley, H. Continuous Base Identification for Single-Molecule Nanopore DNA Sequencing. *Nat. Nanotechnol.* **2009**, *4* (4), 265–270.

(17) Traversi, F.; Raillon, C.; Benameur, S. M.; Liu, K.; Khlybov, S.; Tosun, M.; Krasnozhon, D.; Kis, A.; Radenovic, A. Detecting the Translocation of DNA through a Nanopore Using Graphene Nanoribbons. *Nat. Nanotechnol.* **2013**, *8* (12), 939–945.

(18) Ivanov, A. P.; Instuli, E.; McGilvery, C. M.; Baldwin, G.; McComb, D. W.; Albrecht, T.; Edel, J. B. DNA Tunneling Detector Embedded in a Nanopore. *Nano Lett.* **2011**, *11*, 279–285.

(19) Sze, J. Y. Y.; Ivanov, A. P.; Cass, A. E. G.; Edel, J. B. Single Molecule Multiplexed Nanopore Protein Screening in Human Serum Using Aptamer Modified DNA Carriers. *Nat. Commun.* **2017**, *8* (1), 1552.

(20) Ren, R.; Zhang, Y.; Nadappuram, B. P.; Akpinar, B.; Klenerman, D.; Ivanov, A. P.; Edel, J. B.; Korchev, Y. Nanopore Extended Field-Effect Transistor for Selective Single-Molecule Biosensing. *Nat. Commun.* **2017**, *8* (1), 586.

(21) Heerema, S. J.; Dekker, C. Graphene Nanodevices for DNA Sequencing. *Nat. Nanotechnol.* **2016**, *11* (2), 127–136.

(22) Building a Better Nanopore. *Nat. Nanotechnol.* **2016**, *11* (2), 105–105.

(23) Lindsay, S. The Promises and Challenges of Solid-State Sequencing. *Nat. Nanotechnol.* **2016**, *11* (2), 109–111.

(24) Patolsky, F.; Zheng, G.; Hayden, O.; Lakadamyali, M.; Zhuang, X.; Lieber, C. M. Electrical Detection of Single Viruses. *Proc. Natl. Acad. Sci. U. S. A.* **2004**, *101* (39), 14017–14022.

(25) Yanagi, I.; Oura, T.; Haga, T.; Ando, M.; Yamamoto, J.; Mine, T.; Ishida, T.; Hatano, T.; Akahori, R.; Yokoi, T.; Anazawa, T. Side-Gated Ultrathin-Channel Nanopore FET Sensors. *Nanotechnology* **2016**, *27* (11), 115501.

(26) Zhang, Y.; Clausmeyer, J.; Babakinejad, B.; López Córdoba, A.; Ali, T.; Shevchuk, A.; Takahashi, Y.; Novak, P.; Edwards, C.; Lab, M.; Gopal, S.; Chiappini, C.; Anand, U.; Magnani, L.; Coombes, R. C.; Gorelik, J.; Matsue, T.; Schuhmann, W.; Klenerman, D.; Sviderskaya, E. V.; Korchev, Y. Spearhead Nanometric Field-Effect Transistor Sensors for Single-Cell Analysis. *ACS Nano* **2016**, *10* (3), 3214–3221.

(27) Xie, P.; Xiong, Q.; Fang, Y.; Qing, Q.; Lieber, C. M. Local Electrical Potential Detection of DNA by Nanowire–Nanopore Sensors. *Nat. Nanotechnol.* **2011**, *7* (2), 119–125.

(28) Kim, K. B.; Nam, S. W.; Rooks, M. J.; Rossnagel, S. M. Ionic Field Effect Transistors with Sub-10 Nm Multiple Nanopores. *Nano Lett.* **2009**, *9* (5), 2044–2048.

(29) Luan, B.; Stolovitzky, G.; Martyna, G. Slowing and Controlling the Translocation of DNA in a Solid-State Nanopore. *Nanoscale* **2012**, *4* (4), 1068–1077.

(30) Paik, K. H.; Liu, Y.; Tabard-Cossa, V.; Waugh, M. J.; Huber, D. E.; Provine, J.; Howe, R. T.; Dutton, R. W.; Davis, R. W. Control of DNA Capture by Nanofluidic Transistors. *ACS Nano* **2012**, *6* (8), 6767–6775.

(31) He, Y.; Tsutsui, M.; Fan, C.; Taniguchi, M.; Kawai, T. Controlling DNA Translocation through Gate Modulation of Nanopore Wall Surface Charges. *ACS Nano* **2011**, *5* (7), 5509–5518.

(32) Heerema, S. J.; Vicarelli, L.; Pud, S.; Schouten, R. N.; Zandbergen, H. W.; Dekker, C. Probing DNA Translocations with Inplane Current Signals in a Graphene Nanoribbon with a Nanopore. *ACS Nano* **2018**, *12* (3), 2623–2633.

(33) Puster, M.; Balan, A.; Rodríguez-Manzo, J. A.; Danda, G.; Ahn, J. H.; Parkin, W.; Drndić, M. Cross-Talk Between Ionic and Nanoribbon Current Signals in Graphene Nanoribbon-Nanopore Sensors for Single-Molecule Detection. *Small* **2015**, *11* (47), 6309–6316.

(34) Panday, N.; Qian, G.; Wang, X.; Chang, S.; Pandey, P.; He, J. Simultaneous Ionic Current and Potential Detection of Nanoparticles by a Multifunctional Nanopipette. *ACS Nano* **2016**, *10* (12), 11237–11248.

(35) Ivanov, A.; Actis, P.; Jönsson, P. On-Demand Delivery of Single DNA Molecules Using Nanopipets. *ACS Nano* **2015**, *9* (4), 3587–3595.

(36) Gershow, M.; Golovchenko, J. A. Recapturing and Trapping Single Molecules with a Solid-State Nanopore. *Nat. Nanotechnol.* **2007**, *2* (12), 775–779.

(37) Plesa, C.; van Loo, N.; Dekker, C. DNA Nanopore Translocation in Glutamate Solutions. *Nanoscale* **2015**, *7* (32), 13605–13609.

(38) Crick, C. R.; Albella, P.; Ng, B.; Ivanov, A. P.; Roschuk, T.; Cecchini, M. P.; Bresme, F.; Maier, S. A.; Edel, J. B. Precise Attoliter Temperature Control of Nanopore Sensors Using a Nanoplasmonic Bullseye. *Nano Lett.* **2015**, *15* (1), 553–559.

(39) Karnik, R.; Fan, R.; Yue, M.; Li, D.; Yang, P.; Majumdar, A. Electrostatic Control of Ions and Molecules in Nanofluidic Transistors. *Nano Lett.* **2005**, *5* (5), 943–948.

(40) Crick, C. R.; Sze, J. Y. Y.; Rosillo-Lopez, M.; Salzmann, C. G.; Edel, J. B. Selectively-Sized Graphene-Based Nanopores for In-Situ Single Molecule Sensing. *ACS Appl. Mater. Interfaces* **2015**, *7* (32), 18188–18194.

(41) Gibb, T. R.; Ivanov, A. P.; Edel, J. B.; Albrecht, T. Single Molecule Ionic Current Sensing in Segmented Flow Micro Fl Uidics. *Anal. Chemisry* **2014**, *86*, 1864–1871.

(42) Gong, X.; Patil, A. V.; Ivanov, A. P.; Kong, Q.; Gibb, T.; Dogan, F.; Demello, A. J.; Edel, J. B. Label-Free in-Flow Detection of Single DNA Molecules Using Glass Nanopipettes. *Anal. Chem.* **2014**, *86* (1), 835–841.

(43) Gao, W.; Baker, T. A.; Zhou, L.; Pinnaduwage, D. S.; Kaxiras, E.; Friend, C. M. Chlorine Adsorption on Au(111): Chlorine Overlayer or Surface Chloride? *J. Am. Chem. Soc.* **2008**, *130* (11), 3560–3565.

(44) Wilson, J.; Sarthak, K.; Si, W.; Gao, L. Y.; Aksimentiev, A. Rapid and Accurate Determination of Nanopore Ionic Current Using a Steric Exclusion Model. *ACS Sensors* **2019**, *4* (3), 634–644.

(45) Kesselheim, S.; Muller, W.; Holm, C. Origin of Current Blockades in Nanopore Translocation Experiments. *Phys. Rev. Lett.* **2014**, *112* (1), 18101.

(46) Andersen, T. N.; Perkins, R. S.; Eyring, H. Zero-Charge Potentials of Solid Metals. *J. Am. Chem. Soc.* **1964**, *86* (20), 4496.

(47) Sugimoto, M.; Kato, Y.; Ishida, K.; Hyun, C.; Li, J.; Mitsui, T. DNA Motion Induced by Electrokinetic Flow near an Au Coated Nanopore Surface as Voltage Controlled Gate. *Nanotechnology* **2015**, *26* (6), 065002.

(48) Walba, H.; Isensee, R. W. Acidity Constants of Some Arylimidazoles and Their Cations. *J. Org. Chem.* **1961**, *26* (8), 2789–2791.

(49) Janek, R. P.; Fawcett, W. R.; Ulman, A. Impedance Spectroscopy of Self-Assembled Monolayers on Au(111): Evidence for Complex Double-Layer Structure in Aqueous NaClO4 at the Potential of Zero Charge. *J. Phys. Chem. B* **1997**, *101* (42), 8550–8558.

(50) Ramírez, P.; Andreu, R.; Cuesta, Á.; Calzado, C. J.; Calvente, J. J. Determination of the Potential of Zero Charge of Au(111) Modified with Thiol Monolayers. *Anal. Chem.* **2007**, *79* (17), 6473–6479.

Chapter 5

Selective sensing of proteins and neurotransmitters using aptamer functionalised nanopore field-effect transistors

Contents

Abstract 112

5.1 Introduction 113

5.2 Device fabrication and chemical modification 116

5.3 Optimisation of aptamer-modified nanopore-FETs 119

5.4 Controlling protein transport by aptamer-functionalised nanopores 122

5.5 Detection of neurotransmitters 125

5.5.1 Characterisation of the binding between aptamers and neurotransmitters using electrical measurements 126

5.5.2 Selective single-molecule detection of neurotransmitters 129

5.5.3 Single-molecule binding assay for neurotransmitters 135

5.6 Conclusion and future work 138

5.7 References 140

Abstract

The selective identification and analysis of biologically important proteins and small molecules at physiological concentrations has been a major driving force for advancing novel detection strategies. For example, nanopore sensing represents a promising route towards advancing conventional detection methods due to its single-molecule sensitivity and label-free operation. However, it remains exceptionally challenging to selectively detect and quantify biologically important proteins and small molecules at sufficiently low concentrations. Herein, I propose a novel class of nanopore bio-transistors, which combines the advantages of aptamer recognition chemistry with the single-molecule sensitivity of nanopore sensors. I demonstrate that it is possible to simultaneously detect those analytes and quantify the binding affinity at a single-molecule level through target-induced conformational changes of the aptamers. Moreover, I show that the neurotransmitters can be detected at fM concentrations.

5.1 Introduction

The accurate detection and quantification of biomolecules is one of the most important goals for the development of biosensors[1–3], and it has significant implications for a range of applications, such as early-stage diagnosis and disease screening. However, there is still a significant need to enhance the sensitivity and selectivity, reduce complex sample labelling and simplify the sensor design.[4–8] Whilst conventional electrochemical[9] and optical-based[10] sensors have been developed to address several of these limitations, many analytes still need to be detected with improved sensitivity and selectivity, especially when working with biological samples.[11] Single-molecule methods have been becoming more prominent in recent years, which is mainly due to the fact that they are capable of distinguishing the individual behaviours of biomolecules from the ensemble averaged properties. This creates the possibility to detect low abundant species. A plethora of single-molecule methods[11–14] have been developed and interconnected for certain purposes, such as single-molecule sequencing[11,12], optical and force spectroscopy[13] and cellular biopsy applications[14].

With the increasing significance of single-molecule methods, nanopores[2,3] and field-effect transistors[15,16] have appeared as promising techniques, which is mainly due to their label-free operation. However, both techniques are limited by the lack of sensitivity and selectivity, especially for molecular targets, such as smaller proteins and neurotransmitters. The operating principle of nanopore sensors is inherently simple and relies on electrokinetically or electrophoretically driving the analytes to translocate through a nanopore, which causes a modulation of the ionic current. The resultant electrical signatures can be used to gather information on the translocating, including the length, size, shape and interaction with the nanopore surface.[17–19] However, the sensing process is typically diffusion-limited and can be restricted further because of elecromigration for analytes being neutral or few charges in solution, and it is often not sufficiently sensitive to distinguish analytes with a similar structure and charge. Therefore, different approaches have been developed to further decrease the limit of detection to sub-pM levels by pre-concentrating the analytes in close proximity to the nanopore using specific methods, such as dielectrophoresis[20] or magnetic fields[21]. Moreover, the selective detection of specific analytes from a complex biological background is a major issue that needs addressing. While receptor-modified nanoscale FETs enable the detection of

biological analytes by monitoring the change of transconductance of semiconductors, the Debye screening in physiological conditions limits the gating response of small target molecules with few charges or being neutral in solutions.[16,22]

Recently, nucleic acid aptamers have been used as an artificial receptor to increase the sensitivity and selectivity of both nanopores[23] and field-effect transistors[22]. Selected from SELEX processes, the high specificity and affinity that are afforded from unique molecular conformations enable the selective recognition of the target with enhanced sensitivity.[24] DNA aptamers were specifically chosen due to their enhanced stability of unique molecular structures, such as stem-loops and G-quadruplexes.

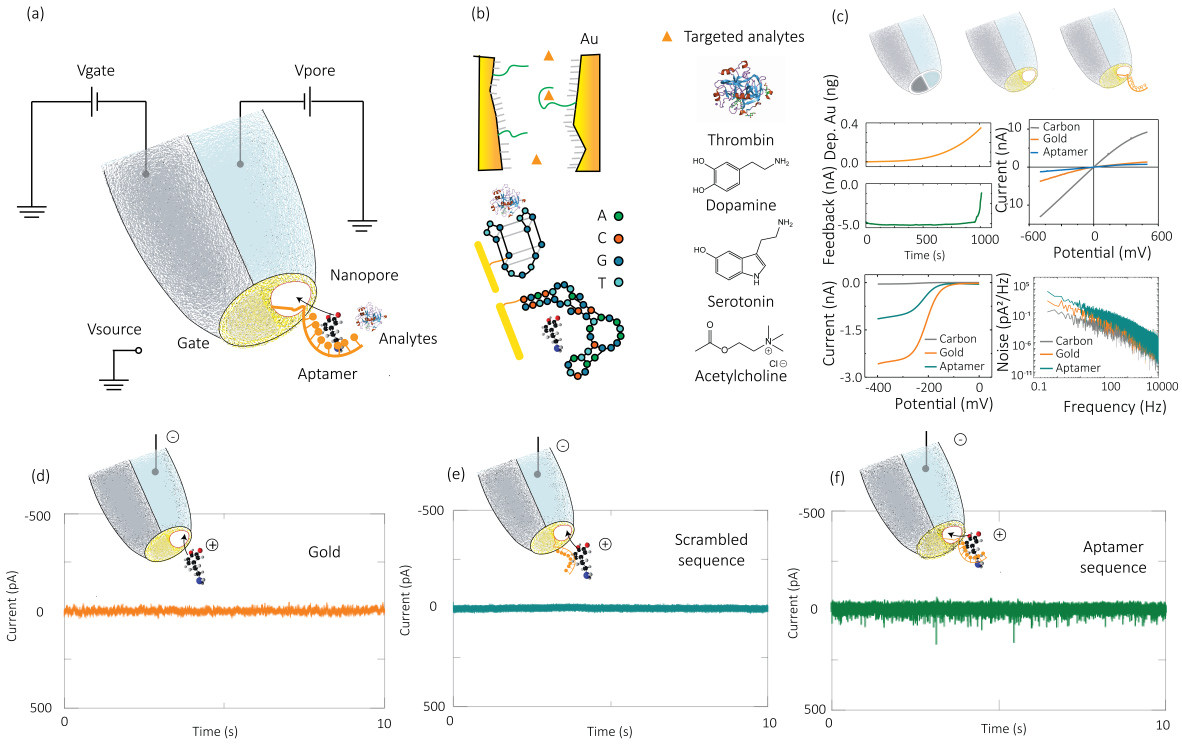


Figure 5-1: The schematic design of aptamer-functionalised nanopore bio-transistors, feedback-controlled fabrication and single-molecule detection of targeted analytes. (a) One barrel was selectively filled with carbon while another barrel (nanopore) was left open. Gold was electrochemically deposited onto carbon. The aptamers were functionalised onto the gold via thiol self-assembly. (b) The schematic design of the nanopore bio-transistor surface chemistry. It includes the sequence information of the aptamers for proteins and neurotransmitters, and the binding mode between the targeted analyte and aptamers. For protein detection, a 15-mer thrombin binding aptamer was used, as the binding occurs

between a G-quadruplex and thrombin. In contrast, for neurotransmitters, the stem-loop aptamer binds to the neurotransmitter via target-induced conformational changes, and the aptamers switch from a duplex to a G-quadruplex conformation upon analyte binding. (c) The feedback-controlled fabrication of nanopore bio-transistors. The electrochemical deposition of gold was performed using a bipotentiostatic configuration, where a reducing potential of -0.73 V was held at the carbon nanoelectrode. The deposition process was monitored by a real-time ionic current flowing through the open barrel due to the potential difference of -0.1 V between the second working electrode and a combined counter/reference electrode in the bath. The gold deposition was stopped at the specific threshold current of -1.5 nA. The gold-deposited device was functionalised by thiolated aptamers. The whole process was monitored by the consecutive change of IV (52 mM $(NH_4)_2SO_3$), as well as the change of the active electrochemical area in the presence of 1 mM $Ru(NH_3)_6Cl_3$. The representative current traces showed the single-molecule translocation of dopamine across (d) gold deposited devices, (e) scrambled sequence functionalised devices and (f) aptamer-functionalised devices. Dopamine was added in the bath.

Herein, I propose a strategy to combine the advantages of nanopore sensors, aptamer molecular recognition chemistry and field-effect transistors (Figure 5-1). For example, nanopores can be functionalised with aptamers to target specific analytes, and this can be further combined with voltage gating to control the physical interactions between the analytes and receptors. I have previously demonstrated the routes towards the fabrication of hybrid nanopore-FET systems for simultaneous single-molecule detection and manipulation.[25] In the present work, we build on these concepts for the selective sensing of small neurotransmitter molecules, including dopamine, serotonin and acetylcholine (Figure 5-1, a–b). Specifically, stem-loop aptamers were attached to the surface of the nanopore, which enabled ligand-induced conformational rearrangements near the nanopore surfaces. Whilst the vast majority of methods for detecting neurotransmitters have a detection limit that ranges from nM to μM[26], the single-molecule detection of neurotransmitters can be achieved at fM level, which is 6–9 magnitudes lower than the conventional electrochemical or optical methods[26].

Name	Sequence Information
Thrombin binding aptamer	/5-ThioMC6-D/GGTTGGTGTGGTTGG
Single base mutation	/5-ThioMC6-D/GGTTGGTGTGGTTTG
Double base mutation	/5-ThioMC6-D/GGTTGGTGTTGTTTG
Random sequence	/5-ThioMC6-D/TATATGACGACGGTG
Dopamine binding aptamer	/5-ThioMC6-D/CGACGCCAGTTTGAA GGTTCGTTCGCAGGTGTGGAGTGACGTCG
Scrambled dopamine aptamer	/5ThioMC6D/GGATATTGCGCGATTCCG GTCGGCAGCTTAGGAAGTGCGGTGTC
Serotonin binding aptamer	/5-ThioMC6-D/CGACTGGTAGGCAGA TAGGGGAAGCTGATTCGATGCGTGGGTCG
Scrambled serotonin aptamer	/5ThioMC6-D/CGTTTGGGGGTAGGAA GCTTATGCCGCGATAAAGGGTAGGGGCC
Complementary sequence of serotonin aptamer	CGACCCACGCATCGAATCAGCTT CCCCTATCTGCCTACCAGTCG
Acetylcholine binding aptamer	/5-ThioMC6-D/AGAGATACTGCCGGTT GCCTTCGACCGCGACGTTGGATTGGTAAC ATAAGGCCACTCCCTTCATGTGGGAT
Scrambled acetylcholine aptamer	/5ThioMC6-D/AGAGATACCTGCCGGTTGCCTTCGA CCGCGACGTTGGATTGGTAACATAAG GCCACTCCCTTCATGTGGGAT

Table 5-1: List of DNA oligonucleotide sequences that are used in this work. All sequences were written in the form from 5' end to 3' end. For thiol-modified DNA oligonucleotides, the oligos were synthesised with an S-trityl-6-mercaptohexyl derivative protecting group. 100 times the excess amount of TCEP (tris (2-carboxyethyl) phosphine) was used to cleave the disulphide bond and form the reactive thiol-modified oligos. The thiol group was separated from the oligo with a C6 spacer arm.

5.2 Device fabrication and chemical modification

Figure 5-1 demonstrates the electrochemical fabrication, chemical modification and device components for our aptamer-functionalised sensors. Each fabrication step was characterised by a combination of I-clamp and V-clamp measurements (Figure 5-2). For the feedback-controlled deposition of gold, a final feedback current of -1.5 nA was chosen, which corresponds to a nanopore diameter of approximately 20 nanometres (nm). To attach aptamers onto the nanopore's surface, the disulfide form of purchased oligonucleotides was pre-treated by tris(2-carboxyethyl)phosphine to form thiol-reactive oligos on 5' end (Scheme

2-2, Table 5-1). The deposited gold was functionalised by the self-assembly of 2 µM thiol oligos of different sequences.

After chemical modification, the mean conductance of the nanopore was decreased due to the attachment of oligonucleotides. As the thiol-modified oligos are negatively charged, the functionalised nanopores showed greater cation selectivity than the gold nanopores.[27] Moreover, the electrochemical surface area of gold was reduced by approximately 60 per cent (%), as seen from the steady-state diffusion limiting currents (Figure 5-2 aiii, inset), which verifies the successful functionalisation of gold.

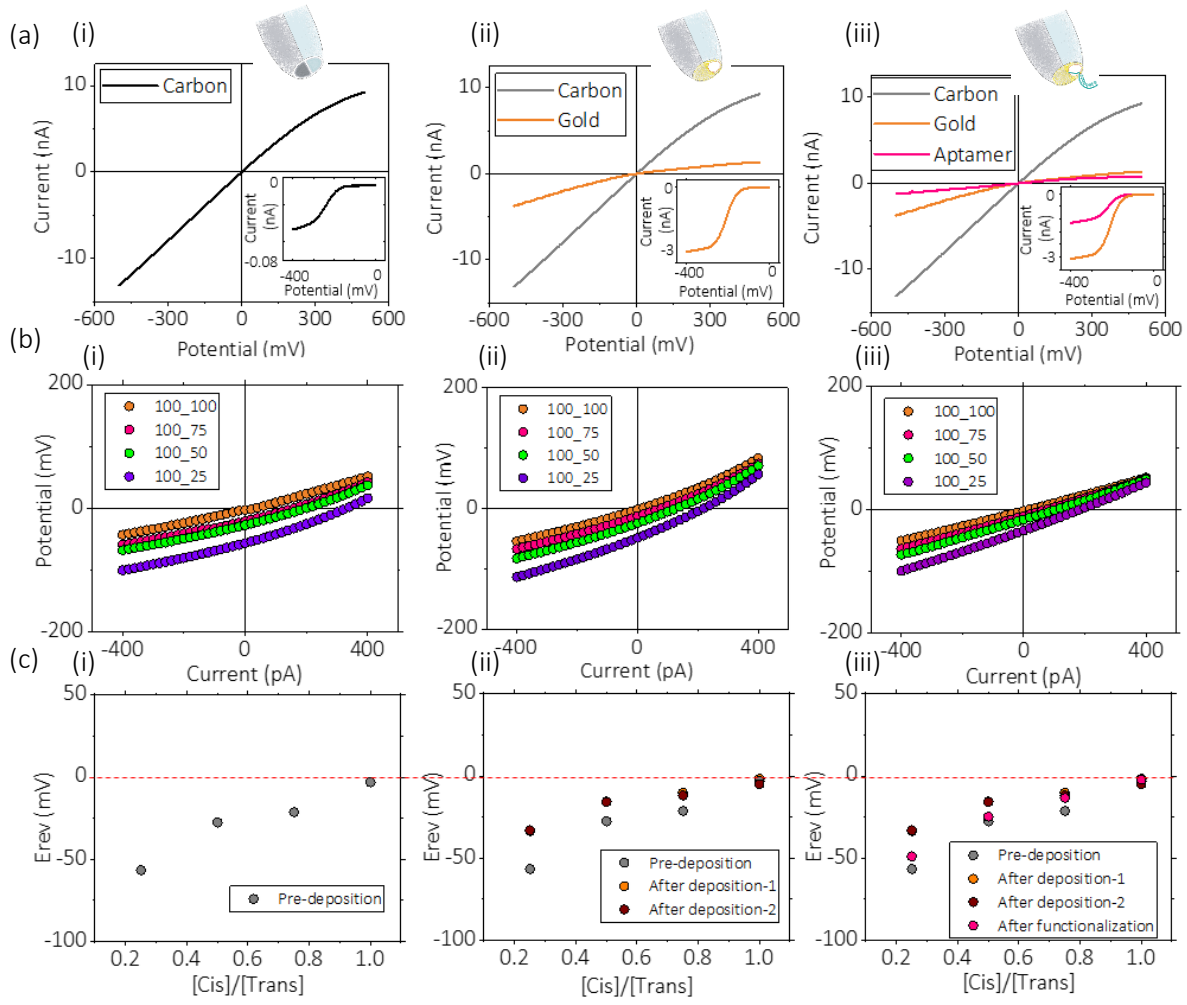


Figure 5-2: The characterisation for the fabrication of nanopore bio-transistors. The process starts with a (i) carbon only device, to form a (ii) gold deposited device via the feedback-controlled deposition of gold, and an (iii) aptamer-functionalised device produced from the surface functionalisation of deposited gold by the thiolated aptamers. To verify the successful fabrication at each step, with (a) I-V measurements demonstrating the consecutive shrinking of nanopore conductance, the inset illustrates

the electrochemical measurements for the active surface area for the carbon nanoelectrode, gold deposited electrode and the aptamer-functionalised electrode. The active surface area was increased after the gold deposition and then decreased after aptamer functionalisation, as seen from the steady-state diffusing limiting current in the presence of 1 mM $Ru(NH_3)_6Cl_3$ upon cathodic polarisation from 0 mV to -400 mV. The whole process was further confirmed by (b), (c) ion-selectivity measurements. The salt concentration on the trans chamber was diluted, while the cis chamber remained unchanged. At each concentration gradient, a reversal potential (E_{rev}) was measured. After the gold deposition, Erev appeared to be more positive, which indicated the reduction of surface charge from a carbon/quartz nanopore to a gold nanopore. Aptamer-functionalized nanopore exhibited a more negative reversal potential compared to the gold deposited device due to the attachment of negatively charged oligonucleotides on the surface. In all cases, the electrolyte in the cis chamber was 100 mM KCl, 10 mM Tris and 1 mM EDTA at pH 8. The concentration of the trans chamber (KCl bath) was varied by serial dilution. Cis means in the nanopipette and trans means the KCl bath.

The specific binding towards different target analytes can be controlled by attaching different aptamers bearing unique molecular structures onto the gold surface (Figure 5-1 b). Further properties of modified nanopores were obtained by analysing the power spectrum density (PSD) of chemically modified nanopores (Figure 5-3). Compared to the gold nanopores, the aptamer-modified nanopores showed a comparable noise at high frequencies with an increase of 1/f noise in the low-frequency regime (f<100 Hz), which is in good agreement with previous literature on functionalising solid-state nanopores with protein receptors[28], lipid bilayers[29] and nuclear pores[30]

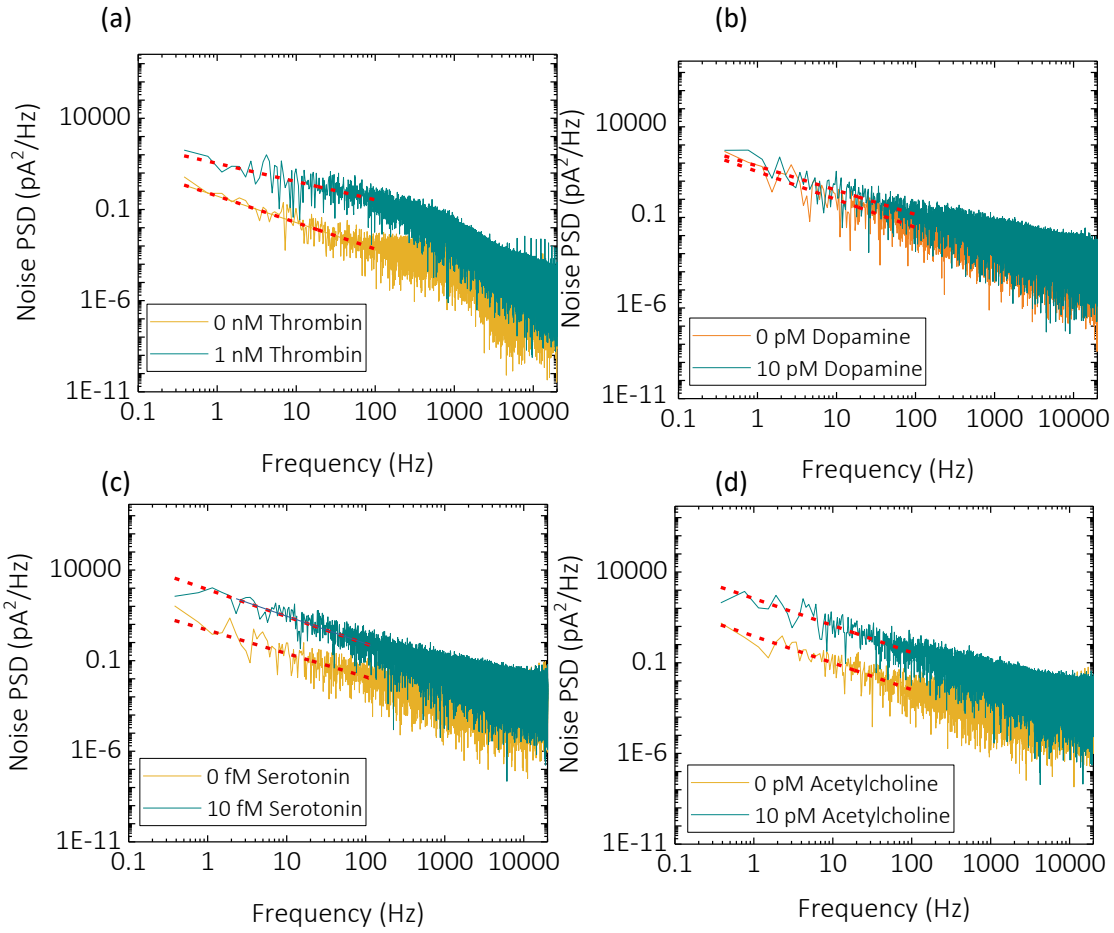


Figure 5-3: Power spectrum density (PSD) for nanopores that are functionalised by different aptamers for (a) thrombin, (b) dopamine, (c) serotonin and (d) acetylcholine, before and after adding the targeted analytes. For all cases, the noise spectra mainly differ in the low-frequency regime (f<100 Hz). In this regime, the power spectra showed 1/f dependence. The specific binding between the aptamer and targeted analyte caused more dynamic fluctuations of thiol-modified oligonucleotides inside the pore. All PSDs were obtained by analysing 10 s current traces for each case. The current traces were low-pass filtered at 30 kHz and sampled at 250 kHz. The red dotted lines represent the linear fitting of PSD at a low-frequency regime. V_{pore} = -500 mV in all cases. The data were obtained from 8 independent nanopores. Analytes were added into the bath.

5.3 Optimisation of aptamer-modified nanopore-FETs

Based on the aptamer-functionalised platform, we chose to investigate thrombin detection as our preliminary target. A 15-mer thrombin binding aptamer[31] bearing a well-studied G-quadruplex structure and a Kd of 25–200 nM[32–34] was functionalised onto gold (Figure 5-1b,

Table 1). The aptamer interacts with the fibrinogen binding site of thrombin. For translocation experiments, the functionalised devices were placed in a solution of 100 mM KCl and 10 mM Tris-EDTA buffer at pH 8, with the carbon barrel and empty barrel as two independent working electrodes and a common reference/ground electrode in the bath. Control experiments using quartz nanopipettes, carbon only and gold deposited nanopipettes produced indistinguishable signals, which means that non-specific interactions are not able to cause modulations in the ionic current.

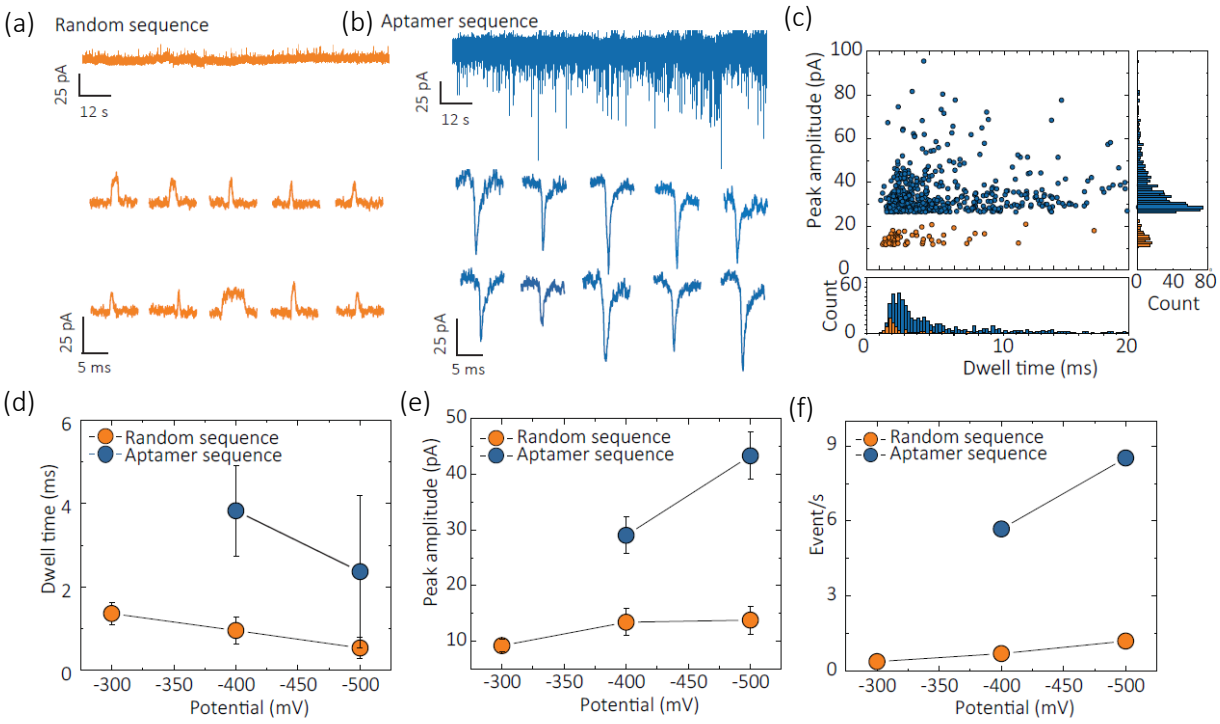


Figure 5-4: The single-molecule detection of thrombin using nanopores functionalised by (a) random sequence and (b) aptamer sequence. Using nanopores functionalised by a random sequence, the translocation of thrombin produced current blockade, whereas, for the aptamer-functionalised nanopore, current enhancement was observed. (c) The specific interactions between the aptamer and thrombin caused a higher peak current and a longer dwell time than the nanopore functionalised by a random sequence. For aptamer-functionalised nanopore, a cut down of peak current was observed for a certain threshold as a result of the binding between aptamer and thrombin. This was further revealed by the voltage dependence of the (d) dwell time, (e) peak amplitude and (f) capture rate. The 1 nM thrombin was added inside the pipette and the translocation occurred from in to out.

Upon the addition of 1 nM thrombin to the aptamer-functionalised nanopipette, the thrombin translocation events could be observed at negative potentials, whereas no translocation signals were observed for bare pipettes, carbon only and gold deposited pipettes. The aptamer-functionalised devices produced single-molecule translocation peaks exhibiting current enhancement (Figure 5-4). To further verify that the obtained signal was due to the specific interaction between the aptamer and thrombin, a random 15-mer sequence (Table 5-1) was also used as a control and revealed limited to no translocation events. However, those that were observed were current blockades as opposed to enhancement. The difference in the direction of translocation peaks was attributed to change in local electrostatic potential leading to attraction between the aptamer and the analyte, causing current enhancement, while in the case of random sequence a repulsive potential was induced, leading to current blockade.[35]

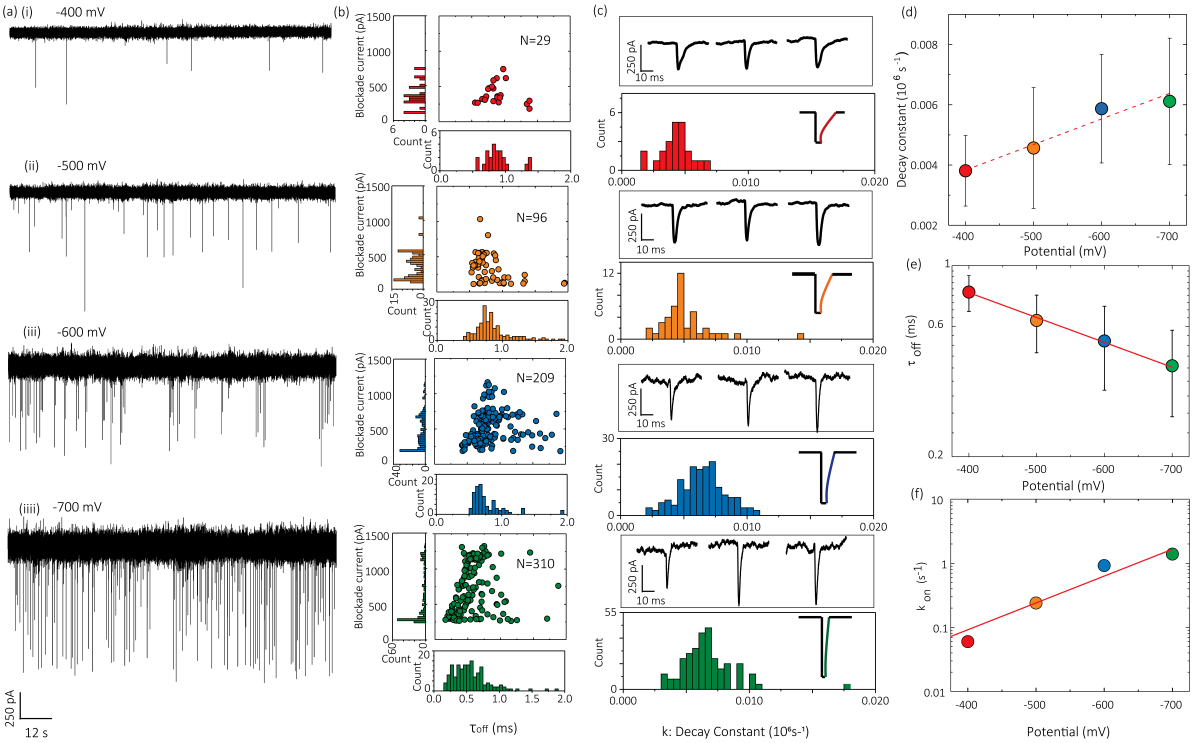


Figure 5-5: The selective single-molecule detection of thrombin using aptamer-functionalised nanopore bio-transistors. (a) The current-time traces showing the voltage dependence of single-molecule thrombin detection from (i) Vpore =-400 mV to (iv) Vpore =-700 mV. (b) A scattered diagram demonstrating the distribution of the blockade current and binding time at different voltages. (c) A unique characteristic for the translocation of thrombin through aptamer-functionalised devices is the

appearance of long tails, and (d) subsequent exponential fitting of the decay gives the distribution of decay constant, which increases linearly with applied voltage. (e) The binding time (τ_{off}, dwell time) decreases exponentially with voltage, and the (f) off rate ($k_{on,}$ capture rate) increases exponentially with voltage. A semi-log plot of the binding time and off rate resulted in a linear trend with increasing V_{pore}. Thrombin was added inside the pipette at 1 nM and the translocation occurred from in to out. Error bars represent the standard deviation of 3 independent measurements.

For aptamer-functionalised devices, increasing the voltage from -400 mV to -700 mV caused a shorter dwell time (0.80 ± 0.12 ms to 0.43 ± 0.15 ms) and a higher blockade current with more translocation events (0.06 s^{-1} to 0.39 s^{-1}) being captured (Figure 5-5), which is similar to the conventional nanopores. The voltage-dependent results also excluded the possibility of the surface absorption of proteins onto gold; in this case, the dwell time is expected to be longer with the increasing voltage.[36] Importantly, an exponential voltage-dependence was obtained for the dwell time (binding time, τ_{off}) (Figure 5-5 b,e) and capture rates (on rates, k_{on}) (Figure 5-5 b,f), which confirms the biomolecular dissociation and association processes. Additionally, the strong voltage dependence of the translocation parameters suggested that most aptamers were located in the position near the nanopipette tip, where the potential field gradient is the highest. Moreover, a closer inspection of the translocation events revealed that most peaks contained a sharp current modulation followed by an exponential decay of the tail. The rate of decay became faster with increasing voltage (Figure 5-5 c-d). As the translocation occurred from tip to bath, the decay of tails corresponds to the interplay of the aptamer-thrombin dragging force against the applied electrophoretic force. The electrophoretic force exerted on the charged analytes scaled linearly with applied voltage, while the receptor–protein interactions remained largely constant[37]. Additionally, the binding stoichiometry between 15-mer TBA and thrombin is 1:1.[38] The decay rate of translocation tails decreased linearly from (0.004 ± 0.001) × 10^6 s^{-1} to (0.006 ± 0.002) × 10^6 s^{-1} with the increasing voltage (Figure 5-5 c-d).

5.4 Controlling protein transport by aptamer-functionalised nanopores

Controlling molecular transport across nanopores is central to many applications in terms of gating DNA single-molecule translocation. While pioneering studies have demonstrated the feasibility of controlling DNA transport by changing the solvent properties[39] and voltage

gating[25], it remains challenging to control the transport of other analytes, especially proteins, which have a more heterogeneous charge distribution and a more complicated shape. The gating of protein transport by surface chemistries have been limited by irreversible binding[40] or non-responsive coatings[41], and so far, they focused on monitoring the change of the ionic current[42] or surface plasmon resonance[43]. In our system, the gating can easily be achieved by changing potential applied onto the gold (Figure 5-6) to modulate single-protein translocation across the nanopore.

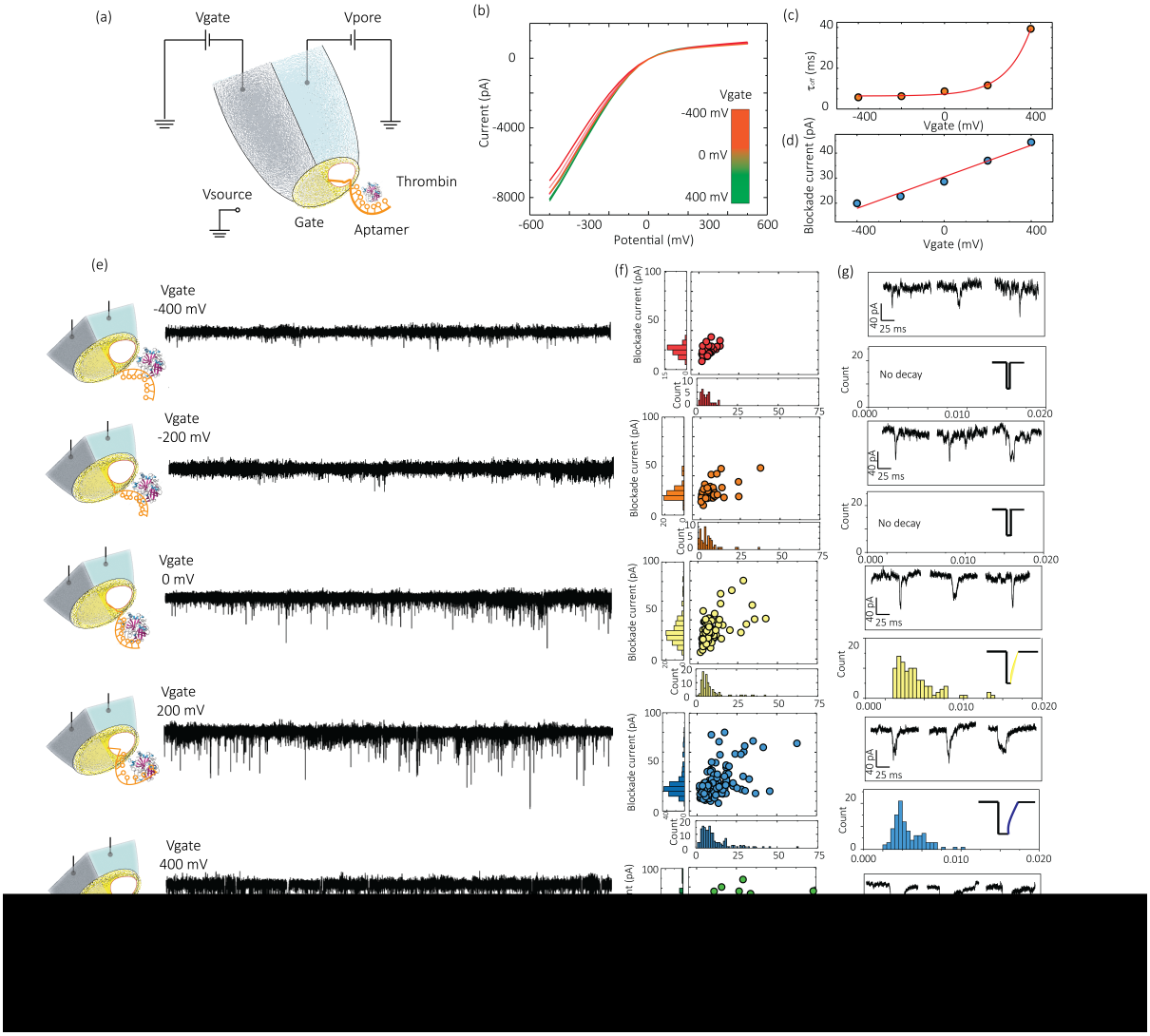


Figure 5-6: The gating of binding affinity and protein transport in an aptamer-functionalised nanopore. (a) Schematic showing that the transistor configuration carbon/gold/aptamer barrel was used as a gate to modulate single-molecule protein translocation. (b) By tuning Vgate from -400 to 400 mV, the regulation of ionic transport across the nanopore was verified by nanopore I-V collected at different gating potentials. From a single-molecule protein translocation study, (c) the dwell time (τ_{off}) was found

to increase as Vgate became more positive, (d) while the blockade current increased as well. (d) This is shown as current–time traces, which demonstrates the gating of single-molecule transport of 1 nM thrombin. Vpore = -400 mV for all cases. Thrombin was added inside the pipette at 1 nM and the translocation occurred from in to out.

By increasing Vgate from -400 mV to 400 mV, the binding time was tuned between 5.7 ms and 39.3 ms, which was accompanied by a linear increase of the blockade current (19.9 ± 5.2 pA to 44.4 ± 27.6 pA) (Figure 5-6 c,e,f,g). Additionally, the decay of tails was dragged to be longer as Vgate becoming more positive (Figure 5-6 g). It was known that the attached DNA oligonucleotide adopted an extended conformation at negative Vgate due to electrostatic repulsion[44], tuning Vgate to be more positive perhaps favoured the binding between G-quadruplexes and thrombin. Therefore, the longer decay was correlated to a binding affinity between the attached aptamers and thrombin as Vgate became more positive.

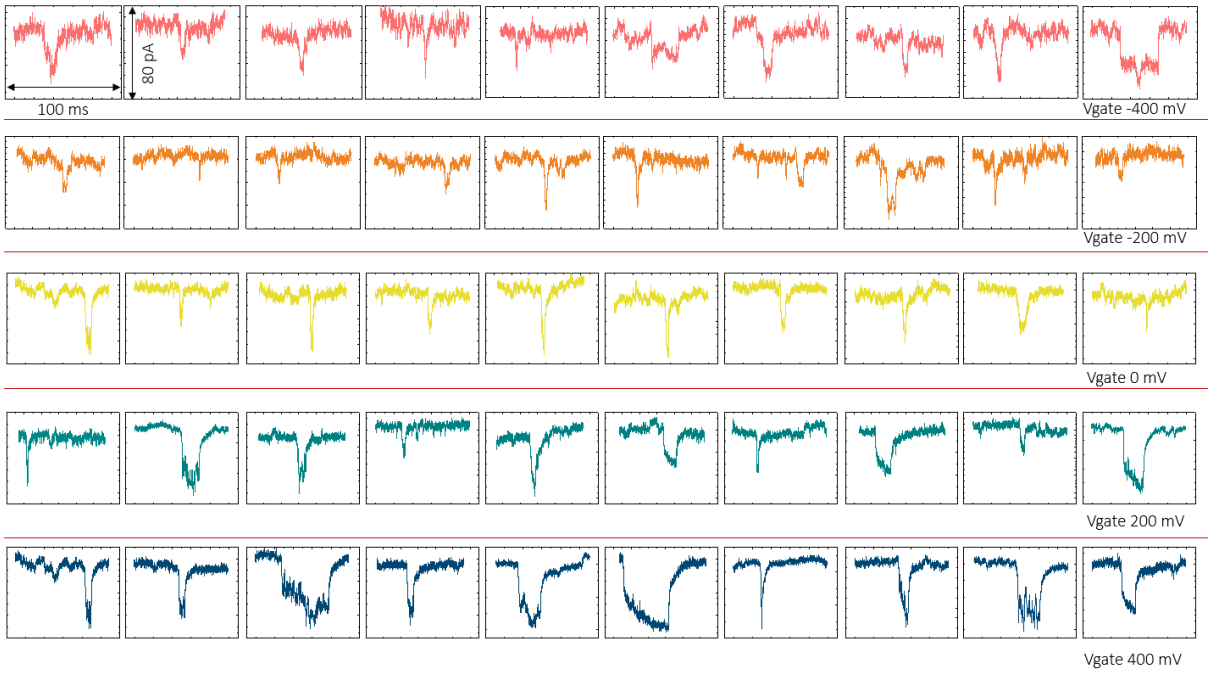


Figure 5-7: More examples of the voltage gating of thrombin from Vgate = - 400 mV to Vgate = 400 mV. Positive Vgate increased the binding time, enhanced the signal-to-noise ratio and slowed the decay for the translocation tails. Vpore = -400 mV for all cases. The experiments were performed in 100 mM KCl, 10 mM Tris and 1 mM EDTA at pH 8. Thrombin was added inside the pipette at 1 nM and the translocation occurred from in to out.

5.5 Detection of neurotransmitters

As the aptamer-functionalised sensors have proved their inherent ability for thrombin detection, we decided to increase the complexity of the aptamer building blocks for targeting the analytes that are even harder to detect. The aptamers[22,45] were specially selected with adaptive-loop binding towards the neurotransmitters, including dopamine, serotonin and acetylcholine (Table 5-1, Figure 5-1b). Importantly, the targeted neurotransmitters (0.15 kDa) are 40000 times smaller than the standard 10 kbp ds-DNA fragment (6500 kDa) for nanopore sensing. Therefore, it is exceptionally challenging to detect small molecules using solid-state nanopores. Consequently, a transducing mechanism is required to convert reversible physical association/dissociation between the targeted analytes and aptamers in the aqueous phase into a high-fidelity electrical signal of the nanopore sensor. The uniqueness of the chosen aptamers lies in the structural properties of bulky stem-loops; more specifically, the structural transformations are responsive down to fM.

5.5.1 Characterisation of the binding between aptamers and neurotransmitters using electrical measurements

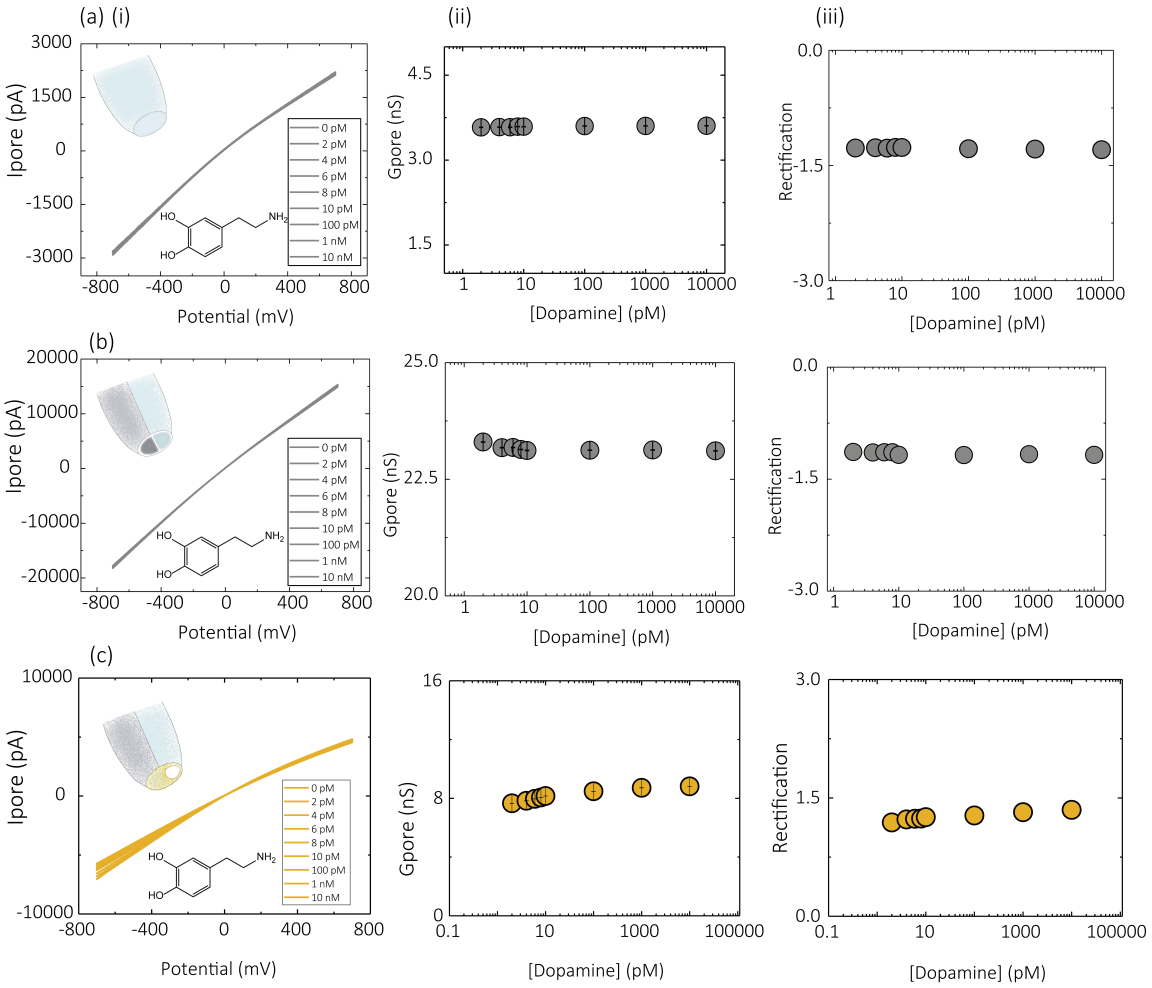


Figure 5-8: I-V characterisation of (a) quartz, (b) carbon only and (c) gold devices against analyte concentration. From the experimental results of quartz and carbon/quartz nanopores, the addition of positively charged analytes, such as dopamine, caused negligible effects on the (i) I-V, (ii) conductance and (iii) rectification ratios. Therefore, the interactions between dopamine and carbon or negatively charged quartz surfaces caused almost no effect on the nanopore I-V characteristics. The nanopore conductance was obtained by a linear fitting from -50 to 50 mV. The experiments were performed in 100 mM KCl, 10 mM Tris and 1 mM EDTA at pH 8. Error bars indicate the standard deviation of 3 independent measurements. Dopamine was added in the bath.

The receptor-modified FETs monitored target binding properties via the change of I-V characteristics.[15,22] As an analogue to this, increasing the concentration of neurotransmitters was found to have a negligible effect on nanopore conductance and rectification ratios for quartz, carbon only and gold nanopipettes. Importantly, we found that the conductance of

aptamer-functionalised nanopores increased with the concentration. (Figure 5-8) I-V studies of functionalised nanopore bio-transistors against the analyte concentration were performed (Figure 5-9). In experiments, the neurotransmitters were added to the KCl bath and the translocation occurred from out to in.

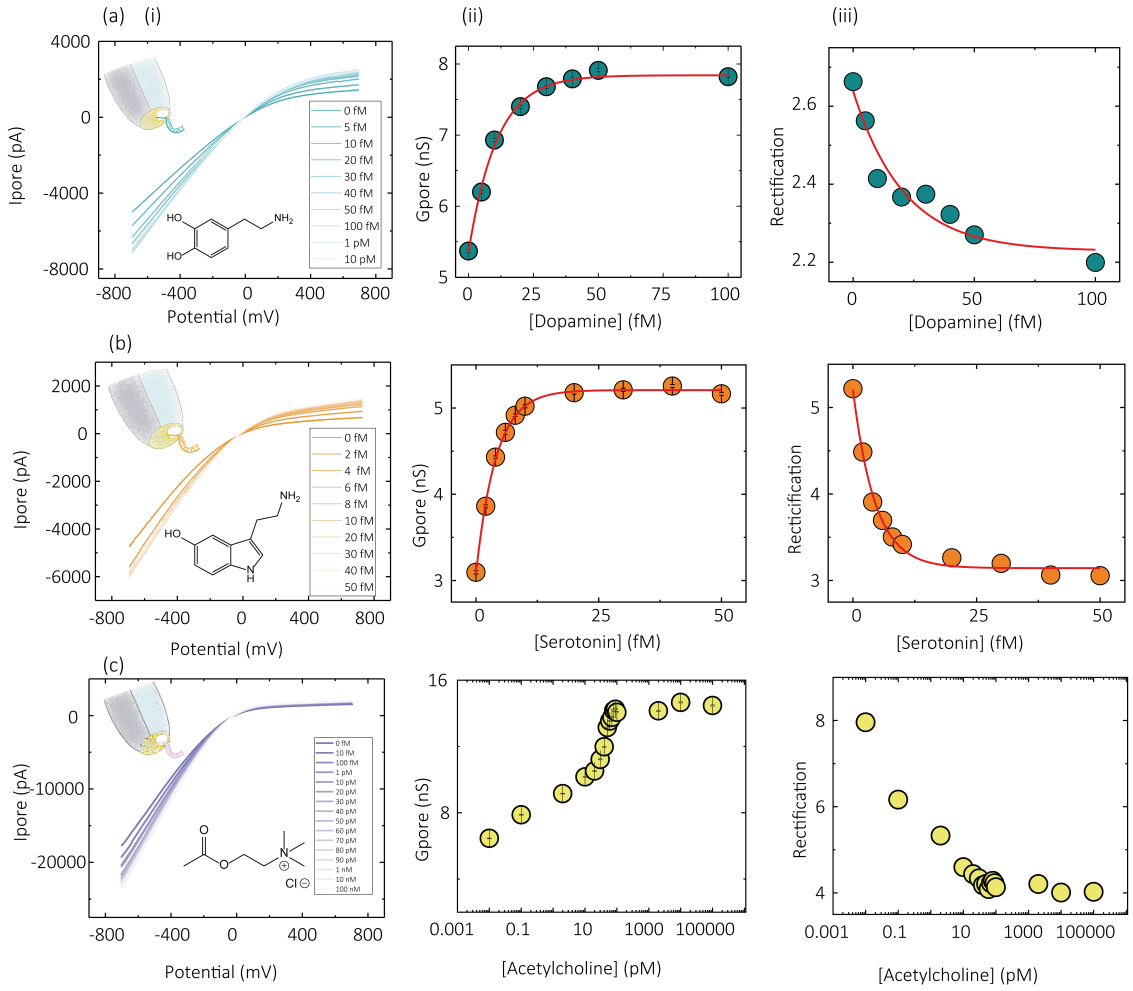


Figure 5-9: I-V characterization of aptamer-functionalised devices against analyte concentration for (a) dopamine, (b) serotonin and (c) acetylcholine. For aptamer-functionalised devices, adding targeted analytes caused a change in the (i) I-V characteristics due to the specific binding. (ii) The conductance decreased with increasing concentration for both dopamine and serotonin aptamer-functionalised devices as a result of forming more G-quadruplexes. Note that the increase of I-V conductance with concentration is consistent with the current enhancement that was obtained for the single-molecule translocation of dopamine and serotonin that was achieved using functionalised nanopore. (iii) The rectification ratios (I_{-500mV}/I_{500mV}) decreased as more positively charged analytes bound with the corresponding aptamer. The sigmodal dependence of acetylcholine is caused by the use of less sensitive aptamers compared to dopamine and serotonin cases where aptamers are responsive down to fM. The targeted analytes were only added to the KCl bath. The nanopore conductance was obtained by a linear

fitting from -50 to 50 mV. The experiments were performed in 100 mM KCl, 10 mM Tris and 1 mM EDTA at pH 8. Error bars indicate the standard deviation of three independent measurements. Dopamine was added in the bath.

For dopamine and serotonin, the experimental results are consistent with the evidence that the aptamers switched from a duplexed conformation to either a parallel or anti-parallel G-quadruplexes, which are more compressed upon analyte binding.[22] Aside from this, the rectification ratio decreased with concentration due to more binding between the positively charged analytes and aptamers. Notably, the acetylcholine aptamer has a similar loop structure to the aptamers for dopamine and serotonin, but with little information on the binding properties and structural transformations. Interestingly, we found the same trend of concentration dependence of conductance and rectification. Based on this, we believed the binding between the aptamer and acetylcholine occurred similarly to the cases of dopamine and serotonin. The fittings of the conductance and rectification data for all three aptamers resulted in binding properties, which are summarised in Table 5-2, that closely match the literature values[22]. In contrast, hybridising the complementary sequence of the aptamer induced a decrease in nanopore conductance, which formed double-stranded DNA in a nanopore (Figure 5-13). Possibly, the charge from the attached oligonucleotides was shifted away from the nanopore surface, which significantly reduced the rectification ratio ($|I_{-500mV}/I_{500\ mV}|$) from 3.8 at 0 fM complementary sequence to 0.66 at 5 pM complementary sequence. The above trend is in good agreement with the results obtained by Hou et al.[46] on a G-quadruplex conformational switching nanochannel. In this case, the translocation of the complementary strand produced a current blockade, which was expected from the decrease in nanopore conductance. Note that the magnitude of the current blockade is independent of the analyte concentration and excludes the possibility that the translocation signals were caused by the local change of the analyte concentration in a nanopore.

5.5.2 Selective single-molecule detection of neurotransmitters

Regarding the thrombin case, the scrambled sequence functionalised nanopore produced no translocation signals, which confirms that the non-specific interactions between the neurotransmitters and the scrambled sequence are unable to cause the modulation of the current baseline. In contrast, the specific interactions between the aptamers and targets are revealed in terms of spikes in the real-time current (Figure 5-1 f and Figure 5-11). This was further proved by the observation that no translocation signals were obtained for the same device when no analytes were added in the bath.

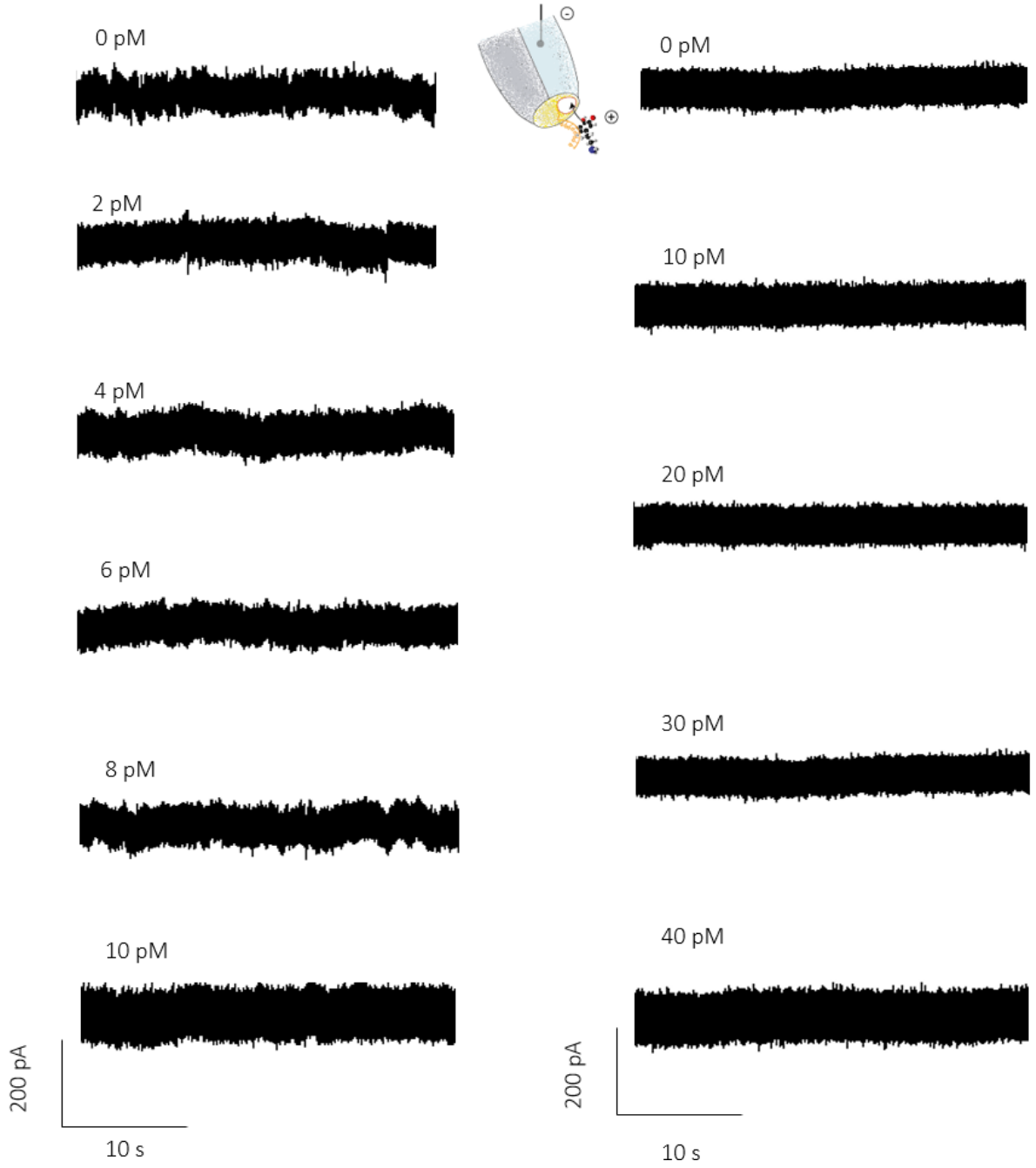


Figure 5-10: The representative current traces for the translocation of dopamine across nanopores functionalised by the scrambled sequence of dopamine aptamer. No distinguishable current modulations were observed. The experiments were conducted at 100 mM KCl, 10 mM Tris and 1 mM EDTA at pH 8. Vpore= -400 mV for all concentrations. The experiments were verified by five independent nanopores functionalised with scrambled sequence of dopamine aptamer. Different concentrations of dopamine were added to the bath and any possible translocations are supposed to occur from out to in.

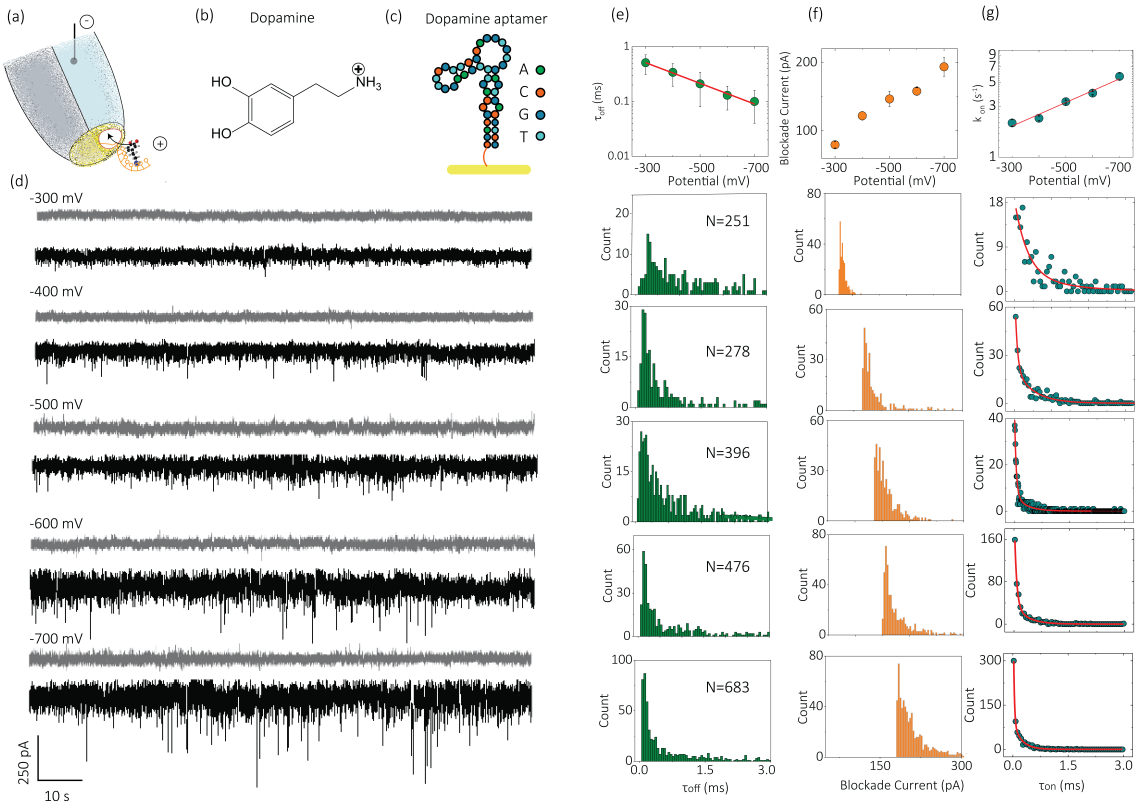


Figure 5-11: Single-molecule detection of dopamine using an aptamer-functionalised nanopore. (a) Single-molecule translocation of (b) dopamine occurred from the electrolyte bath to a nanopore functionalised by (c) dopamine aptamers under a negative V_{pore}, (d) voltage-dependent current–time traces. This illustrates the specific interactions between the stem-loop aptamers and dopamine, as suggested by the contrast between the grey (0 pM dopamine) and black (10 pM dopamine) current traces from the same device. The voltage-dependent results and detailed distribution of the (e) dwell time (dissociation time, τ_{off}), (f) blockade current and (g) on rate (capture rate, k_{on}) with increasing Vpore from -300 to -700 mV. Dopamine was added in the KCl bath, error bars indicate the standard deviation of 3 independent measurements.

In the case of dopamine (Figure 5-11), the translocation caused current enhancement. This is consistent with the evidence from the I-V study that suggests that the aptamer switches from a duplexed conformation to a G-quadruplex upon binding.[22] To further investigate the meaningful features of the collected signals, we hypothesised the binding model proposed by Wei et al.[28] on receptor-modified nanopores. The distribution of interevent time (τ_{off}) was analysed to address whether the obtained signals were due to single-molecule translocation.

In all cases, the exponential dependence of interevent time confirms the stochastic nature of current modulation (Figure 5-11 g), which verifies the single-molecule nature of the collected events[28,47]. Interestingly, the voltage dependence of τ_{off} and k_{on} showed an exponential dependence with applied voltage (Figure 5-11 e,g), which means that the neurotransmitter translocations are predominately governed by ligand-receptor association and dissociation.[28] Additionally, the lack of secondary peaks from individual events confirmed that the translocation signals were caused by the interactions between the targeted analyte and one receptor only. Multiple interactions between the analyte and receptors are expected to induce multi-level translocation events (Figure 5-12).[28] As the strength of the ligand-receptor interactions is strongly related to Debye screening, increasing the salt concentration to 1 M KCl results in the disappearance of translocation signals on the same device.

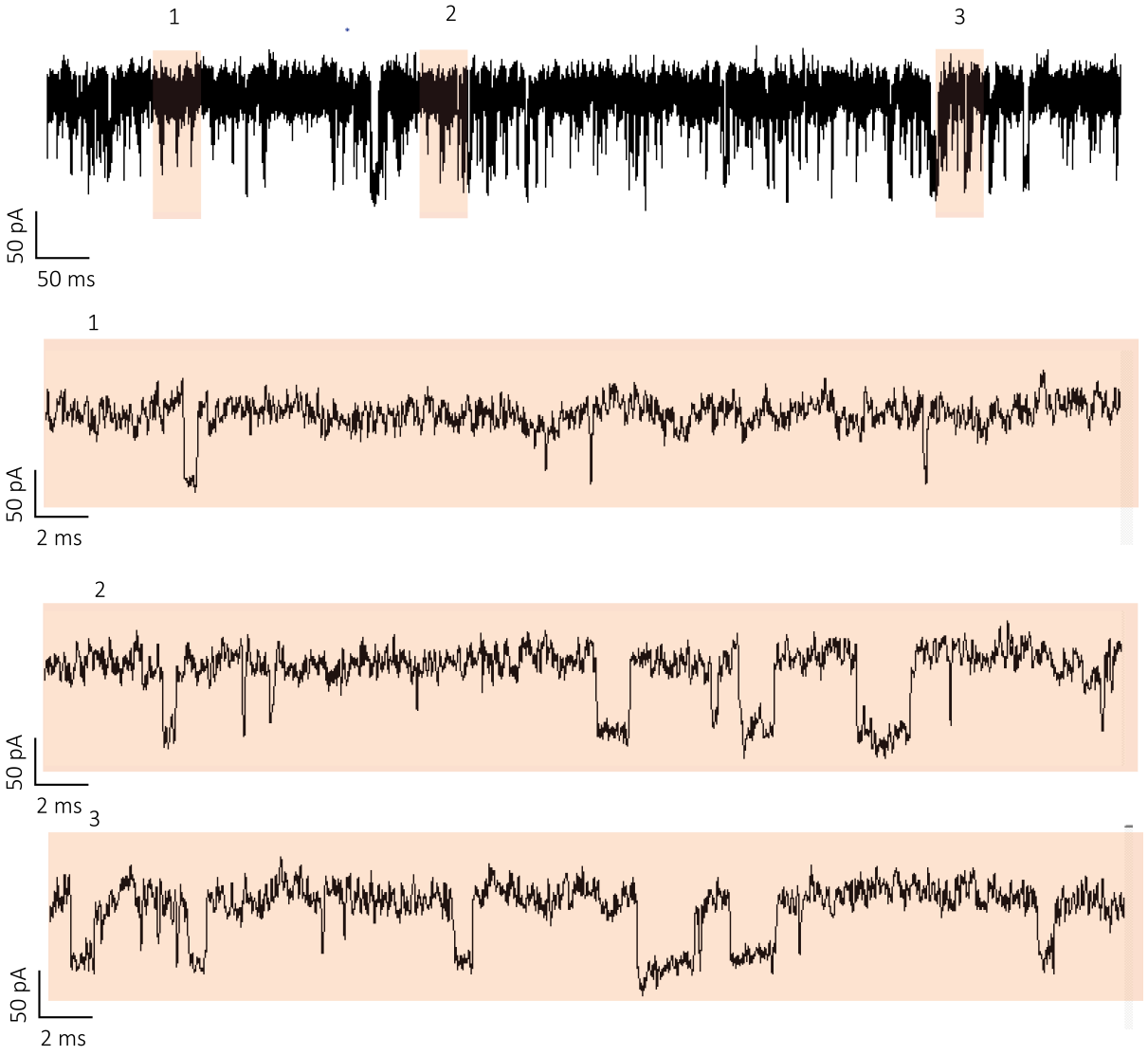


Figure 5-12: The representative current-traces for serotonin showing the shape of the translocation peaks. In most cases, the translocation events were predominately seen as a single and rectangular peak, which suggests that each translocation event was caused by an interaction with one receptor, as multiple receptors are able to cause the inter-transfer of the targeted analyte between different ligands in the nanopore sensing region. The concentration of serotonin is 10 fM added into the KCl bath, and the translocation occurred from bath to tip, Vpore = -500 mV.

Regarding the I-V studies of aptamer binding, a further confirmation of the occurrence of the aptamer-target association and dissociation was made on hybridising the complementary strand to the aptamer. In this case, the formation of ds-DNA, which is more extended inside the nanopore, also caused a current blockade. This is consistent with the results from I-V, where the nanopore rectification was dramatically reduced.

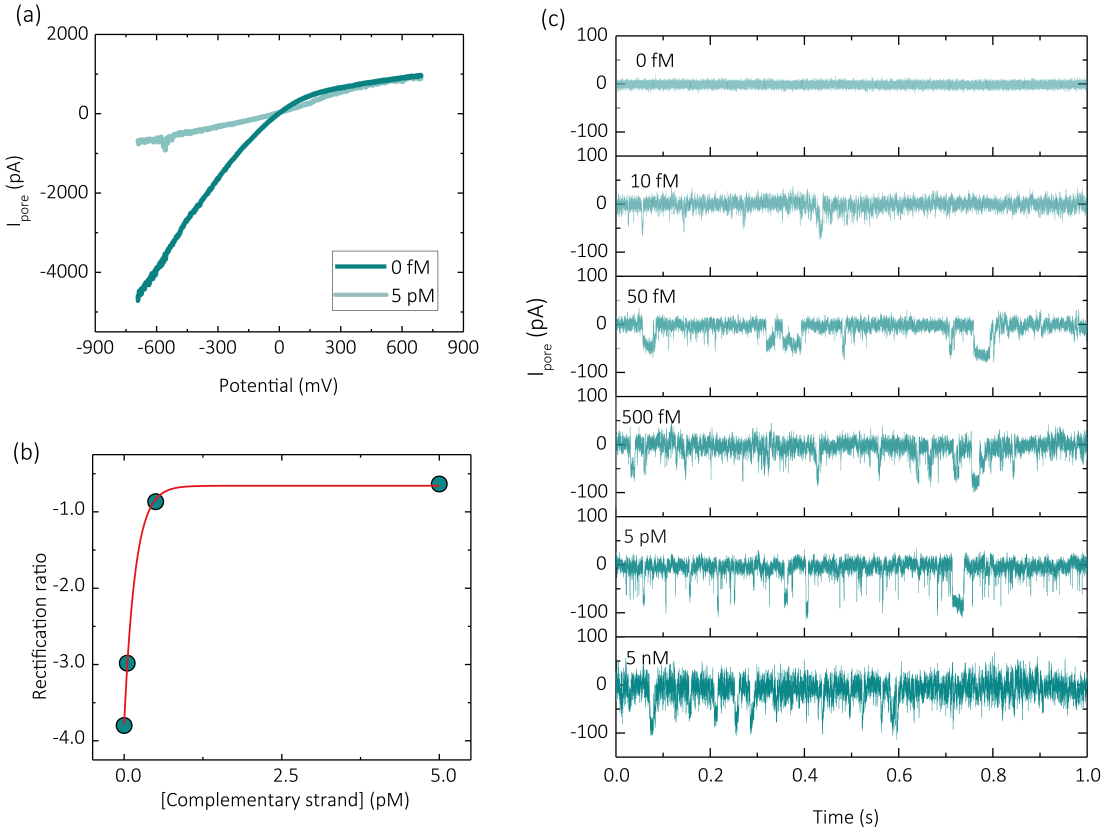


Figure 5-13: The hybridisation of the complementary strand to the nanopore functionalised by the serotonin aptamer. (a) The change of I-V demonstrated the formation of hybridised double-stranded DNA inside the nanopore. (b) The rectification $\left(\left|\frac{I_{-500mV}}{I_{500\ mV}}\right|\right)$ changed from negative rectification to

almost no rectification, and finally, a slightly positive rectification. The decrease of the rectification ratio can be attributed to the formation of ds-DNA in a nanopore, which shifts the negative charge of the attached oligonucleotides away from the surface. Interestingly, the rectification ratios became slightly less than one (i.e. positive rectification) at a 500 fM and 5 pM concentration of the complementary strand. A gold nanopore is expected to have a negative rectification due to the surface absorption of chloride anions. For the functionalised nanopore system, the linear and extended ds-DNA suppresses the chloride absorption. Therefore, it exposes more bare gold surface, which is weakly positively charged[25,48] and causes a positive rectification. (c) The real-time current traces recorded from the same device at different concentrations of the complementary strand. A current blockade was observed that is consistent with the change of I-V. Note that the blockade current is independent of the concentration. Vpore = 600 mV. The translocation of the negatively charged complementary strand occurred from out to in. The complementary strand of serotonin aptamer was added into the KCl bath.

Having verified the occurrence of the association–dissociation processes in a nanopore for dopamine, another two aptamers with similar stem-loop structures were selected for serotonin[22] and acetylcholine[45], respectively (Table 5-1), to bring more diversity to this functionalised nanopore sensing platform. Similar to the dopamine case, the selectivity and voltage dependence of τ_{off} (Figure 5-11 c, Figure 5-14 ai, bi) and k_{on} (Figure 5-11 e, Figure 5-14 aii, bii) were verified to occur like the characteristics of the nanopore binding processes, as mentioned above. Based on the translocation statistics that were already established, the single-molecule detection of serotonin at fM level was demonstrated (Figure 5-14 a), which was a magnitude lower than the typical nanopore sensing concentration and six to nine magnitudes lower than the conventional methods, such as electrochemical and optical measurements.[10,44] This was further demonstrated by the single-molecule detection of non-redox-active neurotransmitters, such as acetylcholine (Figure 5-14 b). This is also possible at pM level by using aptamer-functionalised devices. The label-free feature of nanopore sensing provides a viable way of detecting a range of neurotransmitters without the prerequisite of chemical sample labelling or modification.

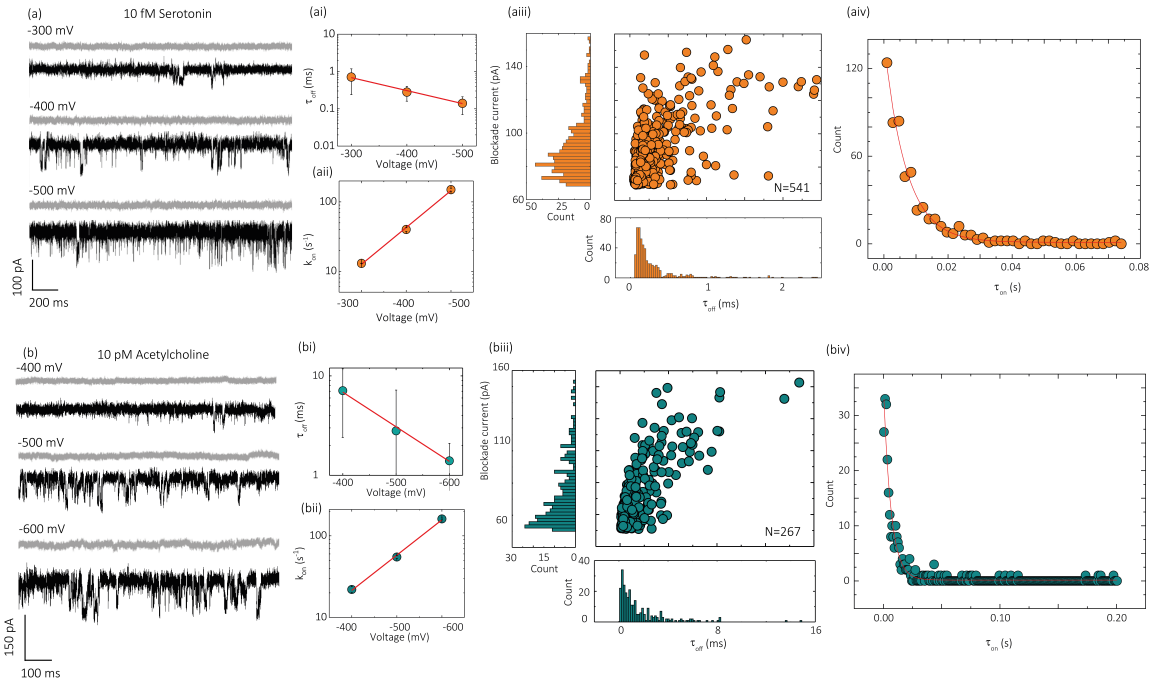


Figure 5-14: The single-molecule sensing of neurotransmitters at fM concentration, and the capability of aptamer-functionalised nanopore bio-transistors to detect non-redox-active neurotransmitters. The single-molecule detection of serotonin at fM level was illustrated by the example of (a) serotonin, while the detection of non-redox-active neurotransmitters was demonstrated by (b) acetylcholine. For both cases, the single-molecule detection was performed via a voltage dependence of (i) dwell time (τ_{off}) and (ii) capture rate (k_{on}), with (iii) scattered diagrams to demonstrate the distribution of the blockade current and binding time at Vpore = -500 mV, and (iv) exponential distribution of interevent time (τ_{on}) demonstrating the single-molecule nature of translocation signals. Serotonin and acetylcholine were added into the KCl bath in all cases. Error bars represent the standard deivation from 3 independent measurements.

5.5.3 Single-molecule binding assay for neurotransmitters

For a more quantitative rationalisation of our experimental results, the calculation of the dissociation constant (K_d) was performed by extrapolating the voltage dependence of τ_{on} and k_{off} to find the values at which no voltage was applied across the nanopore (Figure 5-15). The K_d for dopamine, serotonin and acetylcholine was estimated to be 5 nM, 1.25 pM and 250 pM, respectively.

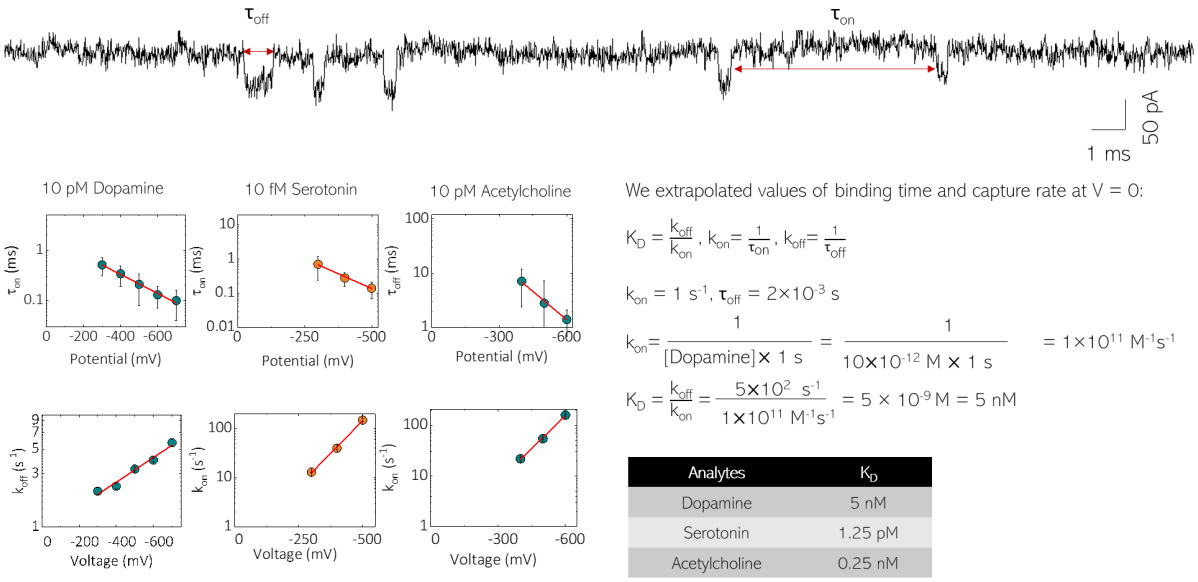


Figure 5-15: Further details of the calculation of K_D from single-molecule translocation data. The voltage dependence of the dwell time (τ_{off}) and capture rate (k_{on}) was extrapolated to discover the values at which no voltage wasapplied to calculate the K_d and compare it with the literature values.

	Dopamine aptamer Dopamine	Serotonin aptamer Serotonin	Acetylcholine aptamer Acetylcholine	Serotonin aptamer Complementary strand
Aptamer structural switching	Duplex –> (parallel or mixed) G4	Duplex –> antiparallel G4	Duplex → likely a G4	Duplex –> hybridised ds-DNA
Conductance	Increase	Increase	Increase	Decrease
Rectification	Decrease	Decrease	Decrease	Decrease
Translocation	Enhancement	Enhancement	Enhancement	Blockade

Table 5-2: The summary of the experimental and literature evidence of the structural switching of aptamers and its relation to I-V and translocation studies. The aptamers switched from a duplex conformation to either a parallel or anti-parallel G-quadruplex, which becomes more compressed upon binding with dopamine or serotonin. This created a knock-on effect on the concentration dependence of nanopore conductance, which increased with more targets being bound, and therefore, more G-quadruplex formations. The rectification decreased due to more binding between the positively charged analytes and the aptamer. This was further reflected in the results of the single-molecule translocation experiments where current enhancement was observed.

In parallel, the concentration dependence of nanopore I-Vs with single-molecule translocation of neurotransmitters (Figure 5-16). Inside the dynamic range where the nanopore conductance increased with concentration, the current enhancement was obtained, which corresponded to the translocation of a single neurotransmitter. In contrast, the current blockade appeared after the concentration dependence of nanopore conductance reached the plateau, which was a result of the interactions between the filled binding sites and the excess neurotransmitters. As noted above, the experimental results were established upon selective detection of targeted analytes. In all cases, the nanopore's functionalised scrambled sequence of corresponding aptamers exhibited no noticeable translocation peaks (Figure 5-10).

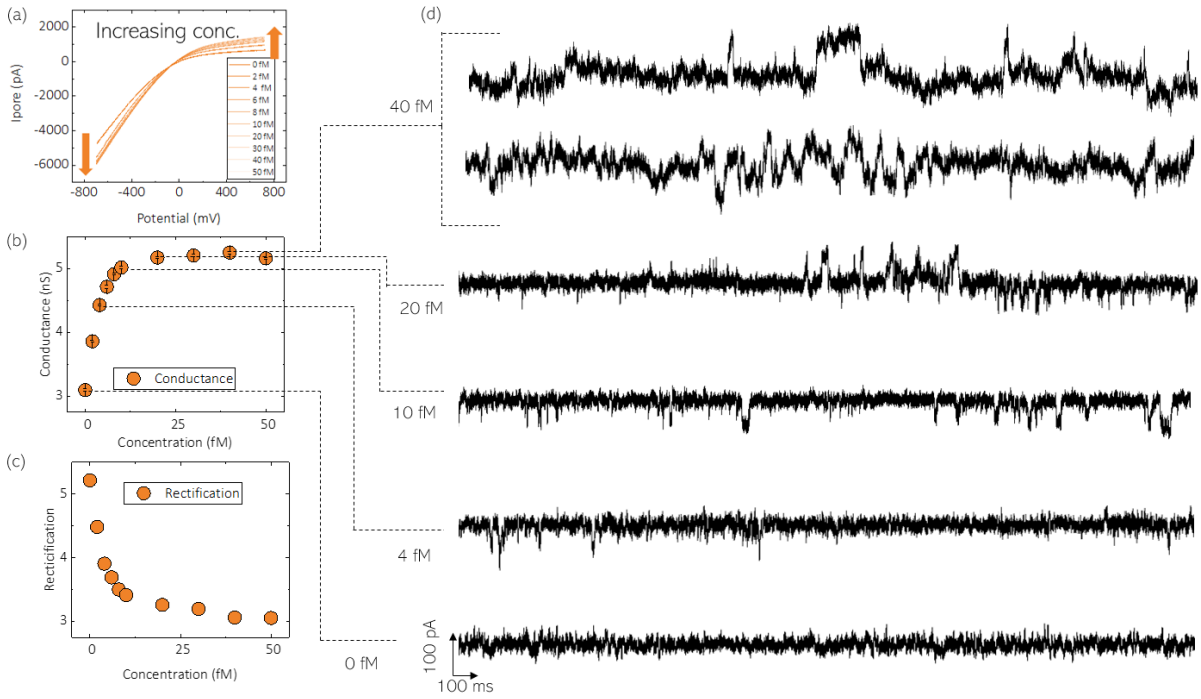


Figure 5-16: The correlation between the concentration dependence of nanopore conductance and the single-molecule translocation of serotonin. Increasing the concentration of serotonin caused the transition from the current enhancement to the current blockade. Within the range where the nanopore conductance increased with concentration, the current enhancement was obtained, whereas the current blockade appeared after the plateau was reached. Vpore = -400 mV and the concentration of serotonin was varied in the KCl bath in all cases. Serotonin was added into the KCl bath.

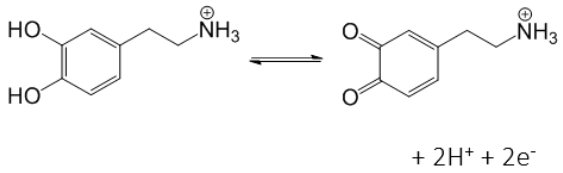
5.6 Conclusion and future work

To conclude, I have developed a novel class of aptamer-functionalised nanopore field-effect transistors for the selective single-molecule detection of proteins and neurotransmitters. The successful assaying of a single protein or neurotransmitter is performed by extracting the binding affinity from the voltage dependence. This correlates with the bulk measurements that validate the robustness of my approach. Due to the increasing abundance of available aptamers for different targets, the versatility of our approach was illustrated for different targets, including both proteins and neurotransmitters. Notably, electrochemically measuring the neurotransmitters is the most predominant sensing method, but the neurotransmitters must be redox-active. Using our approach, it is also possible to detect electronically non-redox-active analytes with single-molecule resolution and that is a significant advantage compared to state-of-the-art electrochemical sensors. By using aptamers with a high specific affinity towards a given analyte, we can achieve the single-molecule detection of neurotransmitters at fM level. Notably, this is six to nine orders of magnitude lower than the conventional methods, such as optical and electrochemical measurements. Furthermore, the crosslinks of binding properties extracted from both single-molecule and bulk measurements for all aptamers and the corresponding neurotransmitters, along with the universal nature sensing platform for producing molecular signatures based on the aptamer structural transformations and receptor-analyte binding for both proteins and small molecules, suggest the potential of using this nanopore sensing system to produce more 'spectroscopic' signals to extract and analyse molecular fingerprints at an ultralow concentration from complex biological backgrounds. Therefore, along with the increasing abundance of aptamers, we foresee an array of more generalised applications that can be achieved by customising aptamers with a desired dynamic range for the targeted analytes through binding chemistries, such as conformational changes. Therefore, further implementation of this in vitro sensing strategy may lead to the detection and quantification of a range of proteins and neurotransmitters both intercellularly and intracellularly, such as in-vitro monitoring of neurontransmitter release in real time.

Although there have been advancements in detecting and quantifying neurotransmitters using this aptamer-modified nanopore bio-transistor sensing platform, there are a few potential improvements that can be still made in the future. The dynamic range of aptamers has critical

implications on the quantification of neurotransmitters. For in vitro applications, the careful selection of aptamers with the desired binding properties is a prerequisite for quantifying neuron activities of interests. Moreover, the precise number and location of the aptamers that are attached inside the nanopore sensing region must be made in a more controlled manner, although this is currently a problem that remains unsolved for solid-state nanopores.

Moreover, the dynamic range of fabricated sensors has important implications in clinical diagnosis and in-vitro monitoring of neuron activities. The aptamer-functionalised nanopore bio-transistors can detect neurotransmitters from fM to nM. A further extension of the dynamic range can be made by customising the aptamers for targeted analytes, each of which has a desired dynamic range for targeted analytes with binding chemistries, such as conformational changes. As aptamer-functionalised nanopore bio-transistors can selectively pre-concentrate analytes on the gate electrode, another route focuses on exploring the electrochemical properties of redox-active neurotransmitters, such as dopamine and serotonin. Proof-of-principle studies have been conducted, as shown in Figure 5-17. The aptamer-functionalised nanopore bio-transistors generated the most significant response in terms of dopamine oxidation, in contrast to those functionalised by scrambled sequence and the gold and carbon gate electrodes.



Scheme 5-1: The electrochemical oxidation of dopamine oxidising phenol groups into ketones and releasing protons.

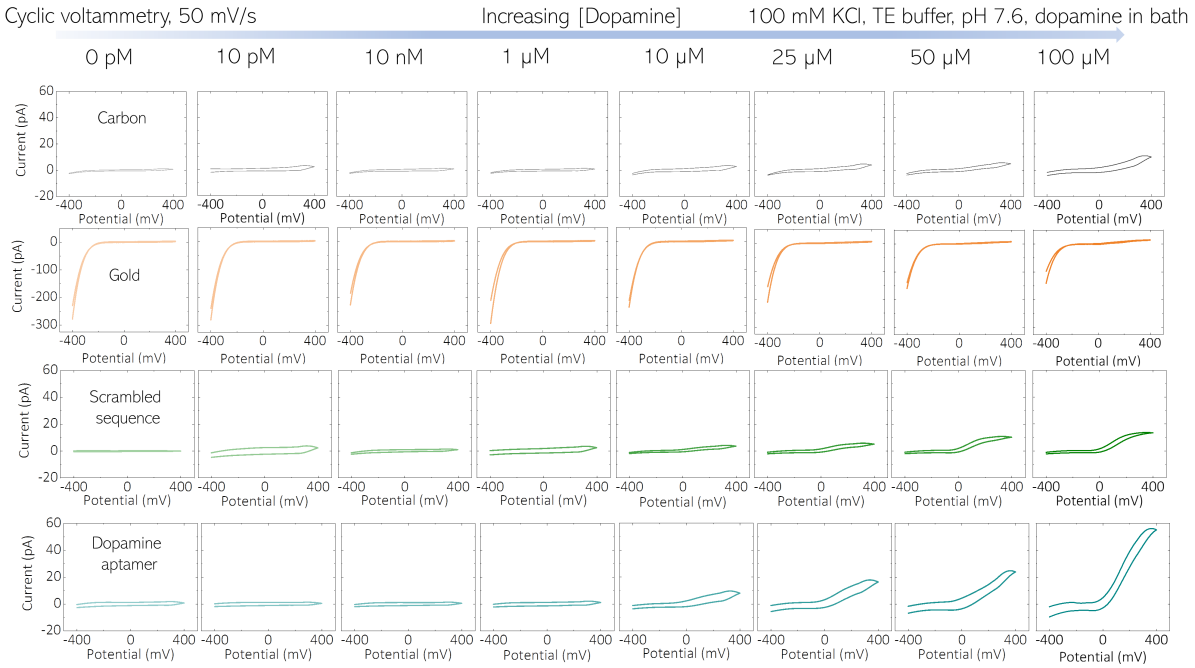


Figure 5-17: The selective electrochemical response for the gate electrodes of aptamer-functionalised nanopore bio-transistors. The electrochemical response from (a) carbon nanoelectrode, (b) gold deposited gate, (c) gold gate functionalised by the scrambled sequence of dopamine aptamer and (d) gold gate functionalised by dopamine aptamer. The aptamer functionalised gate generated the most significant electrochemical response. Dopamine was added into the KCl bath.

5.7 References

(1) Turner, A. P. F. Biosensors: Sense and Sensibility. *Chem. Soc. Rev.* **2013**, *42* (8), 3184–3196.

(2) Miles, B. N.; Ivanov, A. P.; Wilson, K. a; Doğan, F.; Japrung, D.; Edel, J. B. Single Molecule Sensing with Solid-State Nanopores: Novel Materials, Methods, and Applications. *Chem. Soc. Rev.* **2013**, *42* (1), 15–28.

(3) Varongchayakul, N.; Song, J.; Meller, A.; Grinstaff, M. W. Single-Molecule Protein Sensing in a Nanopore: A Tutorial. *Chem. Soc. Rev.* **2018**, *47* (23), 8512–8524.

(4) Cai, S.; Sze, J. Y. Y.; Ivanov, A. P.; Edel, J. B. Small Molecule Electro-Optical Binding Assay Using Nanopores. *Nat. Commun.* **2019**, *10* (1), 1797.

(5) Sze, J. Y. Y.; Ivanov, A. P.; Cass, A. E. G.; Edel, J. B. Single Molecule Multiplexed Nanopore Protein Screening in Human Serum Using Aptamer Modified DNA Carriers. *Nat. Commun.* **2017**, *8* (1), 1552.

(6) Ren, R.; Zhang, Y.; Nadappuram, B. P.; Akpinar, B.; Klenerman, D.; Ivanov, A. P.; Edel, J. B.; Korchev, Y. Nanopore Extended Field-Effect Transistor for Selective Single-Molecule Biosensing. *Nat. Commun.* **2017**, *8* (1), 586.

(7) Pérez-Mitta, G.; Toimil-Molares, M. E.; Trautmann, C.; Marmisollé, W. A.; Azzaroni, O. Molecular Design of Solid-State Nanopores: Fundamental Concepts and Applications. *Adv. Mater.* **2019**, *1901483*, 1–46.

(8) Bayley, H. Single-Molecule DNA Sequencing: Getting to the Bottom of the Well. *Nat. Nanotechnol.* **2017,** 12, 1116-1117.

(9) Abi, A.; Ferapontova, E. E. Unmediated by DNA Electron Transfer in Redox-Labeled DNA Duplexes End-Tethered to Gold Electrodes. *J. Am. Chem. Soc.* **2012**, *134* (35), 14499–14507.

(10) Pradhan, T.; Jung, H. S.; Jang, J. H.; Kim, T. W.; Kang, C.; Kim, J. S. Chemical Sensing of Neurotransmitters. *Chem. Soc. Rev.* **2014**, *43* (13), 4684–4713.

(11) Restrepo-Pérez, L.; Joo, C.; Dekker, C. Paving the Way to Single-Molecule Protein Sequencing. *Nat. Nanotechnol.* **2018**, *13* (9), 786–796.

(12) Harris, T. D.; Buzby, P. R.; Babcock, H.; Beer, E.; Bowers, J.; Braslavsky, I.; Causey, M.; Colonell, J.; Dimeo, J.; Efcavitch, J. W.; Giladi, E.; Gill, J.; Healy, J.; Jarosz, M.; Lapen, D.; Moulton, K.; Quake, S. R.; Steinmann, K.; Thayer, E.; Tyurina, A.; Ward, R.; Weiss, H.; Xie, Z. Single-Molecule DNA Sequencing of a Viral Genome. *Science* **2008**, *320* (5872), 106–109.

(13) Neuman, K. C.; Nagy, a. Single-Molecule Force Spectroscopy: Optical Tweezers, Magnetic Tweezers and Atomic Force Microscopy. *Nat. Methods* **2008**, *5* (6), 491–505.

(14) Nadappuram, B. P.; Cadinu, P.; Barik, A.; Ainscough, A. J.; Devine, M. J.; Kang, M.; Gonzalez-Garcia, J.; Kittler, J. T.; Willison, K. R.; Vilar, R.; Actis, P.; Wojciak-Stothard, B.; Oh, S. H.; Ivanov, A. P.; Edel, J. B. Nanoscale Tweezers for Single-Cell Biopsies. *Nat. Nanotechnol.* **2019**, *14* (1), 80–88.

(15) Zhang, A.; Lieber, C. M. Nano-Bioelectronics. *Chem. Rev.* **2016**, *116*, 215–257.

(16) Gao, N.; Gao, T.; Yang, X.; Dai, X.; Zhou, W.; Zhang, A.; Lieber, C. M. Specific Detection of Biomolecules in Physiological Solutions Using Graphene Transistor Biosensors. *Proc Natl Acad Sci U S A* **2016**, *113* (51), 14633–14638.

(17) Venkatesan, B. M.; Bashir, R. Nanopore Sensors for Nucleic Acid Analysis. *Nat. Nanotechnol.* **2011**, *6* (10), 615–624.

(18) Ying, Y. L.; Yu, R. J.; Hu, Y. X.; Gao, R.; Long, Y. T. Single Antibody-Antigen Interactions Monitored: Via Transient Ionic Current Recording Using Nanopore Sensors. *Chem. Commun.* **2017**, *53* (61), 8620–8623.

(19) Cao, C.; Ying, Y. L.; Hu, Z. L.; Liao, D. F.; Tian, H.; Long, Y. T. Discrimination of Oligonucleotides of Different Lengths with a Wild-Type Aerolysin Nanopore. *Nat. Nanotechnol.* **2016**, *11* (8), 713–718.

(20) Freedman, K. J.; Otto, L. M.; Ivanov, A. P.; Barik, A.; Oh, S.-H.; Edel, J. B. Nanopore Sensing at Ultra-Low Concentrations Using Single-Molecule Dielectrophoretic Trapping. *Nat. Commun.* **2016**, *7*, 10217.

(21) Chuah, K.; Wu, Y.; Vivekchand, S. R. C.; Gaus, K.; Reece, P. J.; Micolich, A. P.; Gooding, J. J. Nanopore Blockade Sensors for Ultrasensitive Detection of Proteins in Complex Biological Samples. *Nat. Commun.* **2019**, *10* (1), 1–9.

(22) Nakatsuka, N.; Yang, K.; Abendroth, J. M.; Cheung, K. M.; Xu, X.; Yang, H.; Zhao, C.; Zhu, B.; Rim, Y. S.; Yang, Y.; Weiss, P. S.; Andrews, A. M. Aptamer – Field-Effect Transistors Overcome Debye Length Limitations for Small-Molecule Sensing. **2018**, *324* (October), 319–324.

(23) Rotem, D.; Jayasinghe, L.; Salichou, M.; Bayley, H. Protein Detection by Nanopores Equipped with Aptamers. *J. Am. Chem. Soc.* **2012**, *134* (5), 2781–2787.

(24) Dunn, M. R.; Jimenez, R. M.; Chaput, J. C. Analysis of Aptamer Discovery and Technology. *Nat. Rev. Chem.* **2017**, *1*, 0073.

(25) Xue, L.; Cadinu, P.; Paulose Nadappuram, B.; Kang, M.; Ma, Y.; Korchev, Y.; Ivanov, A. P.; Edel, J. B. Gated Single-Molecule Transport in Double-Barreled Nanopores. *ACS Appl. Mater. Interfaces* **2018**, *10* (44), 38621–38629.

(26) Pradhan, T.; Jung, H. S.; Jang, J. H.; Kim, T. W.; Kang, C.; Kim, J. S. Chemical Sensing of Neurotransmitters. *Chem. Soc. Rev.* **2014**, *43* (13), 4684–4713.

(27) Rollings, R. C.; Kuan, A. T.; Golovchenko, J. A. Ion Selectivity of Graphene Nanopores. *Nat. Commun.* **2016**, *7*, 11408.

(28) Wei, R.; Gatterdam, V.; Wieneke, R.; Tampé, R.; Rant, U. Stochastic Sensing of Proteins with Receptor-Modified Solid-State Nanopores. *Nat. Nanotechnol.* **2012**, *7* (4), 257–263.

(29) Yusko, E. C.; Johnson, J. M.; Majd, S.; Prangkio, P.; Rollings, R. C.; Li, J.; Yang, J.; Mayer, M. Controlling Protein Translocation through Nanopores with Bio-Inspired Fluid Walls. *Nat. Nanotechnol.* **2011**, *6* (4), 253–260.

(30) Kowalczyk, S. W.; Kapinos, L.; Blosser, T. R.; Magalhães, T.; van Nies, P.; Lim, R. Y. H.; Dekker, C. Single-Molecule Transport across an Individual Biomimetic Nuclear Pore Complex. *Nat. Nanotechnol.* **2011**, *6* (7), 433–438.

(31) Deng, B.; Lin, Y.; Wang, C.; Li, F.; Wang, Z.; Zhang, H.; Li, X. F.; Le, X. C. Aptamer Binding Assays for Proteins: The Thrombin Example-A Review. *Anal. Chim. Acta* **2014**, *837*, 1–15.

(32) Pasternak, A.; Hernandez, F. J.; Rasmussen, L. M.; Vester, B.; Wengel, J. Improved Thrombin Binding Aptamer by Incorporation of a Single Unlocked Nucleic Acid Monomer. *Nucleic Acids Res.* **2011**, *39* (3), 1155–1164.

(33) Bock, L. C.; Griffin, L. C.; Latham, J. A.; Vermaas, E. H.; Toole, J. J. Selection of Single-Stranded DNA Molecules That Bind and Inhibit Human Thrombin. *Nature* **1992**, *355*, 564–566.

(34) Uehara, S.; Shimada, N.; Takeda, Y.; Koyama, Y.; Takei, Y.; Ando, H.; Satoh, S.; UnoKazuo, A. 3' Poly(DA)-Tailed Thrombin DNA Aptamer to Increase DNase-Resistance and Clotting Inhibitory Activity. *Bull. Chem. Soc. Jpn.* **2008**, *81* (11), 1485–1491.

(35) Gershow, M.; Golovchenko, J. A. Recapturing and Trapping Single Molecules with a Solid-State Nanopore. *Nat. Nanotechnol.* **2007**, *2* (12), 775–779.

(36) Sexton, L. T.; Mukaibo, H.; Katira, P.; Hess, H.; Sherrill, S. A.; Horne, L. P.; Martin, C. R. An Adsorption-Based Model for Pulse Duration in Resistive-Pulse Protein Sensing. *J. Am. Chem. Soc.* **2010**, *132* (19), 6755–6763.

(37) Strunz, T.; Oroszlan, K.; Schumakovitch, I.; Güntherodt, H. J.; Hegner, M. Model Energy Landscapes and the Force-Induced Dissociation of Ligand-Receptor Bonds. *Biophys. J.* **2000**, *79* (3), 1206–1212.

(38) Zhang, J.; Loo, R. R. O.; Loo, J. A. Structural Characterization of a Thrombin-Aptamer Complex by High Resolution Native Top-Down Mass Spectrometry. *J. Am. Soc. Mass Spectrom.* **2017**, *28* (9), 1815–1822.

(39) Fologea, D.; Uplinger, J.; Thomas, B.; McNabb, D. S.; Li, J. Slowing DNA Translocation in a Solid-State Nanopore. *Nano Lett.* **2005**, *5* (9), 1734–1737.

(40) Ding, S.; Gao, C.; Gu, L. Q. Capturing Single Molecules of Immunoglobulin and Ricin with an Aptamer-Encoded Glass Nanopore. *Anal. Chem.* **2009**, *81*, 6649–6655.

(41) Wanunu, M.; Meller, A. Chemically Modified Solid-State Nanopores. *Nano Lett.* **2007**, *7* (6), 1580–1585.

(42) Aznar, E.; Oroval, M.; Pascual, L.; Murguía, J. R.; Martínez-Máñez, R.; Sancenón, F. Gated Materials for On-Command Release of Guest Molecules. *Chemical Reviews*. 2016, pp 516–718.

(43) Emilsson, G.; Sakiyama, Y.; Malekian, B.; Xiong, K.; Adali-Kaya, Z.; Lim, R. Y. H.; Dahlin, A. B. Gating Protein Transport in Solid State Nanopores by Single Molecule Recognition. *ACS Cent. Sci.* **2018**, *4* (8), 1007–1014.

(44) Álvarez-Martos, I.; Møller, A.; Ferapontova, E. E. Dopamine Binding and Analysis in Undiluted Human Serum and Blood by the RNA-Aptamer Electrode. *ACS Chem. Neurosci.* **2019**, *10* (3), 1706–1715.

(45) Bruno, J. G.; Carrillo, M. P.; Phillips, T.; King, B. Development of DNA Aptamers for Cytochemical Detection of Acetylcholine. *Vitr. Cell. Dev. Biol. - Anim.* **2008**, *44* (3–4), 63–72.

(46) Hou, X.; Guo, W.; Xia, F.; Nie, F. Q.; Dong, H.; Tian, Y.; Wen, L.; Wang, L.; Cao, L.; Yang, Y.; Xue, J.; Song, Y.; Wang, Y.; Liu, D.; Jiang, L. A Biomimetic Potassium Responsive Nanochannel: G-Quadruplex DNA Conformational Switching in a Synthetic Nanopore. *J. Am. Chem. Soc.* **2009**, *131* (22), 7800–7805.

(47) Iqbal, S. M.; Akin, D.; Bashir, R. Solid-State Nanopore Channels with DNA Selectivity. *Nat. Nanotechnol.* **2007**, *2* (4), 243–248.

(48) Andersen, T. N.; Perkins, R. S.; Eyring, H. Zero-Charge Potentials of Solid Metals. *J. Am. Chem. Soc.* **1964**, *86* (20), 4496.

Chapter 6

Conclusion and future work

6.1 Project aims and outcomes

Harnessing the unique chemical and physical properties of nanopore sensing with advances in new materials and chemistries has been one of the ultimate aims of single-molecule detection. In chapter one, nanopore sensing, as a predominant tool for single-molecule detection of nucleic acids, proteins and glycans, was reviewed from the perspective of new materials and chemistries, with the main challenges including improving controlled fabrication and enhancing selectivity. A plethora of strategies have been innovated to advance nanopore sensing and at the same time to address the challenges described above. Specifically, a method was proposed to fabricate chemically-modified nanopore field-effect transistors to control single-molecule transport and selectively detect proteins and even small molecules.

Chapters two and three outlined the detailed fabrication methodology. As conventional nanopore-FETs are difficult to fabricate via advanced lithography techniques, this problem was addressed using the platform of dual-barrel nanopipettes. In contrast to conventional solid-state nanopore or single-barrel nanopipette platforms, dual-barrel nanopipettes were used in this project mainly due to nanoscale separation of their septum (~ 20 nm). One barrel can be selectively filled with carbon via pyrolysis of butane and another barrel can be used as a nanopore. A feedback-controlled mechanism is needed to accurately deposit gold around the nanopore opening.

It was explained in chapter three that, by using a gold-sulphite plating solution, controllable deposition on the nanoscale was proved to be feasible by using electrochemistry. More importantly, the feedback mechanism was introduced into this system by using a bipotentiostatic configuration to decrease the difficulty of fabrication and increase the device yield. The reproducibility and reliability of the fabrication method were verified through the precise tailoring of nanopore conductance. Surface characterisation, using optical and electron microscopy techniques, verified the deposition pattern and visualised the deposited gold around the nanopore opening. This opens up the possibility of using fabricated devices for nanopore field-effect transistors.

The control of single-molecule transport of DNA can be readily achieved using voltage gating. A reason to choose gold is the ease of its functionalisation by thiolated species. Therefore, gold can be functionalised by two different types of thiols: small molecules and oligonucleotides. Specifically, by using conventional solid-state nanopore or single-barrel nanopipette platforms.

In chapter four, it was shown how voltage gating was implemented into this system by using gold-deposited devices as on/off switches for the single-molecule transport of DNA. This was carried out under optimised electrochemical conditions probed by differential capacitance measurements. It is an important factor that gold can be easily modified by a range of thiolated species by developing an optimised formulation for surface functionalisation. Surface modification of deposited gold by either small molecules or oligonucleotides was successfully established and fully characterised by a combination of different electrochemistry techniques. Small molecules with different charges can be used to tune the surface charge of a nanopore, while oligonucleotides can act as selectivity components that recognise targeted analytes.

More active control of molecular transport was enabled by chemically modifying deposits with a positively charged amine. Functionalised nanopore-FETs are able to control single-molecule transport not only through switching on or off but also by tuning more transport properties, including transport velocity and capture rate, by orders of magnitude.

In chapter five, it was demonstrated how selectivity can be incorporated into this system in the form of aptamer-analyte binding. DNA aptamers bearing unique molecular structures such as G-quadruplex and stem-loop were functionalised onto the surface of gold to target proteins and small molecules such as neurotransmitters. Single-molecule transport of proteins can be detected and controlled using relatively well-characterised aptamers such as a 15-mer thrombin-binding aptamer.

Stem-loop aptamers for dopamine, serotonin and acetylcholine were used to detect these small molecules via target-induced conformational changes down to fM sensitivity. Aside from one-dimensional information obtained using resistive pulse sensing, the binding information can be extracted from the characteristics of single-molecule translocation events and correlated well with bulk measurements of the concentration dependence nanopore I-Vs in terms of conductance and rectification. Detecting neurotransmitters was not only possible by

using aptamer-functionalised nanopores, but also by using the gate electrode for selective electrochemical detection based on the redox properties of neurotransmitters.

6.2 Future work

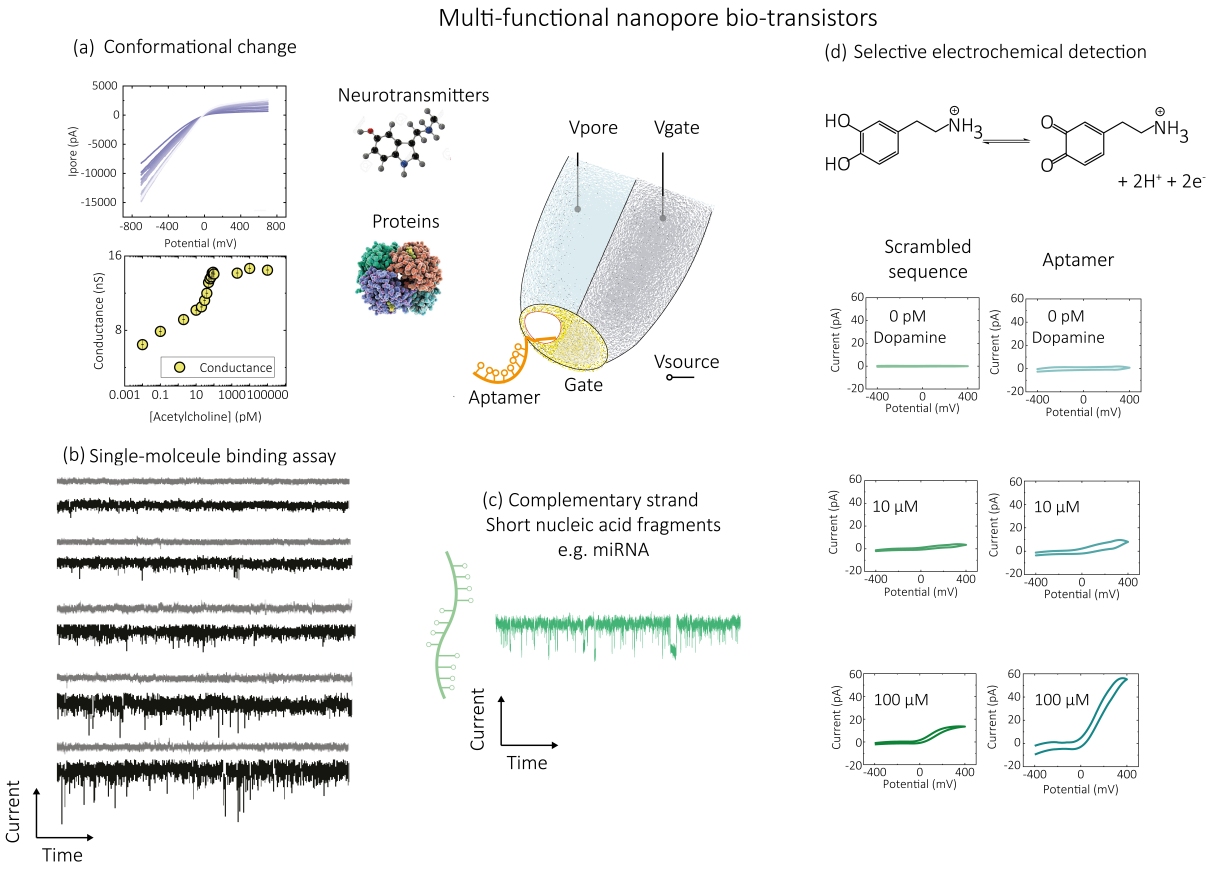


Figure 6-1: Summary of key conclusions and future work based on hybrid nanopore bio-transistors developed in this thesis. Overall, conclusions can be drawn from two different components of the device. (a) For aptamer-functionalised nanopores, the single-molecule detection of neurotransmitters was achieved via the target-induced conformational changes of aptamers functionalised onto the surface of gold. (b) By using aptamers with sufficiently high affinity with the targets, fM sensitivity can be attained. More importantly, the binding kinetics and thermodynamics can be extracted from resistive pulse-sensing methods and correlated with bulk measurements, confirming the robustness of the approach. (c) The strategy proposed in this thesis has implications on the detection of short fragments of nucleic acids via the base-pairing interactions between the target and the complementary strand, suggesting a novel way of detecting important potential biomarkers such as miRNAs. (d) To truly take advantage of this platform, the electrochemistry of the aptamer-functionalised gate was incorporated with a significantly broader dynamic range, up to hundreds of micron molar, from the

oxidation of redox-active neurotransmitters. To summarise, a range of detection methods were integrated into this sensing platform, with different dynamic ranges from fM to µM. Promising applications regarding in-vitro detection of neurontransmitter release can be expected.

In terms of future work, an array of applications can be foreseen, based on what has already been achieved. Coupled with further advances in aptamer customisation, more generalised applications can be achieved by designing aptamers with a desired dynamic range for the selective detection of targeted analytes using a range of sensing modes developed in this platform, using binding chemistries such as conformational changes, to test analytes in complex analyte matrices.

From the concentration dependence of aptamer-binding properties on nanopore FETs, nanopore I-Vs, redox detection of neurotransmitters and single-molecule translocation, studies can be crosslinked on one nanopipette to deliver a comprehensive picture of neuron activities inside living cells.[1–3] Each individual method is capable of revealing different chemical–physical processes occurring inside of a nanopore, either at single-molecule level or at bulk level, covering a broad concentration range from fM to µM. Therefore, a multi-functional probe for living-cell processes can be expected by using the unique features of this sensing platform. Moreover, the developed platform has important implications on the monitoring of a range of neuron activities because of the tuneable dynamic range for each sensing mode.

In recent years, there has been an increasing trend to direct nanopore research towards clinical diagnosis.[4,5] Apart from the conformational changes of aptamers, another area to be explored for selective detection using this platform is the base-pairing interaction between complementary strands. This might form the basis of the in-vitro single-molecule diagnosis of diseases from different biomarkers such as miRNAs, especially at low concentration (fM-pM). Perhaps Oxford Nanopore Technologies can be used as a benchmark where the high-throughput detection and sequencing of targets (in most cases nucleic acids) are facilitated by nanopore arrays in the form of flowcells. Different approaches might emerge for scaling up the operation of solid-state nanopores to cope with the increasing number of innovations in nanopore materials, as partly investigated in this thesis, even though there are currently still some developments to be made on scaling up the operation of solid-state nanopores or

nanopipettes. This will have implications on the detection of disease biomarkers and, consequently, future point-of-care diagnostic devices.

6.3 References

(1) Lussier, F.; Missirlis, D.; Spatz, J. P.; Masson, J. F. Machine-Learning-Driven Surface-Enhanced Raman Scattering Optophysiology Reveals Multiplexed Metabolite Gradients Near Cells. *ACS Nano* **2019**, *13* (2), 1403–1411.

(2) Abdalla, A.; Atcherley, C. W.; Pathirathna, P.; Samaranayake, S.; Qiang, B.; Peña, E.; Morgan, S. L.; Heien, M. L.; Hashemi, P. In Vivo Ambient Serotonin Measurements at Carbon-Fiber Microelectrodes. *Anal. Chem.* **2017**, *89* (18), 9703–9711.

(3) Zhang, Y.; Takahashi, Y.; Hong, S. P.; Liu, F.; Bednarska, J.; Goff, P. S.; Novak, P.; Shevchuk, A.; Gopal, S.; Barozzi, I.; Magnani, L.; Sakai, H.; Suguru, Y.; Fujii, T.; Erofeev, A.; Gorelkin, P.; Majouga, A.; Weiss, D. J.; Edwards, C.; Ivanov, A. P.; Klenerman, D.; Sviderskaya, E. V.; Edel, J. B.; Korchev, Y. High-Resolution Label-Free 3D Mapping of Extracellular PH of Single Living Cells. *Nat. Commun.* **2019**, *10*, 5610.

(4) Galenkamp, N. S.; Soskine, M.; Hermans, J.; Wloka, C.; Maglia, G. Direct Electrical Quantification of Glucose and Asparagine from Bodily Fluids Using Nanopores. *Nat Commun* **2018**, *9* (1), 4085.

(5) Cai, S.; Sze, J. Y. Y.; Ivanov, A. P.; Edel, J. B. Small Molecule Electro-Optical Binding Assay Using Nanopores. *Nat. Commun.* **2019**, *10* (1), 1797.